Portfolio of Measurement, Processing, and Analysis Techniques for Optical Oceanography Data

---

A report created by the students of:

Calibration and Validation for Ocean Color Remote Sensing

University of Maine Darling Marine Center, 11-29 July 2011

Funding provided by NASA

Contributing authors, in alphabetical order by last name:

Ana Arellano, Nathan Briggs, Fang Cao, Alison Chase, Haidi Chen, Apurva Dave, Clemence Goyens, Fernanda Henderikx-Freitas, Courtney Kearney, Malika Kheireddine, Sachi Mishra, Aimee Neeley, Melissa Omand, Leanne Powers, Anthony Reisinger, Sara Rivero, Brandon Russell, Bridget Seegers, Ryan Vandermeulen, Weining Zhu

Table of Contents

Fluorometers

Section Guide

1. Introduction

Fluorescence is the emission of light by a substance after the light has been absorbed. The re-emitted light has a longer wavelength and lower energy than the original light. There are known excitation and emission spectrum for a variety of substance including chlorophyll and CDOM. The fluorescence can therefore be used as a proxy for chlorophyll concentration and CDOM concentration. Chlorophyll absorbs in the blue and fluoresces in the red. CDOM absorbs in the UV and fluoresces blue light. Fluorometers provide the proper excitation light and then measure the emission light that results from the fluorescence. The parameters of fluorescence measured by fluorometers are the emission spectrum and its intensity.

There are a variety of bench top and in-situ fluorometers commercially available. This document covers details of the following fluorometers: Turner Designs 10-AU Fluorometer, TD-700 Fluorometer, Turner Designs C3 with in vivo chlorophyll and CDOM sensors, TD Cyclops-7 CDOM fluorometer, and the Wetlabs ECO FLNTU. This document also covers calibrations, field techniques, and some examples of data analysis/output from a cruise deployment.

2. Turner Designs 10-AU

2.1 Description

The manufacturer's website describes the 10AU Field Fluorometer as a "rugged, field-portable instrument that can be set up for continuous-flow monitoring or discrete samplanalyses" (http://www.turnerdesigns.com/t2/instruments/10au.html). A basic schematic of the instrument design is shown in Figure 1. The manufacturer also provides application-specific optical filters, allowing the user to analyze a variety of compounds, including chlorophyll *a* both *in vivo* (in living cells) and *in vitro* (extracted in solvent). The focus of this report is the Environmental Protection Agency (EPA) standard fluorometric method to measure *in vitro* chlorophyll *a* using a 90% acetone extraction (EPA Standard Method 445.0).

2.2 Instrument set up

Instrument set-up for extractive chlorophyll *a* (Chl *a*) measurement requires optical kit 10-037R (see application note 998-5101). Briefly, the fluorometer excites chlorophyll in 90% acetone using a broad-band blue filter (340-500 nm) and is equipped with a red-sensitive photomultiplier tube (PMT, >665 nm) for fluorescence detection. The output of the PMT is voltage, so one must standardize output voltage to known concentrations of a pure chlorophyll *a* standard (available from Turner Designs). The kit also includes a solid secondary standard to check for instrument drift during experiments. Since liquid chlorophyll *a* is expensive and photosensitive, the secondary standard provides an alternative to repetitive instrument recalibration. A 13 mm cuvette holder is typically used for this method. The 10AU fluorometer User's Manual reports a limit of detection of about 0.025 μg Chl *a* L^{-1} with the 13 mm cuvette holder and is about five times more sensitive with a 25 mm cuvette holder. The EPA Method 445 found a limit of detection closer to 0.05 μg Chl *a* L^{-1} with a limit of linearity of about 250 μg Chl *a* L^{-1}. Both limit of detection and limit of linearity should be periodically checked with a pure sample of chlorophyll *a*.

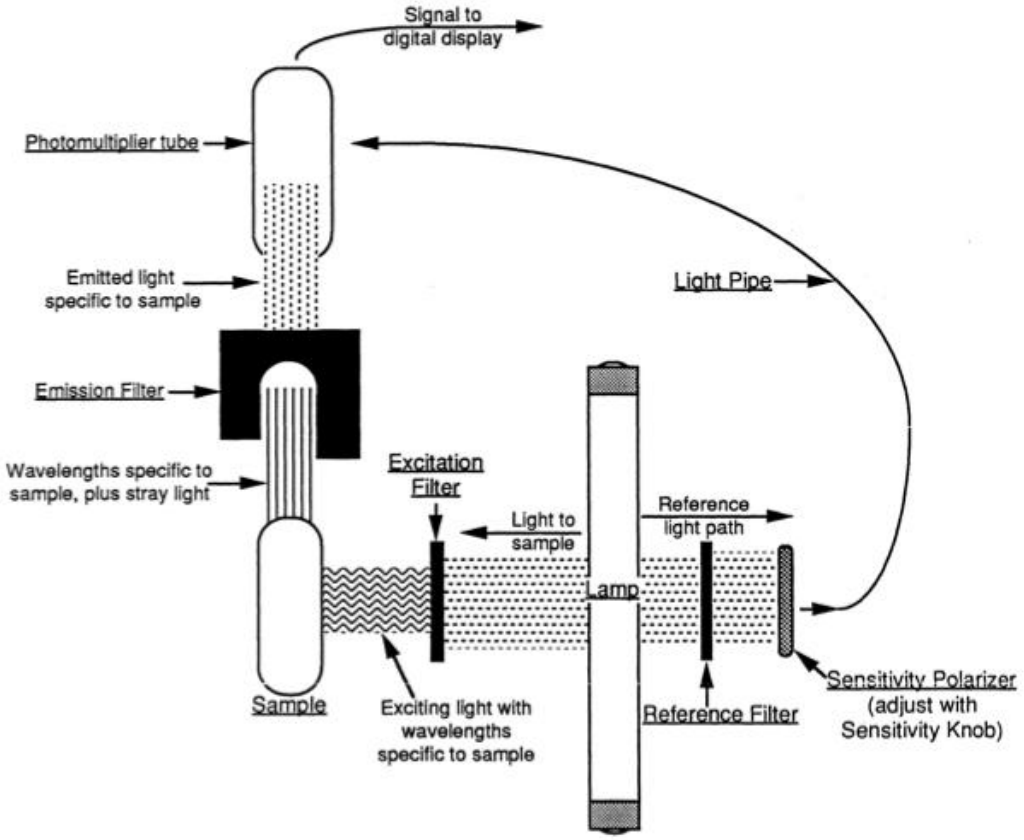

Figure 1. Instrument design of Turner Designs' 10 AU Field Fluorometer as shown in the User's Manual.

2.3 DATA MEASUREMENT

In field samples both chlorophyll *a* and its principle degradation products (the pheopigments pheophytin *a* and pheophorbide *a*, typically seen when cells are in senescence) are usually present. Since this standard method uses a broad-band blue filter to excite fluorescence, both chlorophyll *a* and the pheopigments are excited and measured. Acidifying the samples converts chlorophyll to pheophytin by removing its Mg^{2+} center, so measuring

samples post acidification measures fluorescence due to pheophytin only. To determine both chlorophyll *a* (Chl *a*) and pheophytin *a* (Pheo *a*), use the equations below.

$$[\text{Chl } a] = K (Fm/ Fm-1) \times (Fo - Fa) \times (v/V) \quad (1)$$

$$[\text{Pheo } a] = K (Fm/ Fm-1) \times [(Fm \times Fa - Fo)] \times (v/V) \quad (2)$$

where K is the standard curve's calibration coefficient, Fo is the sample fluorescence before acidification (dark corrected), Fa is the fluorescence after acidification (dark corrected), Fm is the max ratio Fo/Fa of the pure chlorophyll *a* standard, v is the 90% acetone extract volume (0.005 L typically) and V is volume of sample filtered (L).

Fluorometer calibration:

If not already calibrated, calibrate the fluorometer with standard dilutions of a known concentration of pure chlorophyll *a* (Turner Designs) in 90% acetone.

- The slope of the fluorescence (counts) vs. [chl *a*] (mg m^{-3}) gives the calibration coefficient, K.
- To determine Fm, add acid to each dilution and re-measure fluorescence. Fm is equal to the max ratio of fluorescence before acid addition to fluorescence after acid addition (Fo/Fa) for the pure culture).
- The manufacturer recommends recalibration every few months.

Note: Use consistent and careful techniques when sampling and filtering phytoplankton cells for chlorophyll analysis in order to keep the sample's fluorescent signature consistent. Also use proper safety equipment (gloves, goggles, etc.) when handling acid and acetone.

Filtration and Extraction

Prepare vacuum filtering apparatus and place a GF/F filter pad on each filter and insure that the filter cup is secure.

1) Mix sample bottle and add measured volume of sample (usually 50-200 mL depending on sample) to each filter cup.

- Filtering a larger amount of sample will leave more chlorophyll on the filter, and thus more chlorophyll will be extracted in 90% acetone. It may be wise to filter a variety of volumes for each sample to ensure that you take fluorescence measurements that lie within your standard curve, the instrument's limit of detection and the instrument's limit of linearity (Figure 2). Make sure to take 3 replicates of each volume filtered.
- Samples used in the following example were a pure culture of the diatom *Thalassiosira pseudonana* and an unfiltered whole water sample collected in the Damariscotta River Estuary.

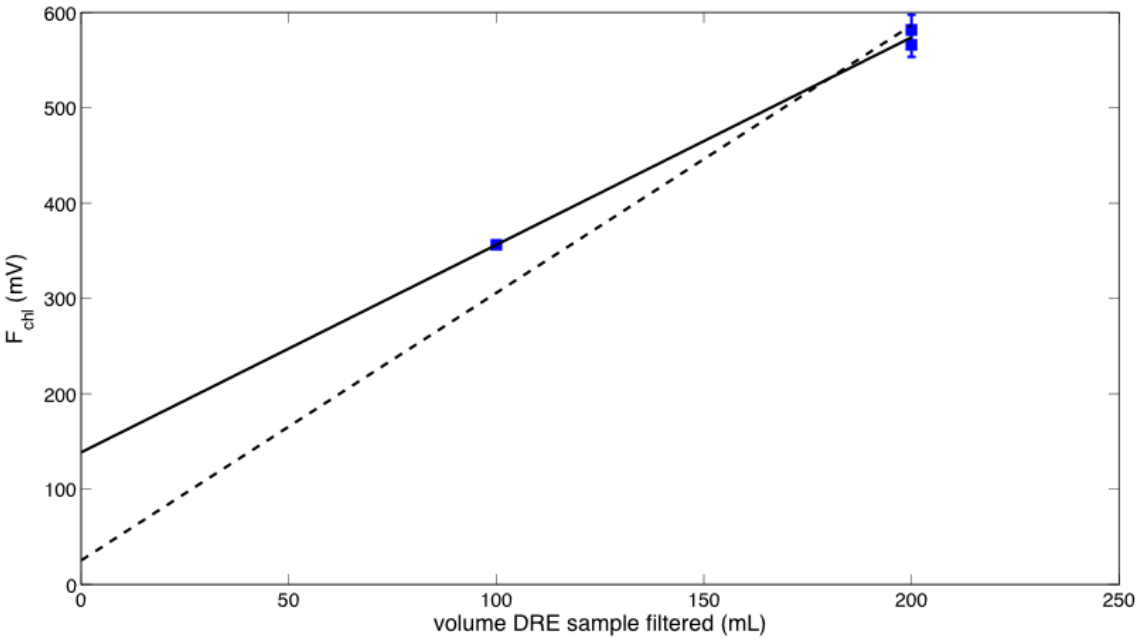

Figure 2. Integrated fluorescence (F_{chl} (mV)) vs. volume Damariscotta Estuary Water filtered (mL). Although only two points are used to fit a line, this chart is an example of how to check the instrument's limit of linearity. When fluorescence no longer increases with increasing volume of sample collected on a filter, the curve will bend over. Note that the solid line is a linear fit through two data points and the dashed line is a linear fit through zero. In this example the limit of linearity is not reached, but it is also not perfectly linear.

2) Filter samples through G/FF with the vacuum pressure below 5 mm Hg and when all water has been filtered, immediately remove filter and submerge in a borosilicate tube with 5 mL 90% acetone.

- Since chlorophyll in acetone bleaches very rapidly, work in dim light and store tubes in dark until you are finished.

3) Place 3 unused filters in 3 separate tubes with 5 mL 90% acetone.

- These tubes will act as blanks for the fluorometer measurements. Blank measurements are necessary because we need to correct for all signal measured that is not due to chlorophyll and pheophytin fluorescence (i.e. the instruments dark signal).

4) Place tubes in freezer for 24 hours to allow chlorophyll and pheophytin to extract from cells into acetone.

Fluorescence Measurement

1) Turn fluorometer on to warm up. Keep room light as dim as possible.

2) Keeping room in dim light, remove tubes from freezer and vortex mix them to complete extraction and to ensure uniform distribution in tube.

3) With forceps, remove filters, replace caps, and wipe finger-prints off each tube.

4) Centrifuge tubes for 5 minutes to remove filter fragments since some G/FF filters are much more prone to disintegration.

- Centrifugation pushes these and other particles to the bottom of the tube. This is an important step because presence of particles in he light path will cause scattering. Both the light emitted from the light source or the light fluorescing in the sample can be scattered into or away from the detector.
- Carefully remove tube from centrifuge being careful to not re-suspend filter pad fragments and particles (for the above mentioned reasons).

5) Measure room temperature. If temperature in the room varies by more than 1-2ºC, the fluorometer should be calibrated with acetone extracts at a range of temperatures; fluorescence quantum yield decreases as a function of increasing temperature. Place the secondary standard in the fluorometer and measure and record the reading.

- The purpose of the secondary standard is to check for instrument drift. During your runs, you should periodically re-run the secondary standard and make sure it is giving you the same amount of fluorescence. If the instrument has drifted during your experiment, you should re-run your blanks.

6) Insert your sample blank tube into the fluorometer, record its reading and call it Fob.

7) Remove tube, add one drop 10% HCl, don't mix, and place back in the fluorometer. This reading is Fab. Repeat for all sample blanks.

8) Insert sample tube in fluorometer and record the reading (this reading is Fo).

9) Remove tube, add one drop 10% HCl, don't mix, and place it back in the fluorometer. Record this reading and call it Fa. Repeat for all samples.

- Also remember to periodically measure the secondary standard and check for instrument drift.

10) When finished empty tubes in hood into an acetone waste container and leave empty tubes in hood (with hood on!) until all acetone has evaporated.

11) Subtract blank readings, Fob and Fab, from Fo and Fa readings, respectively. Using the corrected Fo and Fa values, calculate chlorophyll *a* concentration using equations 1 and 2 above.

2.4 DATA PROCESSING and INTERPRETATION

Use Equations 1 and 2 to calculate Chl *a* and pheo *a* concentrations from raw data (Fo and Fa). Replicates will allow uncertainty estimations. The figure below shows the results of these calculations for chlorophyll determination in both the culture of the diatom *Thalassiosira pseudonana* and the natural sample collected in the Damariscotta River Estuary (Figure 3).

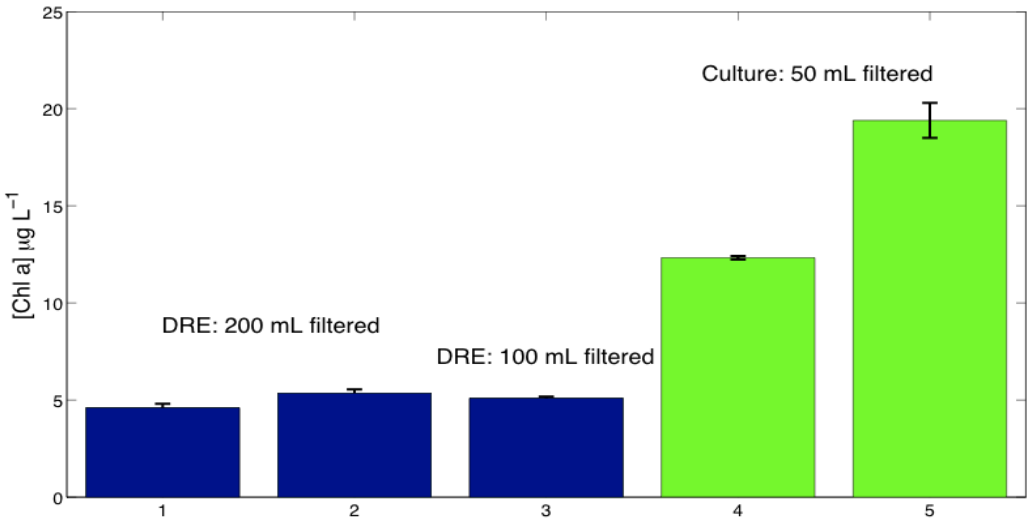

Figure 3. Chlorophyll concentration [Chl] (µg L^{-1}) calculated from raw fluorometer counts using Equations 1 and 2 from a whole water sample collected at the Damariscotta River Estuary (DRE, blue bars) and from a culture of *Thalassiosira pseudonana* (Culture, green bars). Different volumes of DRE sample were filtered (200 mL or 100 mL) and 50 mL samples of two different culture samples were filtered. Each bar on this chart represents the average of 3 extractions from the same sample.

2.5 CAUTIONARY NOTES

Turner Designs 10 AU Field Fluorometer is a stable and easily operated instrument for measuring fluorescence. Despite this fact, one must use caution when assessing chlorophyll concentration as determined using this method. The fluorescence in each sample is described by the equation

$$F = a(\lambda)*E(\lambda)*\Phi_f \qquad (3)$$

where F is the fluorescence of the sample (moles fluoresced photons m^{-3}), $a(\lambda)$ is the absorption coefficient of fluorophore (m^{-1}), $E(\lambda)$ is the excitation energy (mole photons m^{-2}) of the fluorophore and Φ_f is the quantum efficiency of the fluorophore (mole photons fluoresced/mole photons absorbed). Unfortunately factors can affect the $a(\lambda)$, $E(\lambda)$, and Φ_f of

a sample.

First of all, Φ_f is affected by temperature. Increasing temperature exposure tends to decreases the fluorescence quantum yield. One must monitor temperature throughout the course of an experiment and run a recalibration if the temperature drifts more than 1 to 2° C. Interference, a(λ),If suspended particles in the extraction tube are not centrifuged or are resuspended, they will interfere with the excitation light source, increase scattering and give an artificially high reading for Chl *a* fluorescence. Another issue is the use of the broad-pass filter from 340 to 500 nm for chlorophyll *a* excitation since additional chlorophyll pigments absorb light in these wavelengths. Luckily, not all phytoplankton pigments fluoresce when extracted in solvent. However in addition to the degradation product and accessory pigment pheophytin *a*, chlorophyll *b* also fluoresces in acetone. In fact, there may be significant fluorescence from chlorophyll *b* because it absorbs light in this region and may be present in significant concentrations nature. Furthermore, when chlorophyll *b* is acidified, its degradation product is pheophytin *b*, which also absorbs light in this region and fluoresces. This could lead to an underestimation of chlorophyll *a* by 60% in the most extreme case (Turner Designs application note 998_9000). In response to this problem, Welschmeyer (1994) developed a method that avoids the interference of chlorophyll *b* by using a narrow band excitation filter that excites only chlorophyll *a* at 436 nm and a narrow detection filter that detects its emission at 680 nm. This method does not allow for measurement of pheopigment concentration, which has an absorbance peak at 412 nm. If one is interested in a quantitative assessment of all phytoplankton pigments in a sample, high-pressure liquid chromatography (HPLC) techniques are recommended.

3. Turner Designs 700

Because chlorophyll a fluorescence is widely used as a proxy for phytoplankton biomass, variability of its quantum yield of fluorescence is problematic, compromising linearity in the relationship between in vivo fluorescence and concentration. One major driver of fluorescence variability is light, particularly high light. Changes in the apparent quantum yield of fluorescence can occur on time scales from seconds to hours. One of the challenges for ecological and biogeochemical studies is how to better constrain this aspect of variability in the relationship between chlorophyll a fluorescence and concentration.

Instantaneous in-situ measurements of chlorophyll fluorescence are necessary to address questions regarding photo-adaptation of cells to different light conditions, and the Turner Designs TD-700 fluorometer is a viable instrument to provide such estimates. Generally, the emitted light at 680 nm will be directly proportional to the concentration of the chlorophyll in a sample analyzed. Further acidification methods can be performed to obtain chlorophyll concentrations, but they usually are not performed in situ. As the objective here is to observe relative changes in fluorescence counts with different light conditions (which relate to chlorophyll concentration), chlorophyll measurements will not be performed.

3.1 Description

From Turner Designs (http://www.turnerdesigns.com/), the TD-700 Laboratory Fluorometer is a compact and low-cost bench-top fluorometer (Figure 4). The TD-700 is very close in sensitivity to the 10-AU. Its design is based on the idea that proper filter and lamp combination can allow measurement of light and quantification of the compound present. Sensitivity for chlorophyll a measurements range from 0.01 µg/L to about 250 µg/L. Fluorescence measurements are recorded in counts, with an excitation wavelength of 440 nm and emission (measured) range at 680 nm. No special storage conditions are required. For common asked question about the instrument, visit *www.comm-tec.com/Prods/mfgs/TurnerDesigns/.../TD-700%20FAQ.pdf (Turner Designs, 2008,* http://www.turnerdesigns.com/).

Fig. 4. TD-700 bench-top fluorometer (Turner Designs). 12x35 mm round screw top vials hold the samples, which are introduced inside the instrument for reading. A black plastic standard accompanies the instrument for necessary calibrations.

In-vivo measurements of fluorescence using TD-700.

Both in vivo and in vitro measurements can be performed with this instrument. The main difference between the procedures includes ways of monitoring light to which samples are exposed to (as in the natural environment small variations in light can change the quantum efficiency of living cells, and therefore result in variation of fluorescence readings. In the laboratory however, light intensity and exposure can be monitored and controlled). As an example, let's consider a culture of *Thalassiosira pseudonana*, and assess the variations in fluorescence readings in a natural environment, where irradiance intensities change in diverse time scales (direct or indirect sunlight). Therefore, fluorescence measurements will be made for samples progressively exposed to natural illumination, against samples kept protected from sunlight. Relative fluorescence measurements will also be calibrated against filtered sea water samples (theoretically equivalent to a zero concentration of particles, and therefore useful to provide background information on the quantities measured and stability of the instrument). Photo-synthetically available radiation (PAR) will be measured simultaneously to support data interpretation.

3.2 Physical setup

Necessary materials include: TD-700, located as close to where the samples will be exposed to illumination as possible; solid calibration standard provided with instrument to follow sensor drift; labels to identify sample tubes; filtered sea-water blank (0.2 um filtered) in tube sample to be exposed to illumination; triplicates of culture in tube samples that will be exposed to illumination, with known volume and concentration; triplicates of culture in tube samples that will be constantly maintained in the dark, with same volume and concentration as the light-exposed samples; cooler with sea water to keep dark culture samples; water container to hold light-exposed samples while under sun illumination (preferably ambient water to prevent variations in temperature that might affect quantum efficiency), absorbing paper to clean tubes before they are inserted in the fluorometer; alarm clock to monitor the time each sample gets exposed to the light in between measurements; PAR meter (measured in $\mu mol/m^2s$, positioned in a constantly un-shaded location to measure changes in incident light).

3.3 Procedure

1) Allow the fluorometer to warm-up for the time specified in the User's Manual (a "countdown" clock will show the remaining time on the screen). Make sure the lamp is functioning by checking the lamp view port on the back panel of the instrument.
2) Place triplicates of culture samples in the water container, in the natural light. Define time they will be exposed to (e.g. record fluorescence); maintain dark samples in cooler, away from natural sunlight.

3) Place solid standard in fluorometer, wait until counts stabilize (~10 s), record the fluorescence counts. TD-700 will internally take that count into consideration when retrieving fluorescence counts of the samples.
4) Mix and read filtered seawater blank in known volume tube, record fluorescence counts; Record time of each measurement for each sample.
5) Mix, read and record fluorescence for light-exposed samples, one tube at a time. Keep remaining samples exposed to illumination in between each measurement to avoid recovery and adaptation to low light conditions.
6) Mix, read and record dark-adapted samples, one at a time. Return tubes to cooler immediately after reading.
7) Keep samples exposed to illumination for 5 more minutes, and repeat 4-6. Repeat experiment as many times as possible throughout the day.
8) In the end of experiment, record fluorescence from the solid blank again, to be aware of any sensor drift.
9) Obtain PAR data (if connected to a computer), or record it at the time of each measurement (if data can't be stored automatically).

Important:

- Fluorometer should be placed close to cultures;

- Don't forget to mix tubes before each reading, inverting them upside down a couple of times. Be consistent with all tubes. Dry the outside of the tubes before each reading.

- Keep light-sample tubes in a horizontal position in the water container to prevent settling of particles to the bottom and packaging (which might affect quantum efficiency).

- Depending on the concentration of the culture chosen, the settling of particles in the tube in the moment of reading might affect the stabilization of fluorescence counts. If the counts do not stabilize, wait around 10 seconds and record counts.

- This experiment should be performed in a sunny day for clear results.

Supporting data

It is possible to convert fluorescence counts to chlorophyll concentration, if at least one chlorophyll concentration is known for a certain culture and volume. The relationship can result from a simple linear regression (assuming every phytoplankton has chlorophyll a, and chlorophyll a is fluorescent at 680 nm, and therefore the more chlorophyll a cell has the more it should fluoresce). More robust algorithms are also available, with variable uncertainties. An example include Mignot et al. ("From the shape of the vertical profile of in vivo fluorescence to Chlorophyll-a concentration", Biogeosciences Discussions, 2011, vol 8, Issue 2, pp.3697-3737).

The document available at www.turnerdesigns.com/t2/doc/appnotes/S-0003.pdfi, from Turner Designs, has a comprehensive set of questions and answers regarding Fluorometric

Chlorophyll Analysis, including general methods for chlorophyll extractions and equations transforming the fluorescence counts into chlorophyll estimates.

3.4 Data processing

Below (Table 1) is an extract of a real data sheet collected with TD-700 for *Thalassiosira pseudonana*, for which results will be presented in the next session. Even though it is not the ideal situation, here is shown one sample blank for sea water, two samples for culture kept in the dark, and three replicates of culture kept in the light. Time of each measurement and instantaneous PAR were annotated. Each tube was filled with 50 mL of water + culture or filtered sea water (0.2 μm). Fluorescence counts for the equipment's Solid Standard are not shown, but were consistent before and after the experiment. TD-700 takes the initial solid standard measurement into consideration when computing the fluorescence counts for the samples.

Table 1. Extract of the raw data obtained in the field using TD-700.

Time	**PAR**	**Sky**	**sea water blank**	**dark 1**	**dark 2**	**cult 1**	**cult 2**	**cult 3**	**Who sampled**
14:06	782	cloudy	4.4	178.7	177.6	214.4	197.5	187.4	Person a
14:11	871	cloudy	4.4	202.4	210.7	199.8	198.5	194	Person a
14:16	2258	sunny	4.6	200.7	195.5	174.1	172	164	Person a
14:21	2186	sunny	4.7	206	196	146.2	145	144.2	Person b
…	…		…	…	…	…	…	…	
17:58	565	sunny	4.6	184.2	203.3	210	188	191.7	Person b
18:17	531.1	sunny	4.7	211	200	190.4	183.4	186.6	Person b

The concentration of the cultures was not known (even though each 50 mL tube culture sample had the same concentration), so the values retrieved cannot be directly compared with other experiments. It is believed to be useful, however, to compare data from the same population, and therefore test the effect of quenching and photo-adaptation of phytoplankton cultures when exposed to natural light variations throughout a certain day (if there is an effect at all).

Basic statistics can be obtained by calculating average and standard deviation of dark 1 and dark 2, and culture 1, 2 and 3. Sea water blank measurements are subtracted from each sample to account for a background fluorescence signal in the filtered sea water. The average of dark

measurements can be used in the normalization of the data, especially when trying to compare parallel experiments happening throughout the same day, as shown below.

3.5 Results and Interpretation

Figure 5 shows two parallel experiments to assess quenching of a culture of *Thalassiosira pseudonana:* one running from 2 pm to 6:24 pm on July 14th 2011, in Coastal Maine (USA), and another starting at 4:40 and ending at 6:24 pm. Measurements were taken at approximately every 5 minutes. Replicas of fluorescence measurements were only obtained in the first hour of the first experiment, but throughout the entire second experiment. Fluorescence is normalized to the average to the dark samples of each experiment, to allow inter-comparison of magnitudes.

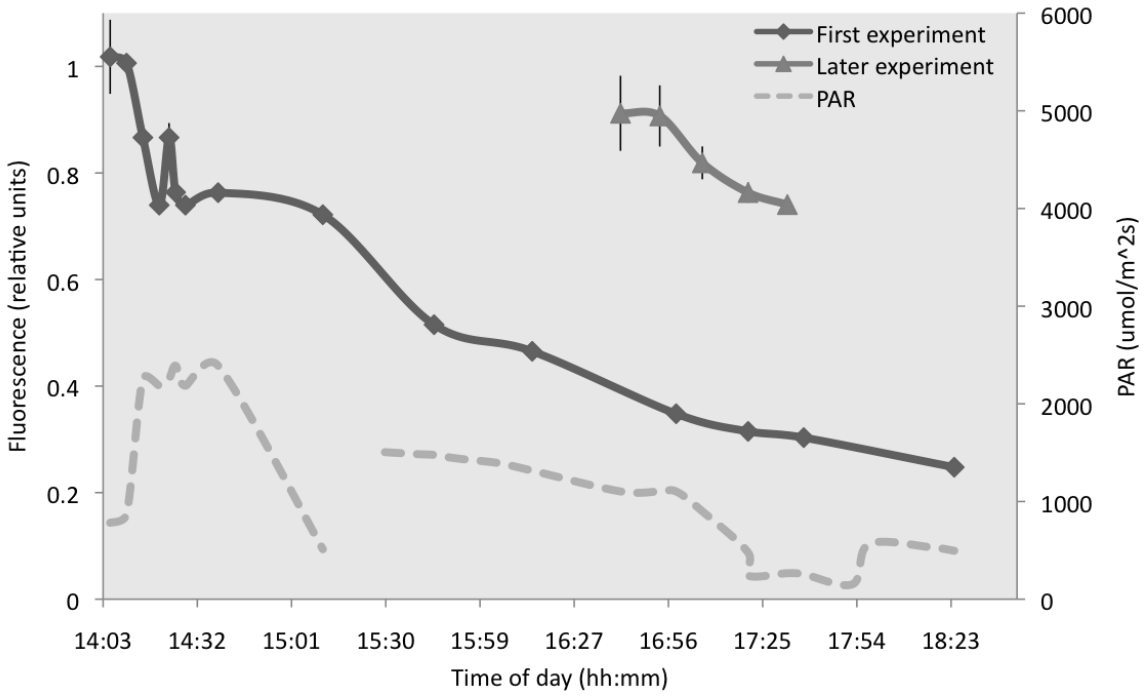

Figure 5. Interpolated fluorescence measurements of *Thalassiosira pseudonana* exposed to natural illumination *t*hroughout a day (2-6 pm), normalized to fluorescence of cultures preserved in the dark. The first experiment, darker grey, represents the same culture followed throughout the day. The second experiment, lighter grey, represents cultures exposed to sunlight from 4-6 pm. All cultures analyzed had the same volume (50 ml) and concentration (not recorded). PAR measurements were obtained for most of the afternoon (gap around 3:15 pm). Replicas were not available for experiment 1 between 3-6 pm.

When quenching occurs, i.e. when the quantum efficiency of cells is modified, one would expect to see a decrease in fluorescence as a function of exposure to high light conditions, and Figure 5 clearly shows that relationship for both experiments. The fact that sun illumination varied considerably throughout the afternoon (PAR), however, makes it hard to infer whether there is a linear relationship between exposure to light and decrease in fluorescence.

Before 3:30 pm (Figure 5), it is possible to note the presence of clouds during the experiment (backed up by field annotations), especially during the first hour of observations, which results in rather unreliable readings, as cells have the ability to quickly recover and increase their quantum efficiency.

In Figure 6 below, PAR is plotted against the dark-normalized fluorescence for the same observations of Figure 5, and no clear relationship between both variables can be seen, and that can be related to 1) the short duration of experiments; and 2) the fact that weather conditions were not ideal for a detailed quenching experiment and tracking of the light history and its impact on the culture considered. Issues with dark cultures could also be observed, as the oscillation of fluorescence measurements (in an environment that was expected to remain fairly constant) could relate to interactions between the light source inside TD-700 and the cultures. The increase in fluorescence counts in the dark measurement was especially noted in the field when the sample was left in the equipment for a longer period of time.

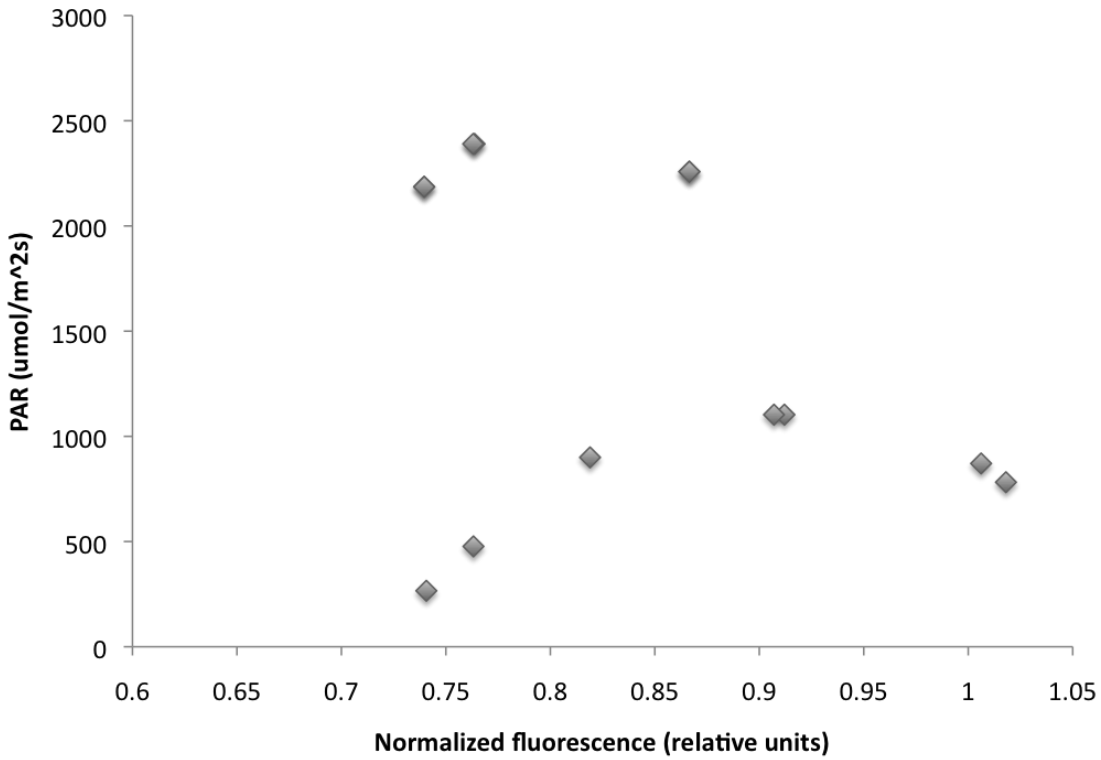

Figure 6. Dark-normalized fluorescence against PAR for experiments 1 and 2 (shown in figure X). Note that there is no clear relationship between the two variables, which can be related to the constantly changing weather conditions during the experiment, as well as the limited number of samples/replicas measured and the duration of the experiment.

Rather than instantaneous light, a comparison with total photons reaching the samples would probably show a more direct relationship between exposure to light and decrease in

fluorescence. Repeated analysis during longer periods of the day (especially in clear sky conditions), more structured sampling strategies (larger number of samples), support of a laboratory simulation of quenching based on controlled changes in solar radiation, as well as data on coefficient of absorption of the culture and chlorophyll a estimations could be used to support the analysis.

4. Wetlabs ECO FLNTU

4.1 Description

The ECO FLNTU is an *in situ* combination fluorometer and turbidity sensor. It measures chlorophyll fluorescence at 470 nm and turbidity at 700 nm. The fluorometer operates by exciting material in the water with a low-power blue LED beam. Subsequent florescence is measured by a detector equipped with an interference filter in order to ensure that no scattered excitation light is counted in the measurement. Turbidity is measured simultaneously by detecting the scattered light from a red LED beam. While these sensors may be used to quickly measure relative amounts of chlorophyll, CDOM, uranine, phycocyanin, or phycoerythrin, the user should be aware that calibration of the sensor with carefully laboratory measurements is required in order to obtain reliable readings for concentration output.

The user guide may be found at the following link:

http://www.wetlabs.com/products/pub/eco/flntuac.pdf

Figure 7: ECO FLNTU sensor, taken from Wetlabs specification sheet (http://www.wetlabs.com/products/pub/specsheets/flntussh.pdf)

4.2 Data Measurement

Dark measurement

This measurement is used to derive the background noise of the sensor. This value will later be subtracted from the readings. Black electrical tape is placed over the detector window, and the sensor is run for approximately 10 – 15 seconds while submerged in tap water. For a comparison of dark samples taken in and out of water of different types, refer to Appendix A.

Blank measurement

**In the lab, black buckets may be used to hold all water samples for sensor readings in order to minimize any ambient light from reflecting into the detector of the sensors.*

Blanks are used for determining how the sensor will record in the presence of medium (water) without the addition of sample, and are essentially a zero concentration reading. Depending on the user's needs, one can use ultrapure type 1 water or freshly filtered seawater (FSW); note that small phytoplankton may fall through the filter. Ideally, the blank water should be as similar to the sample water as possible in terms of inert components. As long as there is no interference with dissolved components in the water, FSW may be used.

1) Fill bucket with sufficient volume of FSW.

2) Gently lower sensor into the water, lightly moving around the bucket to stir. Test distance from bucket wall to ensure that the wall does not contribute to the measurement.
3) Start readings and record for 10 – 15 seconds.

Sample measurement

For this demonstration, two tasks were examined. The first task was to calibrate the chlorophyll fluorometer, and the second task was to examine the effects of increased turbidity on a constant chlorophyll fluorescence reading. The following section describes the laboratory setup and procedure for each task.

Task 1 (Chl. Fluorescence) – Dark and blank readings are performed as outlined above, using ultrapure and FSW. Incremental additions of *Thalassiosira* culture are added using a clean graduated cylinder. All samples are mixed before sensor readings begin. All readings take place for 10 – 15 sec. Additions are performed as follows:

Sample	Added culture (mL)	Cumulative addition (mL)	Total water volume (mL)
1	50	50	8050
2	100	150	8150
3	200	350	8350
4	400	750	8750
5	800	1550	9550

Following the final measurement for the *Thalassiosira* culture + SW mixture, a 500 mL sample is taken from the bucket for subsequent laboratory analysis of Chlorophyll-a concentration.

Task 2 (Effect of turbidity) - Dark and blank readings are performed as outlined above, using FSW. Reading are taken from the black bucket after performing incremental additions of Arizona Clay (40 mg / mL) using a clean 1 mL pipette to the end-point *Thalassiosira* series. All samples are mixed before sensor readings begin. All readings take place for 10 – 15 sec. Additions are performed as follows:

Sample	Added culture (mL)	Added clay soln. (mL)	Total added clay solution (mL)
6	1550	0.5	0.5
7	1550	1.0	1.5
8	1550	1.5	3.0
9	1550	3.0	6.0
10	1550	6.0	12.0

4.3 Data Processing

In order to examine the experimental effects of contaminant addition, the user first needs to process data carefully, ensuring that the data output is accurate. For fluorescence, there are a few simple steps required to go from raw counts to workable data.

1) Open raw data with data analysis tool, such as Microsoft Excel or Matlab.

a. While the instrument outputs several files, it is recommended that the data sets be compiled into a single file for ease of workload and calculations.

2) Beginning with dark reading, perform median and standard deviation calculations.
3) Repeat the above procedure for all FSW and sample data.
4) Set up a table like the following and place values into their respective position:

EX.	A	B	C	D	E	F	G	H
1		*Thal.*/ clay addition (mL)	Cumul. addition (mL)	Total volume (mL)	Dark (med)	RAW Sample (med)	Corrected Sample (med)	Turbid. (NTU)
2	FSW							
3	Sam 1							
4	Sam 2							
5	Sam 3							
6	Sam 4							
7	Sam 5							

5) The corrected sample (Column G) is derived from the following equation:
   a. Corrected Sample (G) = RAW sample (F) – Dark (E)

Now that data is corrected, the user can proceed to derive relationships from the data Remember that the highest fluorescence corresponds to the 500 mL sample that is analyzed for Chlorophyll a in the lab. Fluorescence is a function of concentration (C), excitation light (E(□)),and quantum efficiency (□$_r$), the latter two of which are held constant through the measurement. Therefore, since fluorescence is directly proportional to concentration, one can use the wet laboratory results of chlorophyll find concentrations at other fluorescence values. For a working example of the following spreadsheet instructions, follow this link.

1) Obtain final chlorophyll concentration from the lab extraction measurements.

Perform the following calculations:

NOTE: the next two calculations are only performed on the final sample point that corresponds to the concentration that was taken to the lab.

2) Calculate the mass of total chlorophyll in SW at the last point.
   a. Lab concentration in □g /L (step 1) * total cumulative volume (*SW + culture*)
3) Calculate the concentration of phytoplankton culture in the last sample.
   a. Mass of chlorophyll in SW (step 2) / total cumulative volume (*culture only*)

The following calculations can now be performed on the rest of the sample set.

4) For the rest of the samples, calculate the mass of chlorophyll added *at each dilution*:
   a. Concentration of phytoplankton culture (step 3) * volume of culture added at each dilution.
5) Calculate the mass of chlorophyll *in solution* (cumulative addition) at each dilution.
   a. Mass of chlorophyll added *at each dilution* (step 4) + mass of chlorophyll *in solution* at previous dilution.
6) Finally, find the concentration of chlorophyll in solution for all data points.
   a. Mass of chlorophyll *in solution* (Step 5) / total cumulative volume of solution *at that dilution*.

7) Plot corrected fluorescence counts (FU) as a function of concentration of chlorophyll a in solution (Step 6). Use equation to convert fluorescence to chlorophyll concentration.

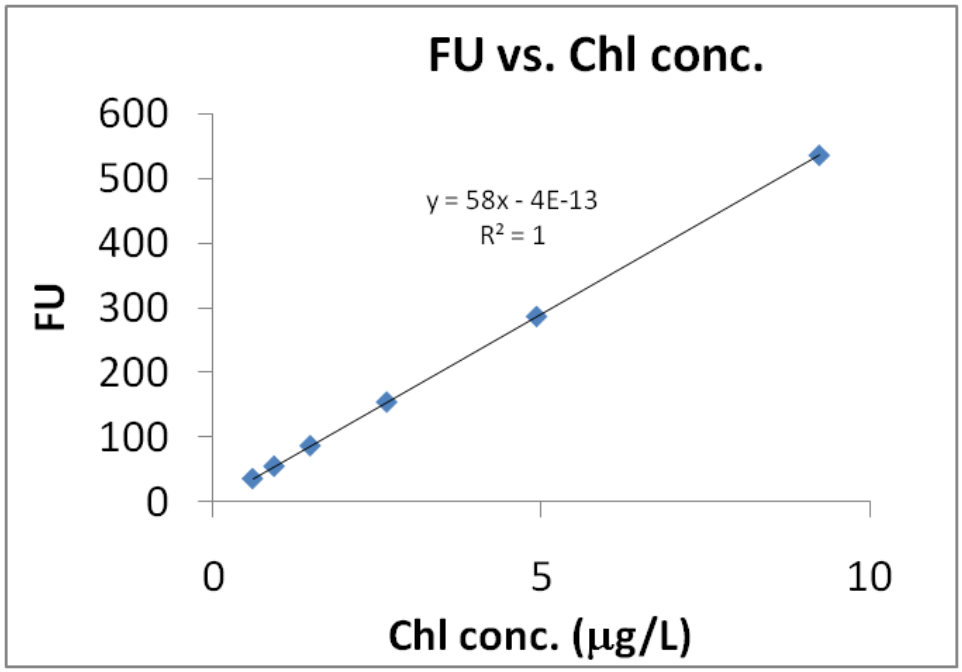

Figure 8: Plot of fluorescence as a function of chlorophyll concentration.

4.4 Data Results and Discussion

The previous section described how to calibrate the instrument. With trustworthy data, the next task is to determine how increased turbidity (and subsequent scattering of light) will affect the chlorophyll fluorescence values along the pathlength. The goal is to find at what point data becomes suspect as a result of the scattering properties of the water. Figure 9 illustrates an interesting trend. The red line shows the very gradual increase of turbidity counts as a result of phytoplankton additions. The blue line shows the dramatic increase of turbidity with the additions of clay solution, as described by Task 2 in the Data Measurement section.

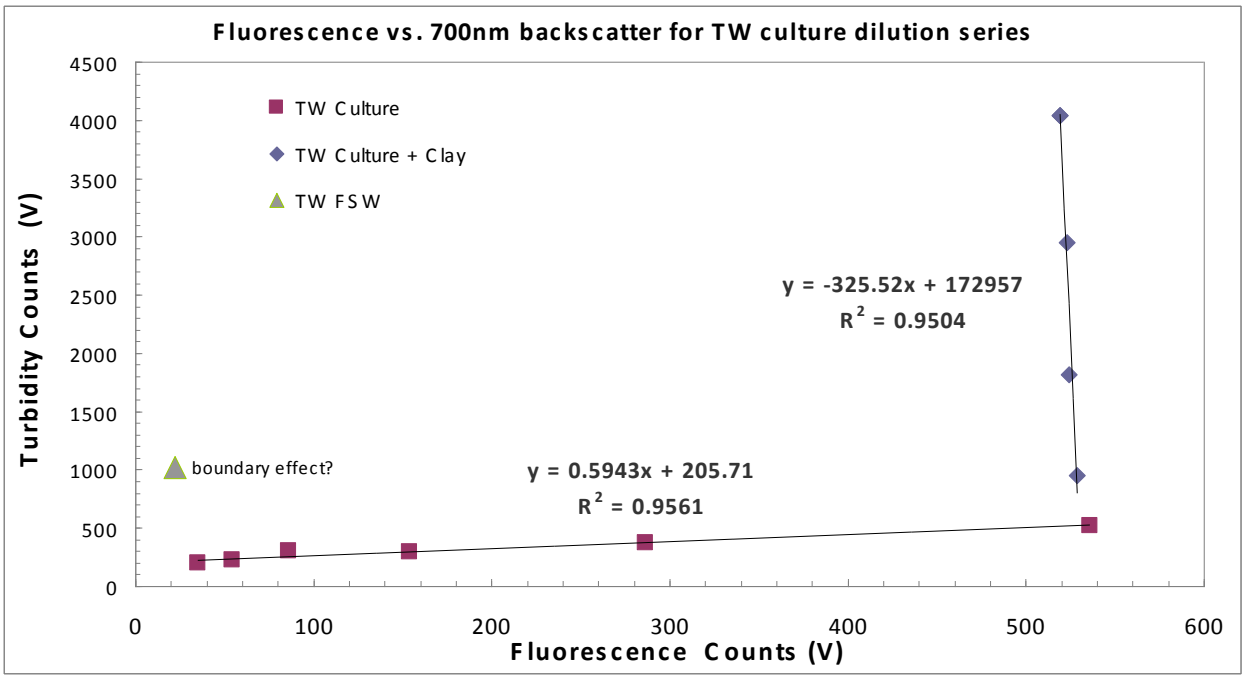

Figure 9: Turbidity counts as a function of sample additions for Task 1 and 2.

Zooming in on the blue line (Figure 10) shows another interesting trend in which the relative fluorescence appears to decrease with the addition of more clay material, even as the culture concentration remains unchanged.

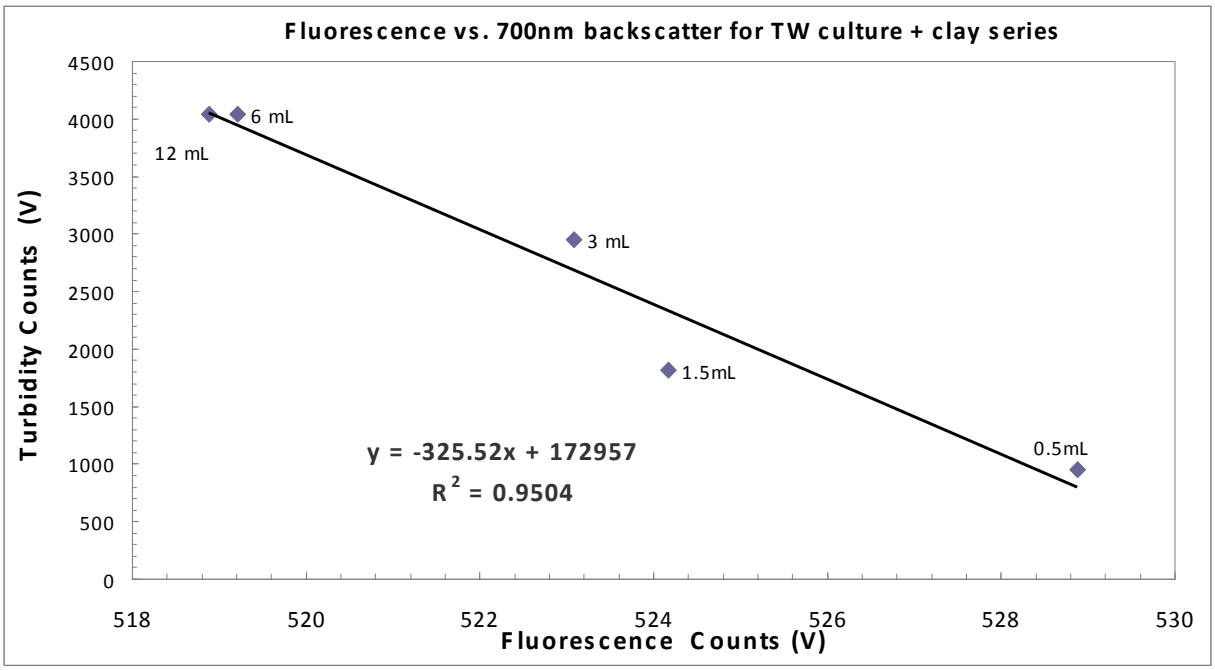

Figure 10: Turbidity counts as a function of fluorescence

Finally, the cumulative decrease in fluorescence with each clay solution addition is subtracted from the fluorescence due to only chlorophyll at the Task 1 endpoint (before the addition of clay). Figure 11 shows the apparent decrease in chlorophyll a concentrations with the addition of clay particles. Therefore, the data shows that clay particles have the potential to change the calibrated concentration of chlorophyll when measured by fluorescence.

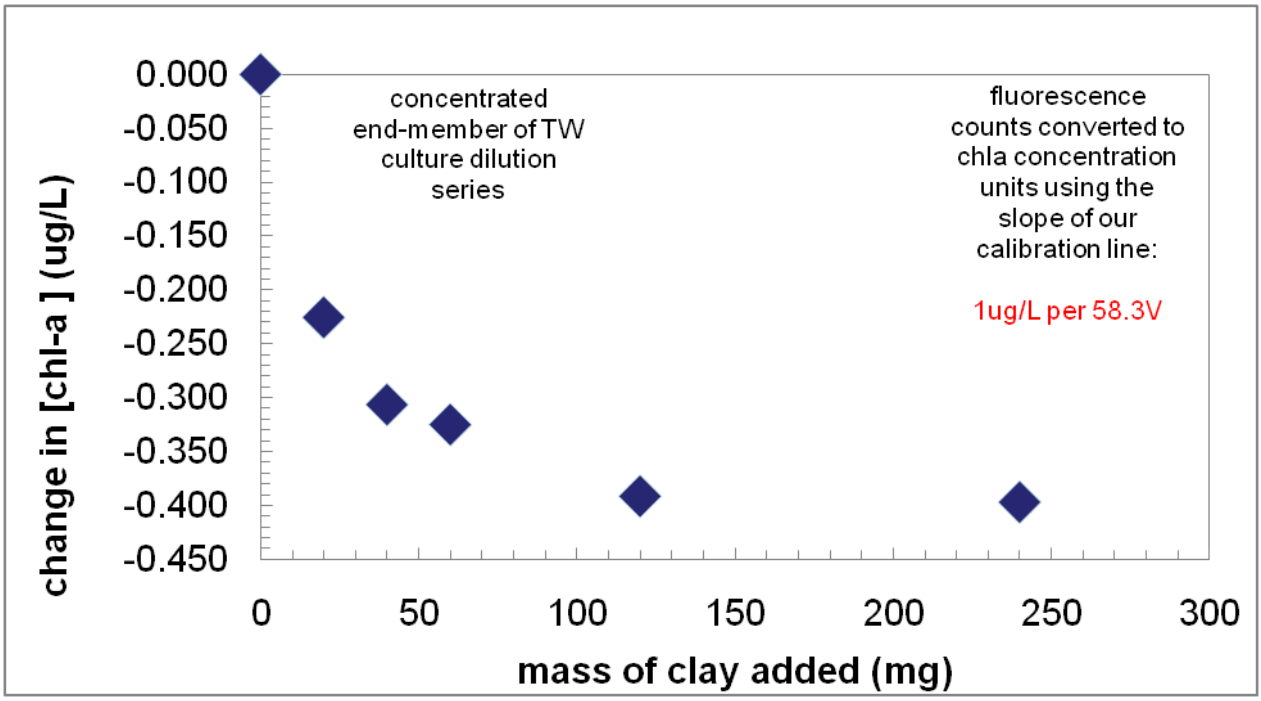

Figure 11: Relative change in chlorophyll-a concentration as a function of clay mass added. For this demonstration, there is up to a -0.4 □g/L bias in the *in situ* chlorophyll fluorescence due to additions of particulate matter in a controlled environement.

4.5 Cautionary Notes

- The presence of high concentrations of particulate matter may affect the results of calibrated chlorophyll output. The upper thresholds of the sensor should be explored for a given water type.
- The health of phytoplankton will impact fluorescence response per unit of chlorophyll. Healthy phytoplankton will have lower fluorescence per unit.
- Light quenching of phytoplankton will produce a lower fluorescence per unit chlorophyll compared to dark-adapted phytoplankton. Also the amount of chlorophyll per cell can changed depending on light availability.
- Cell package (morphology) composition and shape can influence fluorescence.

5. Turner Designs Cyclops-7

5.1 Description

Turner Designs makes a variety of submersible fluorometers. The Ocean Optics course used a Cyclops-7 CDOM fluorometer and a turbidity sensor, and therefore these will be covered in more detail. The Cyclops-7 is a compact and high performance sensor and is available in a wide range of sensors with ultraviolet to infrared excitation wavelengths. Ultrabright LEDs

are used as the excitation source. Infrared light is used for turbidity measurement, ultraviolet (no color) 350 nm light is used for CDOM excitation, and CDOM emission is measured at 450nm. The acceptance angle is at 140 degrees with the source beam. An interference filter is used to reduce scattered excitation light. The Turner Designs submersible C3 fluorometer can include up to three optical sensors from ultraviolet to infrared.

Details about the instruments are available on the Turner Designs website.

Cyclops-7 Submersible

http://www.turnerdesigns.com/t2/instruments/cyclops7.html

Cyclops-7 CDOM Submersible

http://www.turnerdesigns.com/t2/doc/appnotes/S-0081.pdf

C3 Submersible Fluorometer

http://www.turnerdesigns.com/t2/instruments/c3.html

The "how to" of data measurements

5.2 Instrument Setup

The C3 and Cyclops 7 are durable in-situ instruments. They typically would be attached to an optics package or mooring. However, both instruments are of manageable size and could be used as handheld sensors. The smaller size of the Cyclops 7 makes it especially suitable for handheld measurements. The Cyclops 7 sensors have variable gain settings, which is automatic with the yellow DataBank or using special cables.

The instrument setup is straightforward, but one should remember when attaching to mooring and optics packages to insure that the instruments will not be impacted by other instruments' excitation lights. Calibration is a necessary first step to getting reliable, interpretable measurements.

5.3 Calibration Procedure

The calibration of both turbidity and CDOM sensors is done through a serial dilution. It is important to measure dark counts and blanks whenever a calibration is completed. In the lab, black, non-reflective buckets should be used for all sensor readings, in order to minimize any ambient light reflecting into the sensors' detectors.

Dark measurement

This measurement is used to determine the background noise of the sensor. This value should later be subtracted from the readings.

There are numerous ways to measure dark counts: in the air in a dark room, or covering the detector window with black electrical tape (either in the air or in the water). Covering the sensor with black tape and submerging it in tap water was the method.

Table 2. Comparison of protocols for measuring dark counts with a Cyclops-7 CDOM fluorometer. Each dark measurement was repeated by Group 1 and Group 2 using a single fluorometer.

	Group 1 Counts ± SD	**Group 2 Count ± SD**
Dark Room	53.1±11.4	n/a
Taped sensor in air	46.6±14.74	45.6±9.85
Taped sensor in tap water	50.5±8.81	50±6.18
Taped sensor in FSW	n/a	52.6±10.43

Blank measurement

Blanks show how the sensor responds to the medium (in this case, water) without the addition of sample, and is essentially a zero concentration reading. Depending on the user's needs, one can use Milli-Q water or filtered seawater (FSW). Ideally, the blank water should be as similar to the sample water as possible in terms of inert components. As long as there is no interference with dissolved components in the water, FSW may be used.

1) Fill bucket with FSW.
2) Gently lower sensor into the water, lightly moving around the bucket to stir, and to determine the appropriate distance to maintain from the bucket walls/bottom to avoid surface effects.
3) Start readings and record for 10 – 15 seconds.

Sample measurement

For this experiment, two main tasks were completed. The first task was to calibrate the sensor's response to CDOM fluorescence, and the second task was to examine the effects of increased turbidity on the CDOM fluorescence reading. The following section describes the laboratory setup and procedure for each task.

CDOM calibrations were completed by using 0.2 μm filtered seawater (FSW) as a blank; for this application, water from the Damariscotta River Estuary was the blank and CDOM-rich water was incrementally added for the 'calibration'. The calibration was done in a black, non-reflective, 12-15 L bucket. The black buckets minimize reflection of stray light to the detector. The bucket was initially filled with 600 mL of FSW. CDOM was added to the blank in a series of steps to create a calibration curve. The CDOM added was 0.2 μm filtered water from Biscay Pond (Bristol, ME, USA), which is a local pond with high CDOM.

Table 2 shows the CDOM addition series used here. After the final CDOM addition, a sample was collected from the bucket for CDOM absorption measurement, and its absorption spectrum was determined on a Cary 50 spectrophotometer. The a_{CDOM}(450nm) value was used as the a_CDOM of highest point in the calibration curve.

Several details should be kept in mind during calibration. It is important that cumulative and added volumes are recorded after each CDOM addition. Also, during a calibration measurement, the sensor should be kept moving and in the middle of the bucket. After each CDOM addition, the sample should be stirred to ensure that the CDOM is evenly distributed.

After the CDOM dilution series is complete and a sample is removed for spectrophotometer measurements, then a turbidity dilution series was run in the same water using Arizona Clay (40 mg/ml). This addition allows for a measurement of the effect of turbidity on CDOM fluorescence. Incremental additions of Arizona Clay (40 mg /ml) to the CDOM series were made using a clean 1 ml pipette. All samples were mixed before sensor readings began. All readings took place for 10 – 15 seconds.

CDOM Calibration Task Summary List

Task 1- Dark readings

Task 2- Blank readings

Task 3- CDOM dilution series

Task 4- Turbidity dilutions series

Data Processing

For both fluorescence and turbidity, there are a few simple steps required to go from raw counts to workable data.

1) Open raw data with data analysis tool, such as Excel.
    a. While the instrument outputs several files, it is recommended that the data sets be compiled into a single file for ease of workload and calculations.
2) Beginning with dark reading, perform median and standard deviation calculations.
3) Repeat the above procedure for all sample data.
4) Set up a table like the following and place values into their respective position.
5) The corrected sample is derived from the following equation:
    a. Corrected Sample = RAW sample – Dark
    b. Calibration samples = corrected sample – corrected FSW

	CDOM added (ml)	Total volume (ml)	Dark (mV)	Blank FSW (mV)	Raw counts (mV)	Corrected Count (mV)	a_CDOM (± SE)
FSW	0	600	50.5 ±8.4	1615.5 ±7.2	1657.8±10.1	1607.3±25.8	0 ±0.11
Sam 1	200	800	50.5 ±8.4	1615.5 ±7.2	2084.1±5.6	2033.6±21.2	0.16± 0.04
Sam 2	400	1000	50.5 ±8.4	1615.5 ±7.2	2443.7±2.7	2393.2±18.3	0.29± 0.01
Sam 3	600	1200	50.5 ±8.4	1615.5 ±7.2	2443.7±11.7	2752.7±27.3	0.41± 0.09
Sam 4	800	1400	50.5 ±8.4	1615.5 ±7.2	3123.2±9.3	3072.7±24.9	0.53± 0.05
Sam 5	1200	1800	50.5 ±8.4	1615.5 ±7.2	3706.5±12.1	3656±27.7	0.75± 0.07

Table 3. Example of CDOM calibration results. The values are ± standard deviation.

Now that data are corrected, the user can proceed to derive relationships from the data. Since fluorescence is directly proportional to a_CDOM, one can use the Cary spectrophotometer a_CDOM results to find a_CDOM at other fluorescence values.

1) Obtain a_CDOM from the lab for the final dilution in the series.
2) Perform the following calculations:
    a. NOTE: the next step is only performed on the final sample that corresponds to the a_CDOM that was actually measured in the lab.
3) Calculate the a_CDOM per ml of pond water added at the last point.
    a. a_CDOM (step 1)/($\text{Volume}_{\text{final dilution}}$ - $\text{Volume}_{\text{FSW}}$)
    This step corrects for the background CDOM fluorescence in the FSW.
4) Now the amount of a_CDOM per ml pond water has been determined and the following
    calculations can now be performed on the rest of the sample set.
    a. For the rest of the samples, calculate the amount of fluorescence that results from
    the CDOM additions.
    ($\text{Volume}_{\text{sample}}$ -$\text{Volume}_{\text{FSW}}$)*a_CDOM (per ml from step 3a)= a_CDOM at sample
5) Plot corrected fluorescence counts as a function of a_CDOM in solution (value from step
    4a) Use equation to convert fluorescence to a_CDOM. Slope equals fluorescence/a_CDOM.

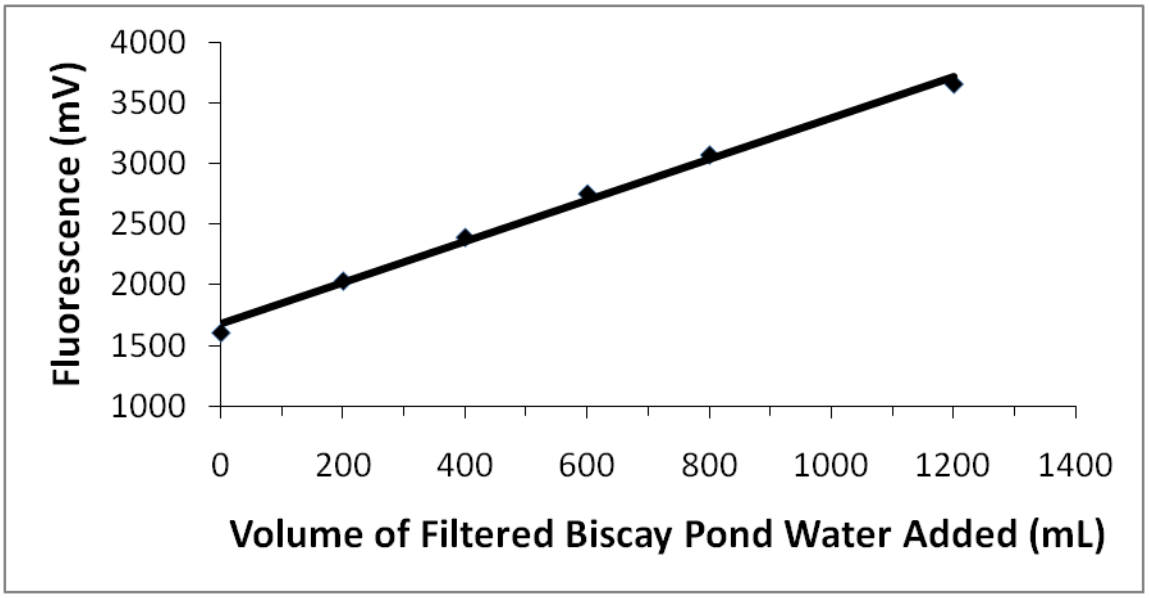

Figure 12. CDOM fluorescence vs. CDOM volume added. The standard deviation is contained within the mark.

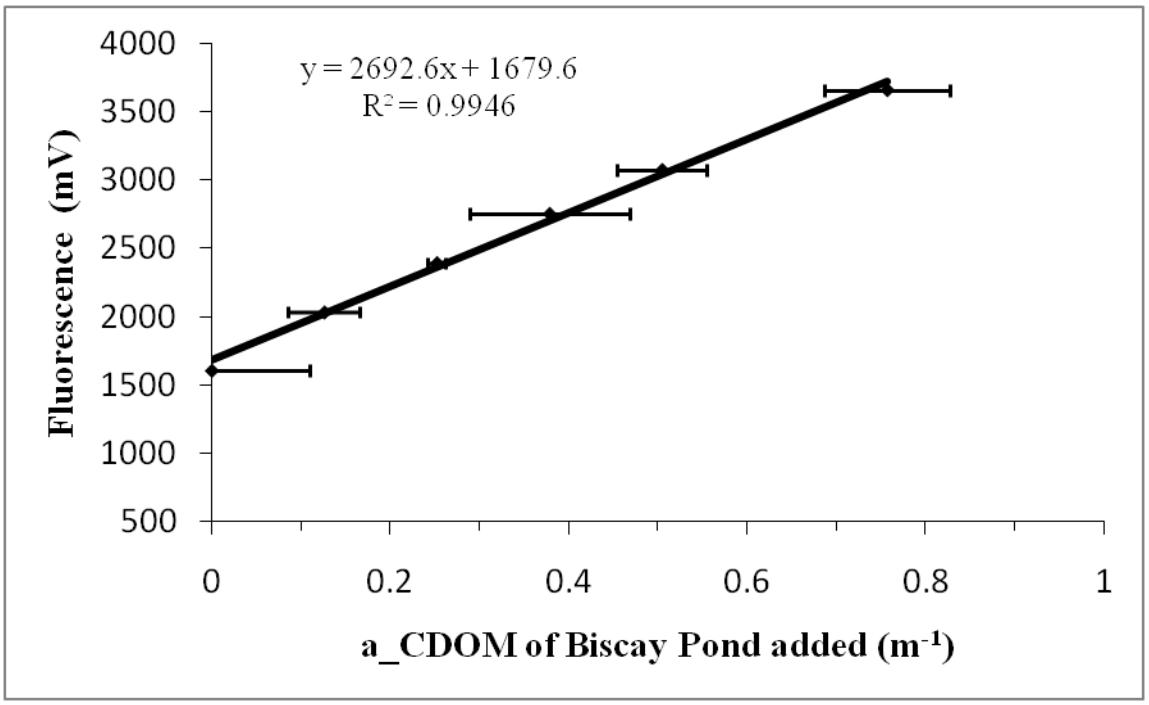

Figure 13. Final fluorescence vs. a_CDOM calibration curve. The slope of the curve gives the relationship of fluorescence to a_CDOM. The fluorescence errors are contained within the symbols.

5.4 Data Results and Discussion

The previous section described how to calibrate the instrument. With trustworthy data, the next task was to determine how increased turbidity (and subsequent scattering of light) would affect the a_CDOM values along the path length. The goal was to find at what point data becomes suspect as a result of the scattering properties of the water. Figure 3 illustrates an interesting trend and the clear impact of turbidity on a_CDOM.

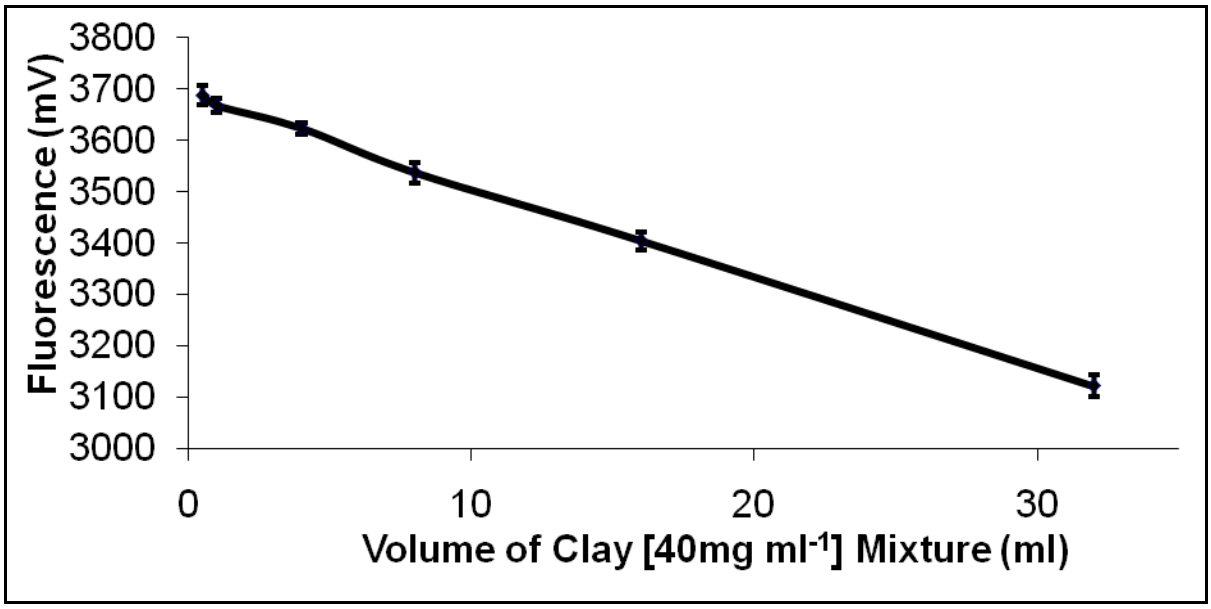

Figure 14. The influence of turbidity on CDOM fluorescence. The addition of turbidity (clay) into a sample causes a decrease in CDOM fluorescence although there is no actually reduction in CDOM.

5.5 Cautionary Notes

- Turbidity has the potential to change calibrated results, because of scattering and shading output (Figure 3).

6. Field Techniques and Cruise Data

6.1 Field collection

The following section regards data collected on July 20, 2011 in the Gulf of Maine at 43°44.9N, 69° 29.9E. The conditions were nearly blue sky with 3 knot wind and 1 foot swell.

A Wetlabs ECO-FL Fluorometer was deployed as part of the optics package. One cast was completed with black electrical tape over the sensors for dark count measurements.

Discrete depths (surface, 5, 10, and 15 m) were sampled for chlorophyll a analysis during a regular cast. Samples were collected with several vertically mounted 5-L Niskin bottles, spaced apart in 5-m intervals and connected to the steel profiling cable holding the optics package. Upon completion of the short profile, the samples were removed from the cable and immediately dispensed into pre-cleaned opaque 250 mL bottles. The bottles and caps were rinsed with seawater sample three times before the final collection took place.

Samples were kept cool using ice, and were subsequently filtered and analyzed on the Turner Designs 10-AU Fluorometer within 12 hours of collection (see section II for analysis protocol).

6.2 Data Processing

Summary of the processing steps:

1. Subtract the dark counts.
2. Check for offset with CTD depth and fluorometer measurements.
3. Using discrete chlorophyll samples, perform a least squares fit to relate the fluorescence output to chlorophyll concentration. The slope of the regression is fluorescence per unit chlorophyll, and therefore can be used to convert FU into chlorophyll concentration.

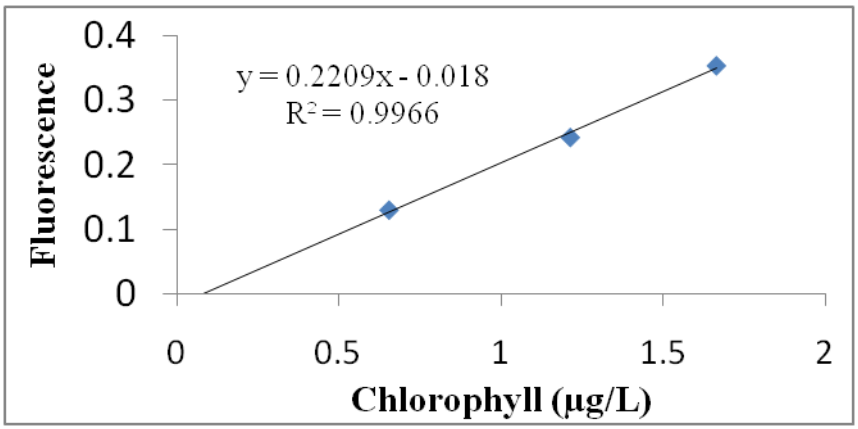

Figure 15. Linear regression of the fluorescence output to chlorophyll concentration.

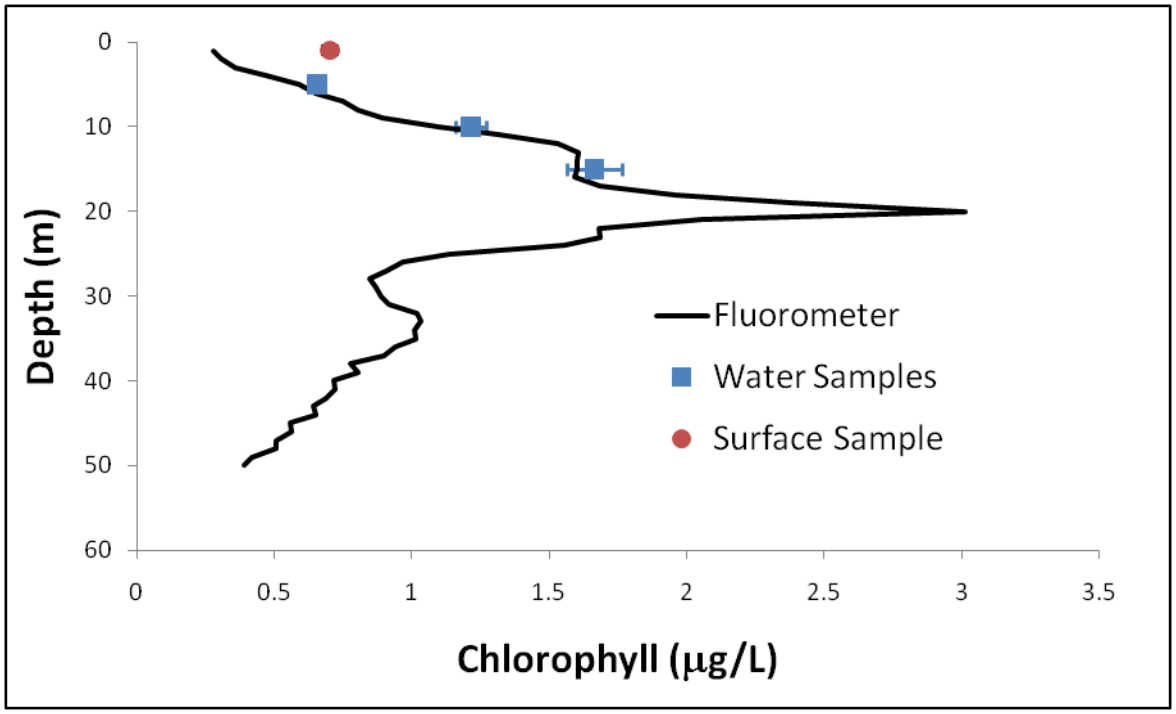

Figure 16. [Chl] (µg L^{-1}) depth profiles from fluorometer and discrete samples collected off the coast of Maine (43º 44.9' N, 69º 29.9' W) on July 20, 2011. Water samples [Chl] (µg L^{-1}) were calculated from fluorescence measurements of acetone extractions of GF/F filtered samples of each depth collected. Surface sample was not included in the regression due to the influence of quenching.

6.3 Cautionary notes

NOTE: It is important to note that if seawater is pumped through the fluorometer in a closed flow-tube configuration, then there will be a time delay between when the temperature of the water sample is measured and when it passes through the instrument. This delay will be especially prevalent if water is run through a filter before entering the instrumentation, as is done when measuring optical properties of CDOM and particulates. The most common plumbing sequence involves passing water first through a CTD and then to other instruments within the package. Instrumentation measurements are automatically synchronized to CTD measurements by time. If the fluorometer is used in a pumped mode during a vertical profile, then the instrument will, for any time dependent CTD reading, actually be exposed to water that passed through the CTD earlier. For example, if water entering the pump passes through a CTD and then takes 8 seconds to reach the fluorometer, then the fluorometer data must be offset by 8 seconds to determine the actual temperature and salinity of the water sample. Time correction should be taken into account for all instruments in a serial plumbing system. The exact correction will depend on set-up and must be measured by the user. This correction step is critical in applying the correct temperature/salinity coefficients.

7. References

Application Notes: http://www.turnerdesigns.com/t2/doc/appnotes/algal.html Chlorophyll measurements with the 10AU Field Fluorometer (**998-5101**); A Procedure for Measuring Extracted Chlorophyll a free from the Errors Associated with Chlorophyll b and Pheopigments (**998-9000**)

Collins, G.B., and E.J. Arar. 1997. EPA Method 445.0. *In Vitro* Determination of Chlorophyll *a* and Pheophytin *a* in Marine and Freshwater Algae by Fluorescence. Revision 1.2, September 1997. U.S. Environmental Protection Agency, Cincinnati. 22 pp.

Manufacturer Website: http://www.turnerdesigns.com/t2/instruments/10au.html

Mignot, A., Claustre, H., D'Ortenzio, F., Xing X., Poteau A., Ras, J. (2011) From the shape of the vertical profile of in vivo fluorescence to Chlorophyll-a concentration, *Biogeosciences Discussions*, 8, 2, 3697-3737.

Model 10 AU User's Manual: www.turnerdesigns.com/t2/doc/manuals/10-AU_OP_MAN.pdf

Turner Designs (2008). Frequently Asked Questions: Fluorometric Chlorophyll Analysis. Available at *www.turnerdesigns.com/t2/doc/appnotes/S-0003.pdf.*

Welschmeyer, N.A. 1994. Fluorometric analysis of chlorophyll *a* in the presence of chlorophyll *b*and pheopigments. Limnology and Oceanography 39: 1985-1992.

8. Appendix A

Dark current comparison

Calibration	Group1 Avg (mV)	SD	Group 2 Avg mV	SD
Dark Room	53.1	11.40	n/a	
Tape Air	46.6	14.74	45.6	9.85
Tape Tap Water	50.5	8.81	50	6.18
Tape FSW	n/a		52.6	10.43

Table 3: Comparison of methods for dark count measurements.

Cary 50 Spectrophotometer

Section Guide

1. Instrument Description

CDOM absorbance (A, dimensionless) is measured on a bench-top spectrophotometer (Cary-50 UV-Visible spectrophotometer with single beam). It measures the amount of light a sample absorbs from UV-VIS (200-800 nm) electromagnetic radiation.

(Cary-50 spectrophotometer, Agilent)

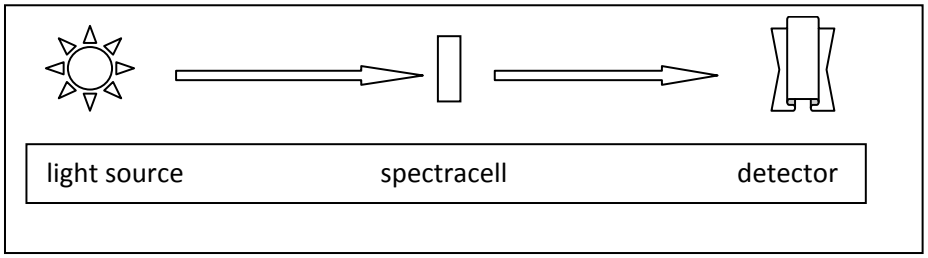

When a light beam (a stream of photons) passes through the sample molecule (analyte), the molecule will absorb the photon and the absorption will reduce the number of photons and the intensity of the light beam. By passing a single beam of light through the sample from a Xenon lamp as the source of UV-Vis radiation, the spectrophotometer can measure the intensity of the light reaching the detector and the intensity absorbed by the analyte.

The following website contains instrument information:

Agilent Cary 50 Spectrophotometer website

2. Data measurement procedures

2.1Protocol for CDOM Measurement

1. Set the scan limits to 200-800 nm and the medium scan speed
2. Pre-clean the quartz cuvette with RBS detergent first, and residual water should be wiped ONLY with lens paper.
3. Warm up the samples to room temperature.
4. Blank the instrument with Type 1 water that has been treated with a UV oxidizing cartridge (spectrum at all wavelength should be 0) before running samples.
5. After blank, run three independent samples of Type 1 water to confirm that all readings are zero. This information will be included in the uncertainty budget.
6. To measure a sample, fill the cuvette with the sample ONLY by holding the non-optical surfaces carefully, wipe any water residual attached to the cuvette with lens paper and make sure there is no finger prints on the optical surface and no bubbles inside the cuvette (to remove the bubbles, tab the cuvette gently with finger).
7. Look through the cuvette to ensure that there are no visual in-homogeneities (bubbles, residual mixing/turbulence between fresh and salt water sample, particles), place the cuvette into the sample holder in the spectrophotometer in EXACTLY the same orientation every time and do the measurement (dot on cuvette faces the same direction and larger cuvette is tipped back) and perform scan.
8. Rinse the cuvette at least three times with a few mL of samples to remove the residual of previous sample and continue with samples
9. Insert a blank measurement multiple times between samples sample to test for instrument drift.

2.2 Protocol for QFT (Quantative Filter Technique) measurement

1. After filtration, place all filter pads immediately on moist Kimwipes in a Petri dish in dim light; note and record position of filters. Hold filter with forceps by the clean edge only (don't scrape filtered material off the pad).
2. For a blank, moisten a G/FF filter pad with Type 1 water
3. Set scan limits to 300 –800 nm and medium scan speed\
4. Blank the spectrophotometer with air and save that as baseline.
5. Scan Milli-Q-blank. Rotate position and repeat for total of three scans.
6. Scan seawater blanks and samples. Rotate each filter and rescan. Check
7. After scan, measure the diameter of the filtered area with the calipers.
8. To measure a_{NAP}, use the Kishino methanol extraction (under hood):
    a. Place sample and blank filters on filter rack under hood with no vacuum and add about 15 mL of hot 100% methanol,
    b. Wait about 10 minutes, turn on vacuum, and rinse filter with filtered seawater, including under filter cup flanges,
    c. Carefully remove filter (it will be easy to tear) and rescan.

The target absorbance values are ~ 0.1 – 0.2 for the red peak and 0.4 – 0.5 for the blue peak. It is important not to load too much material onto the filter, which can result in an 'artificial' pigment package effect (i.e. pigment packaging by methodology, not by physiology).

3. Data Processing

3.1 Measuring CDOM with the Cary 50 spectrophotometer.

Absorption by colored dissolved organic matter (CDOM) can be measured with a cuvette which may vary in size and is filled with a filtrate of a given water sample. Different sized cuvettes should be considered based on the quantity of CDOM in the water; for example if there appears to be a small amount a cuvette with a longer pathlength should be used, but if the sample has high amounts of CDOM a 1cm cuvette should be used.

3.1.1 Example of absorption by CDOM for a sample of water collected off of the Darling Marine Center dock, where 250mL was filtered through a 2μm filter and collected.

Step 1: subtract the blank spectrum from the raw sample spectrum.

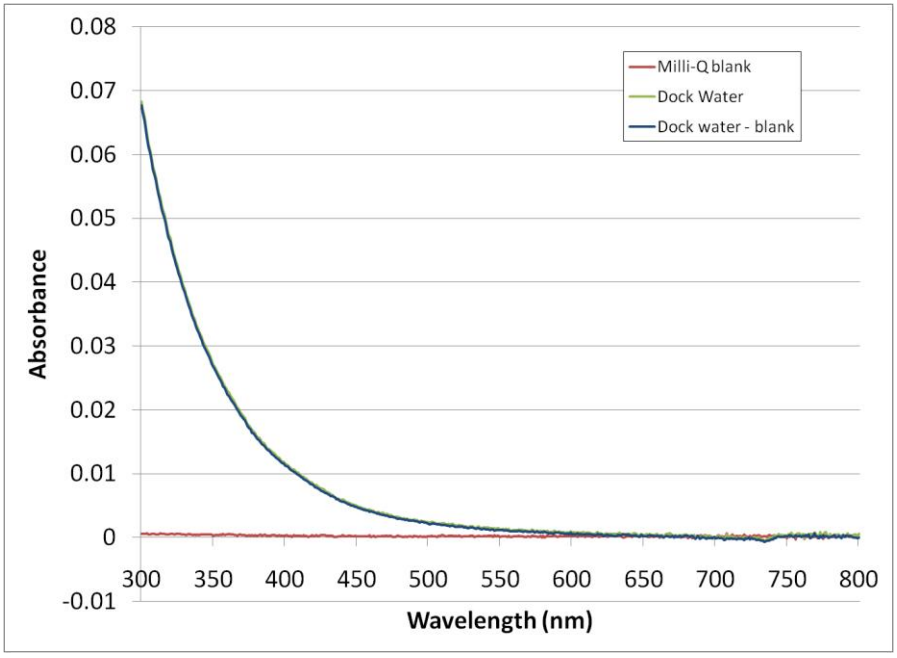

Figure 3.1. Absorbance measured by the Cary 50 Spectrophotometer of filtered water collected at the DMC dock shown in green, a Milli-Q water blank spectrum, and the spectrum of the filtered dock water with the blank subtracted.

The flat spectrum of the Type 1 water blank (red like in the above figure) demonstrates that the instrument was correctly zeroed. After the blank spectrum has been subtracted from the sample, absorbance can be converted to absorption by CDOM using:

$$a_{CDOM}(\lambda) = 2.304 * A(\lambda) * L^{-1}$$

Where L is the pathlength of the cuvette used.

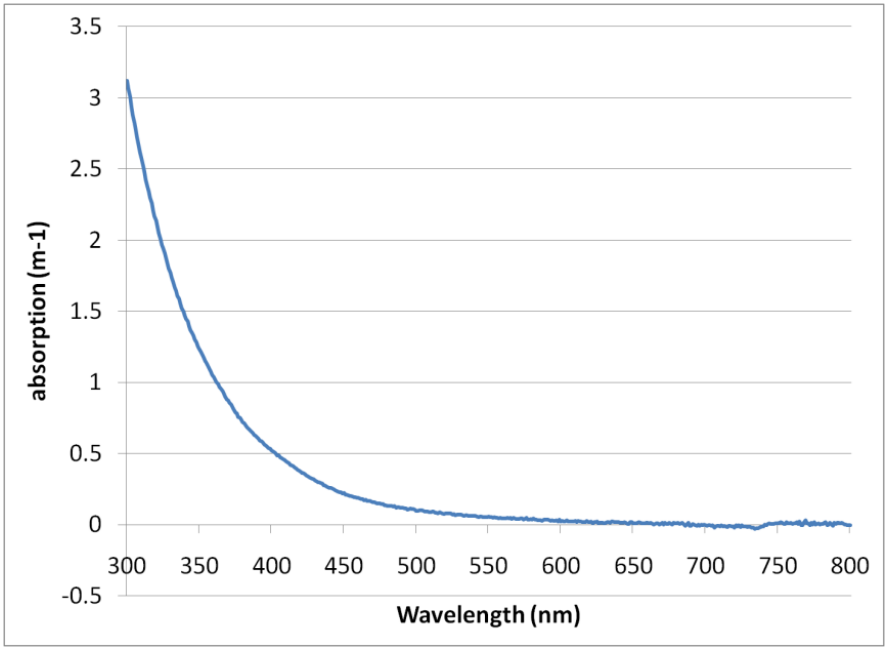

Figure 3.2. Spectrum of absorption (m^{-1}) by CDOM for water collected at the Darling Marine Center dock.

3.2 Particulate absorption using the Quantitative Filter Technique

3.2.1 Example of data processing procedure using a *Thalassiosira weissflogii* culture with 100mL of sample filtered.

Raw data is collected using the Cary 50 spectrophotometer (section 2.) The spec measures dimensionless absorbance, and this data must be corrected using a blank and converted to absorption, which has units of m^{-1}.

Step 1: Adjust or null spectrum in 730-750 nm range (Fig 3.3).

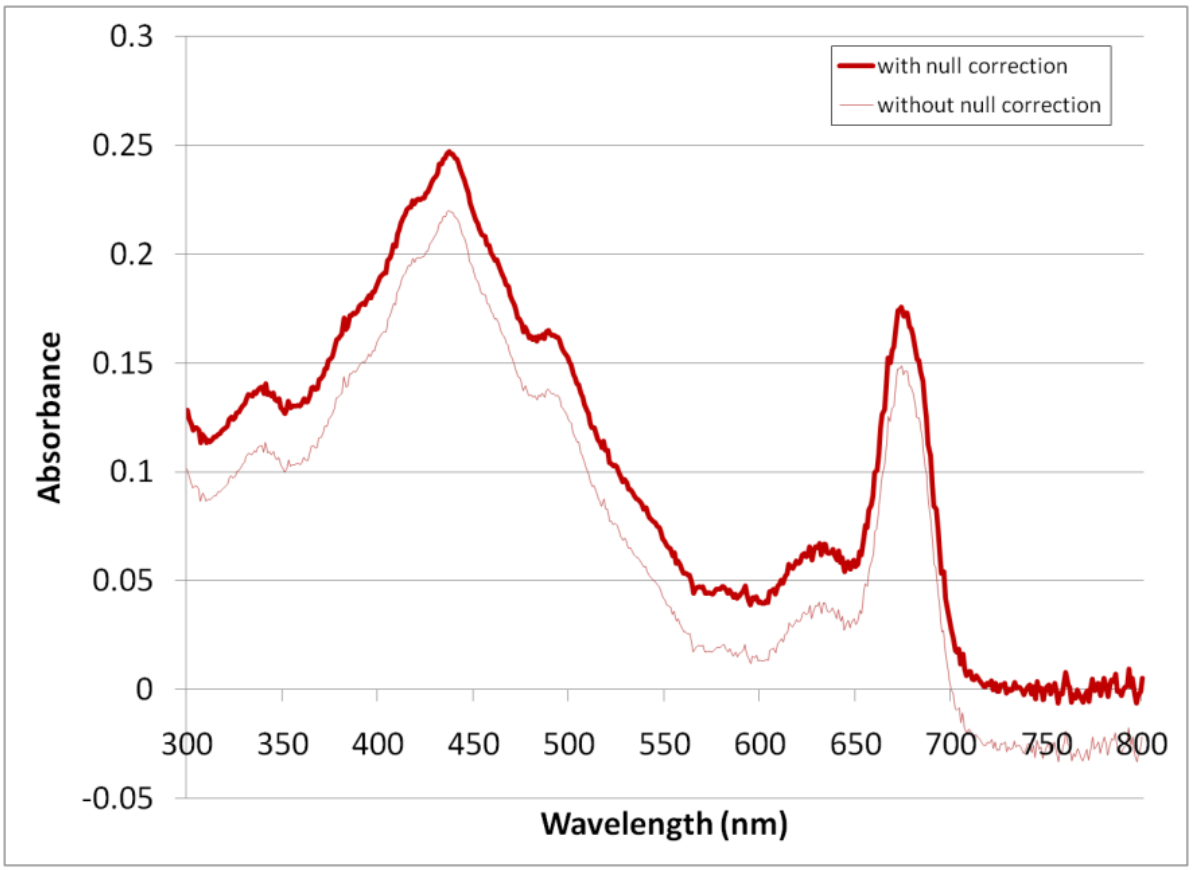

Figure 3.3. Absorbance measured by the Cary 50 spectrophotometer. The thin line has not had a null correction applied, while the thicker line has. Note that the 720nm to 800nm region of the spectrum now goes to approximately zero absorbance.

Step 2: Subtract the blank spectrum

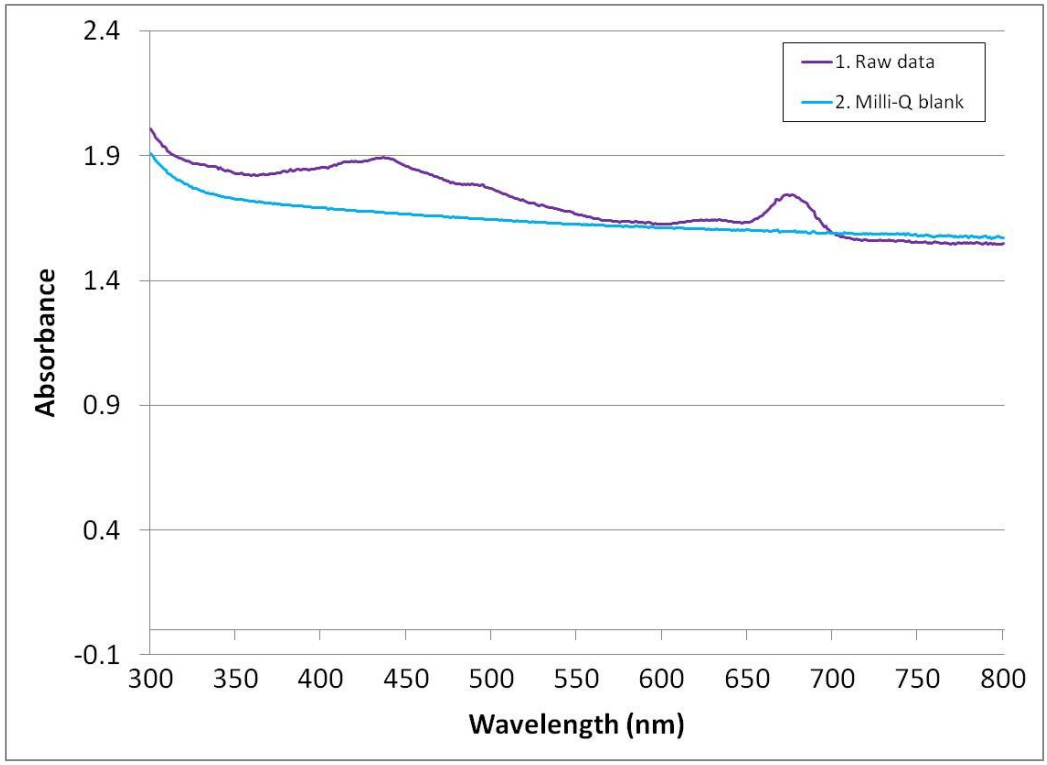

Figure 3.4. Absorbance spectra measured by the Cary 50 spectrophotometer. The purple line shows the raw data, the cyan line shows the Milli-Q blank, and the green line show the raw data with the blank subtracted from it. Note that once the data has been blank corrected, the red region of the spectrum is near zero absorbance.

Absorbance on the filter is theoretically zero or negligible into the NIR region. However, there may be some signal due to the different water content or manufacturing of the filter pads. Therefore, it may be necessary to use an average value from the 730nm to 750nm region of the spectrum and subtract this value from the entire spectrum to correct for this small scattering effect by the filter pads (Pegau et al. 2002). The final absorbance spectrum with this "null" correction made using the 730nm to 750nm region can be seen in Figure 3.2.

After the raw data has been corrected, absorbance can be converted to particulate absorption using

$$A_{\beta\text{-corrected}}(\lambda) = 0.378\,\{A_{pad}(\lambda) - [A_{blank}(\lambda) - A_{null}(\text{“}\lambda\text{”})]\} + 0.523\,\{A_{pad}(\lambda) - [A_{blank}(\lambda) - A_{null}(\text{“}\lambda\text{”})]\}^2$$

$$a_{\mathbf{part}}(\lambda) = \frac{2.303 * 100}{pathlength} * A_{\mathbf{\beta\text{-}corrected}}(\lambda)$$

$$pathlength = \frac{\text{Volume filtered } (cm^3)}{\text{Area of the filter } (cm^2)}$$

Absorbance is multiplied by 2.303 to convert from log base$_{10}$ to natural log. The 100 in the numerator converts cm to m. The β correction accounts for the increase in the effective or geometric pathlength of the filter pad due to presence of the particles that have been filtered onto the pad. The above equation for $A_{\beta\text{-corrected}}$ was determined by Cleveland and Weidemann (1993).

Using absorption by total particles and non-algal particle absorption (obtained using the methanol extraction technique, see section 2.), absorption by phytoplankton can be determined using

$$a_{part}(\lambda) = a_{phyt}(\lambda) + a_{NAP}(\lambda)$$

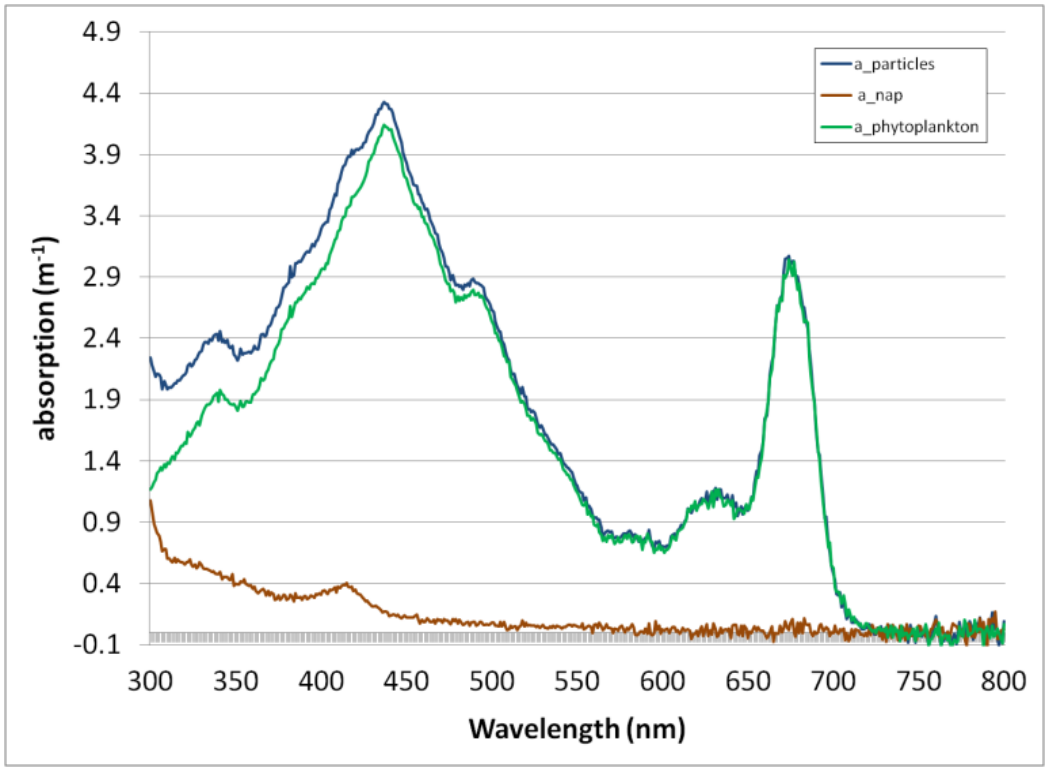

Figure 3.5. Absorption by total particles shown in blue, absorption by non-algal particles after applying methanol shown in brown, and absorption by phytoplankton shown in green

4. Data interpretation and analysis

4.1 CDOM absorption

CDOM (chromophoric or colored dissolved organic matter) absorbs most strongly in the blue (UV-A) part of the spectrum (320-400nm; Nelson and Siegel 2001). Because it absorbs primarily in the blue, CDOM exhibits a yellowish color. The shape and magnitude CDOM absorption spectra and slope can provide information about the concentration and chemical composition dissolved components of the water of interest although the character of the slope is still not fully understood (Ocean Optics protocols rev 4, volume IV; Coble 2007). The CDOM spectral slope provides information about the origin of the dissolved material in the water column, whether it is old, refractive materials or new biological materials. From the satellite ocean color perspective it is necessary to study CDOM in the global oceans because it interferes with the measurement of particulate absorption at 440nm causing an overestimation of Chl *a* by remote sensing (Del Vecchio and Subramaniam 2004). CDOM is found in high concentrations on the coasts where river runoff is influential. CDOM concentration decreases as salinity increases. On these land/ocean boundaries, there is no strong correlation between Chl *a* concentration and CDOM, which suggests that is CDOM is terrestrial in origin (DelVecchio and Subramaniam 2004). CDOM can also be measured in the open ocean. The source of this CDOM has been debated and some have suggested it is of terrestrial origin (Nelson and Siegel 2001; that which has become entrained in currents), new production by bacteria (such as is suggested in the Sargasso Sea; Nelson et al. 2004), release into the water column by the resuspension of sediments (Chen 1999; Nelson and Siegel 2001 or the product of a long-term breakdown of marine productivity (Kalle 1966; Bricaud et al 1981; Hedges et al 1997; Nelson and Siegel 2001). See figure 4.1 below extracted from Coble 2007.

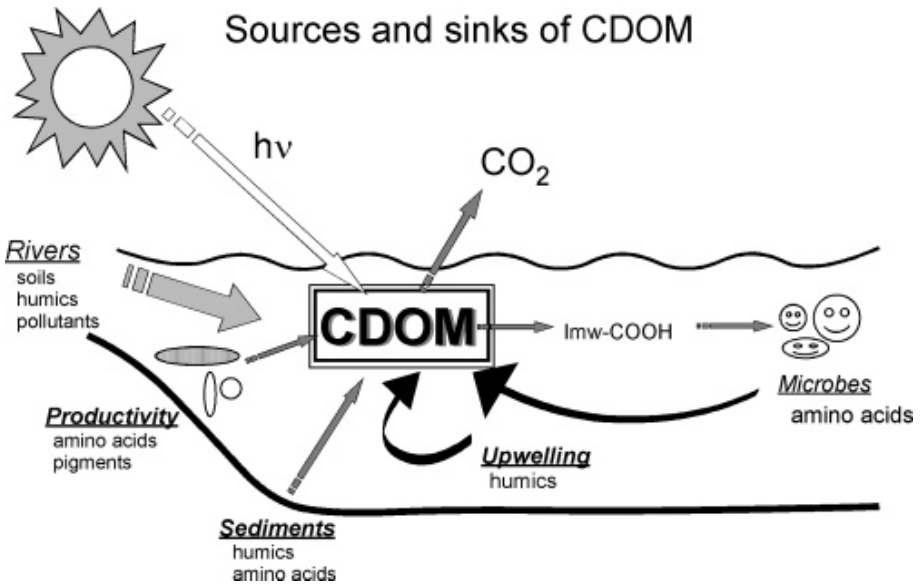

Figure 4.1: Various sources and sinks of CDOM in the coastal and open ocean (Coble 2007).

The definition of the absorption coefficient of CDOM or $a_{CDOM}(\lambda)$ is any 'dissolved' material that is less than 0.2 μm in size. However, in coastal waters it is possible to filter using a nominal 0.7 μm Whatman GF/F filter (to get rid of large particles which dominate). The spectral slope (S) of CDOM is calculated as (Coble 2007):

$$a(\lambda)=a(\lambda_0)e^{-S(\lambda-\lambda 0)}$$

where $a(\lambda)$ is the absorption coefficient at some λ, $a(\lambda_0)$ is the absorption coefficient at a reference λ and S is the spectral slope (Coble 2007).

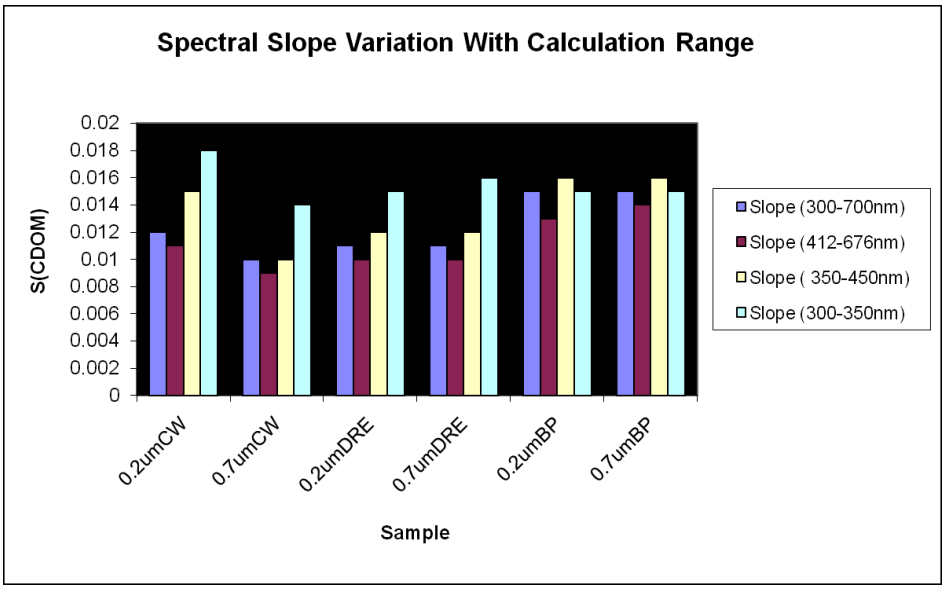

Figure 4.2: The effect of λ_0 choice on spectral slope calculation.

When choosing a reference λ for the spectral slope calculation, it is important to pick a wavelength that is in a reasonable range of the wavelength of interest. Note in figure 4.2, the CDOM spectral slope varies dramatically depending on reference wavelength range. Moreover it is recommended that when comparing your spectral slopes with published values that those values were calculated with a comparable reference wavelength to yours.

4.2 QFT Technique for measuring particulate absorption

Total particle absorption (a_{part}) includes both absorption from phytoplankton ($a_{phyt;}$ polar pigments) and compounds that are not actively contributing to photosynthesis or nonalgal particles ($a_{NAP;}$ inorganic mineral particles, organic particles, detrital material and no-phytoplanktonic living organisms). The a_{NAP} can also include non-methanol extractable

pigments like phycobilins. In order to separate the different components contributing to the total particle absorption, the Quantitative Filter Technique or QFT, can be used. As discussed earlier, the total absorbance of particles is measured on a filter pad. The filter pad is then extracted with methanol thereby leaving all compounds not extractable by methanol on the filter. The absorbance on the filter due to pigments, or a_{phyt} is calculated by the following equation:

$$a_{phyt} = a_{part} - a_{NAP}$$

The shape and magnitude of the spectrum before and after subtraction of a_{NAP} from a_{part} can provide information about the concentration and chemical composition of the particulate constituents of the water column (Ocean Optics protocols rev 4, vol IV). Figure 3.3 shows the total absorption spectra of a culture, *Thalassiosira weissflogii*. The small magnitude of a_{NAP} shows that there is very little NAP in the culture, which is to be expected. These absorption spectra a comparable to what might be expected in Case 1 waters, where there are very few particles and most of the absorption is due to phytoplankton (Ocean Optics protocols rev 4, vol IV). The shape of the a_{phyt} can provide a broad understanding of the composition of the photosynthetic and photoprotective pigments contributing to the overall absorption. Not only can the a_{phyt} tell you about the composition of the particles, but also the a_{NAP} can tell a story. For example, in Figure 3.3, the small bump in the a_{NAP} at approximately 425 nm may be due to absorption of another phytoplankton cell component.

Other pigments that can be extrapolated from the absorption spectrum, and tell you something about phytoplankton community structure, include Chl *b*, Chl *c*, and fucoxanthin (Figure 4.3).

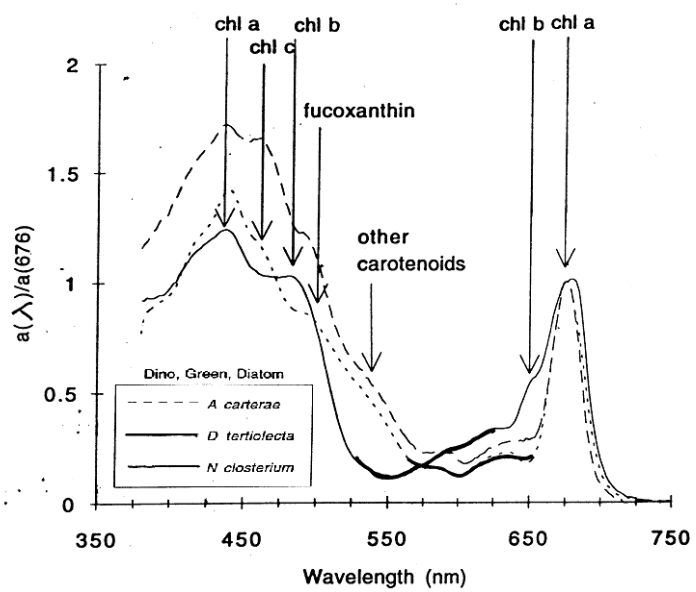

Figure 4.3: Peak characteristics of a_{phyt}

Pigment packaging effects can also occur, masking the true spectral composition of the particles (Figure 4.3; Morel and Bricaud 1981).This can be caused by phytoplankton photoacclimation (i.e. increased photosynthetic pigments in response to low light levels or vice versa; Staehr et al 2002) as well as temperature and nutrient availability (Staehr et al. 2002). Pigment packaging can also be determined by cell size (larger cells can have more pigments packed in than small cells).

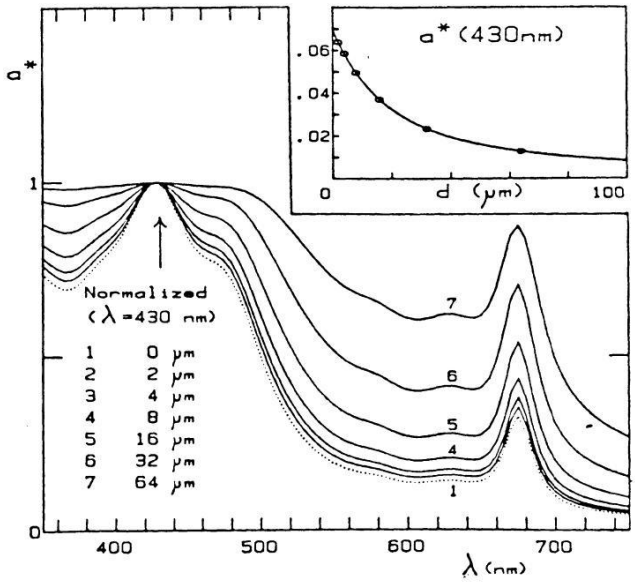

Fig. 2. Change in spectral absorption values with variable cell size (diameter, d, in μm) whereas the cell material forming the cells remains unchanged. The spectral absorption values of this material, somewhat arbitrarily adopted, are shown as the dotted curve. All curves are normalized, at $\lambda = 430$ nm, to evidence the progressive deformation. The variations with size of the specific absolute value at 430 nm (m^2 mg^{-1} Chl a) are shown in inset, under the same assumption of a constant absorption of the cell material ($a_{cm} = 2 \times 10^5$ m^{-1} at 430 nm) and with the additional assumption of a constant intracellular pigment concentration ($c_i = 2.86 \times 10^6$ mg Chl a m^{-3}).

Figure 4.4: Pigment packaging effects on a_{phyt}

Babin et al. 2003 found that in oligotrophic waters, blue to red absorption ratios decreasing with increasing total chl *a* concentration. This was not found to be true for the North Sea and Adriatic Sea (blue and black dots, respectively), which are more eutrophic waters (Figure 4.5).

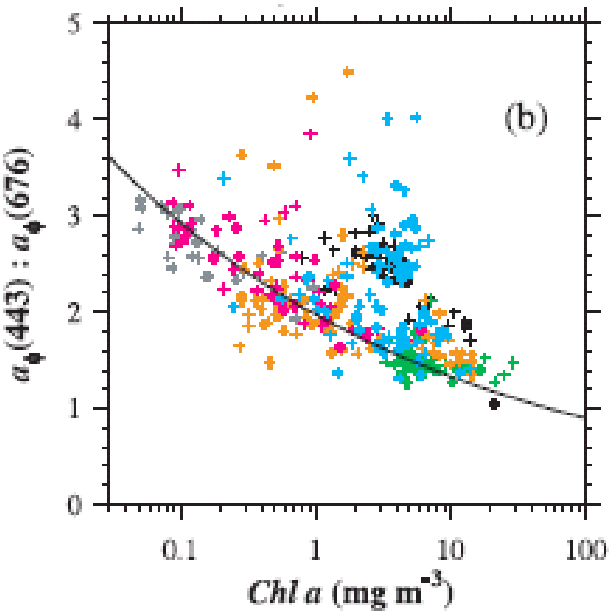

Figure 4.5: red-to-blue absorption ratios in different bodies of water

This phenomenon may be caused by the pigment packaging effect as a part of photoacclimation from oligotrophic to eutrophic waters (Yentsch and Phinney 1989; Bricaud et al 1995) or changes in the relative abundance of accessory pigments (Chl c, Chl b and carotenoids; Bricaud et al 1995; Fig 4.6). Low nutrient waters are typically represented by low chlorophyll because smaller cells (i.e. those that need less nutrients) dominate over larger cells. Here we would see a large red-to-blue pigment ratio (high Chl *a*). High chlorophyll waters are typically dominated by large cells that exhibit pigment packaging effects. Abs/Chl *a* is low in packaged cells but over all light absorption is high.

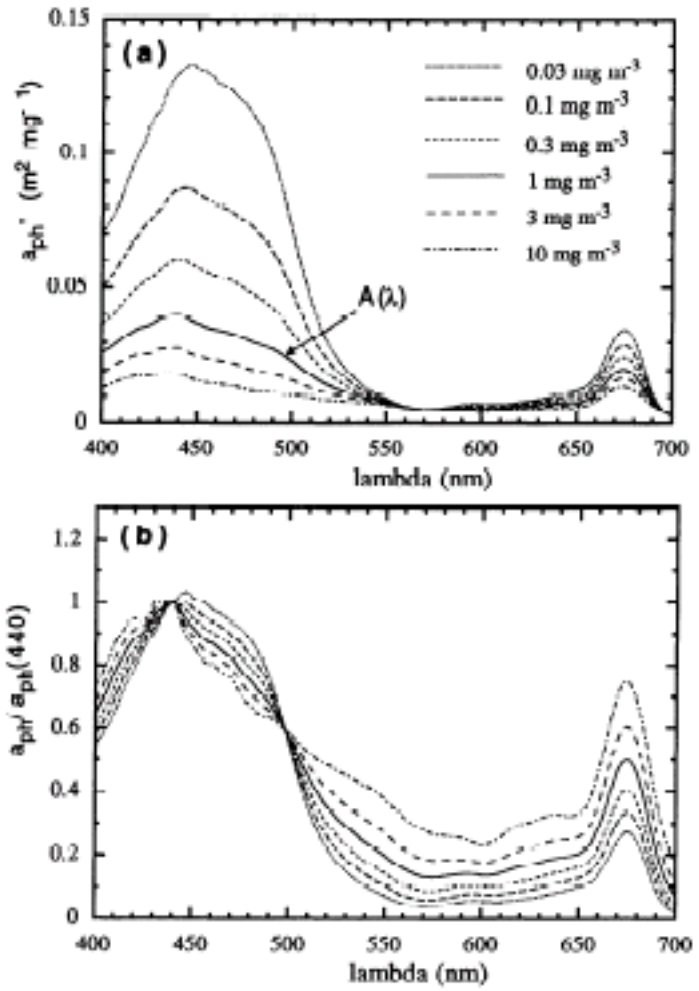

Figure 4.6: Response of absorption in response to Chl *a* concentration

Although this technique is labeled as 'quantitative' some might question this label. As observed in figure 4.4, it is clear that pigment package effects by phytoplankton can severely diminish the important pigment feature of an absorption spectrum. However this can also occur when too much material is loaded onto a filter, which can also act as an 'artificial' package effect (i.e. packaging by methodology, not by physiology). In doing so, the quantitative aspect of this method is lost. Moreover, the uneven distribution of material on the filter also inhibits the quantitative value of the data. A combination of a quantitative absorption value from another instrument, such as an ACS or AC-9, with the qualitative absorption values from the QFT could provide valuable information. The optimal solution is to calculate, in relative units, the proportion of a_{NAP} to a_{phyt} and apply those values to the quantitative absorption measurements, retrieving absorption values for all components. When out in the field, and water column profiles are acquired, it is preferable to choose QFT or pigment sampling depths based on either a density profile or the wavelength dependent absorption in the water column (i.e. changes in absorbance wavelength ratios). Ideally, this type of measurement would provide information on changes in phytoplankton type or particle type throughout the water column (phytoplankton vs. NAP; M.J. Perry, personal communication).

REFERENCES

Bricaud, A., Babin, M., Morel, A. and Claustre, H. (1995). Variability in the chlorophyll-specific absorption coefficients of natural phytoplankton: Analysis and paramaterization. Journal of Geophysical Research 100: 13,321-13,332.

Cleveland, J.S., and A.D. Weidemann, 1993: Quantifying absorption by aquatic particles: A multiple scattering correction for glass-fiber filters. *Limnology and Oceanography.* 38: 1321-1327.

Coble, P.G. (2007). Marine Optical Biogeochemsitry: The chemistry of ocean color. Chemistry Review 107: 402-418.

Del Vecchio, R. and Subramaniam, A. (2004). Influence of the Amazon River on the surface optical properties of the western tropical North Atlantic Ocean 109: C11001, doi10.1029/2004JC002503.

Morel, A. and A. Bricaud (1981). Theoretical results concerning light absorption in a discrete medium, and application to specific absorption of phytoplankton, Deep-Sea Research, 28, 1375-1393.

Nelson, N.B., Carlson, C.A. and Steinberg, D.K. (2004). Production of chromophoric dissolved organic matter by Sargasso Sea microbes. Marine Chemistry 89: 273-287.

Nelson, N.B. and Siegel, D.A. (2001). Chromophoric DOM in the Open Ocean. In: D. Hansell and C. Carlson, Editors, Biogeochemistry of Marine Dissolved Organic Matter, Academic Press, San Diego, CA.

Pegau, S., J.Ronald V. Zaneveld, B. Gregg Mitchell, James L. Mueller, M. Kahru, J. Wieland and M. Stramska. 2002. Ocean Optics Protocols For Satellite Ocean Color Sensor Validation,

Revision 4, Volume IV: Inherent Optical Properties: Instruments, Characterizations, Field Measurements and Data Analysis Protocols. Edited by Mueller, J. L., G.S. Fargion and C R. McClain. NASA/TM-2003-211621/Rev4-Vol.IV. Greenbelt, Maryland.

Staehr, P.A., Henriksen, P. and Markager, S. (2002). Photoacclimation of four marine phytoplankton species to irradiance and nutrient availability. Marine Ecology Progress Series 238: 47-59.

Yentsch, C.S. and Phinney, D.A. (1989). A bridge between ocean optics and microbial ecology. Limnology and Oceanography 34: 1694-1705

WET Labs C-Star Transmissometer

Section Guide

Product website (includes user manual):
http://www.wetlabs.com/products/transmissometers/transmissometers.htm

1. Introduction

The C-Star measures light transmittance at a single wavelength over a known path-length. By comparing a known light output to a received signal, beam attenuation (c) can be calculated. Losses of light propagation through water can be attributed to both scattering and absorption. Suspended particles, phytoplankton, bacteria and dissolved organic matter contribute to the losses sensed by the instruments, and several C-Star models are available for measuring these components. The light source is a single LED with a reported bandwidth (FWHM) of ~20nm for most models. The acceptance angle of the detector is reported as 1.1954°. Multiple configurations and options are available from the manufacturer. These include:

- LED wavelength tuned to application
    - 370, 470, 530, 650nm
- 10cm and 25cm pathlength
- Open transmission path or flow tube
- Power and data cable configuration

The C-Star instrument can be used in-lab, or mounted to instrument packages for in-situ measurements. The following procedure is for in-lab use. If deployed as part of an instrument package, the C-Star may be connected to a datalogger. Consult the user manual and manufacturer for more information. A schematic of the instrument is included (Fig 1).

2. Theory of Operation

C-Star data output is measured as voltage. The voltage output (V_{sig}) is proportional to the amount of light received by the detector. With the instrument in water, the output voltage should vary from a minimum value equaling the inherent sensor noise, or dark value (V_{dark}: obtained by a blocked beam reading) to a maximum signal equal to the voltage obtained during the pure water calibration (V_{ref}). The ratio of the signal output to the calibration output is the transmittance ratio (Tr) and will vary from 0 to 100 percent.

$$Tr = (V_{sig}-V_{dark}) / (V_{ref}-V_{dark})$$

Transmittance is related to the beam attenuation coefficient (c) by the relationship:

$$Tr = e^{-cx}$$

where x is path-length (m) through the water volume. Beam attenuation can be calculated as:

$$c = - 1/x * \ln (Tr)$$

The beam attenuation coefficient is calculated from C-Star voltage output readings by:

$$c = - 1/x * \ln [(V_{sig} - V_{dark}) / (V_{ref} – V_{dark})]$$

3. Considerations for Laboratory and In-Situ Usage

The following procedure and data acquired apply to laboratory use of a nominal 650nm model with 10cm path and flow tube. The instrument was connected to an in-lab power supply/voltage regulator set to 12V and monitored using a voltmeter (Figs. 2-4). If the instrument is connected to a computer monitoring system (optional from manufacturer), count values from supplied software will be used in all calculations in place of voltage values. The supplied software computes signal counts in relation to factory pure water calibration values. It will also apply factory determined temperature correction. This is particularly important if the instrument is used in-situ and connected to an instrumentation package. Temperature dependent variation is largely due to fluctuations in LED output. Instrument response according to pressure will also be more important for in-situ measurements, and pressure testing may be conducted to determine correction coefficients. Alternatively, if the instrument is to be used for oceanographic profiling, a temperature/pressure correction coefficient may be obtained by first performing a profile with the instrument's detector completely blacked out with electrical tape.

For laboratory measurements, temperature correction may be less important if samples are maintained at the same temperature as a reference standard. This reference standard is then used to calculate attenuation of the sample without the need to correct for temperature relative to manufacturer calibration. A similar procedure may be used to obtain attenuation due to the

particulate component of a water sample independent of the effects of CDOM and absorption by water. The original raw water sample may be passed through a 0.2μm filter, and the resulting filtrate used as a reference. This also eliminates the need for salinity correction.

If deployed in the field as part of an instrumentation package, calibration and correction will follow the same principles but will be application-specific. An example of calibration and correction procedures for use of the C-Star with Sea-Bird data collection equipment is included in the ancillary material (Cstar_seabird_calibration.pdf).

It is important to note that if seawater is pumped through the C-Star in a closed flow-tube configuration, then there will be a time delay between when the temperature of the water sample is measured and when it passes through the instrument. This delay will be especially prevalent if water is run through a filter before entering the instrumentation, as is done when measuring optical properties of CDOM and particulates. The most common plumbing sequence involves passing water first through a CTD and then to other instruments within the package. Instrumentation measurements are automatically synchronized to CTD measurements by time. If the C-Star is used in a pumped mode during a vertical profile, then the instrument will, for any time dependent CTD reading, actually be exposed to water that passed through the CTD earlier. For example, if water entering the pump passes through a CTD and then takes 8 seconds to reach the C-Star, then the C-Star data must be offset by 8 seconds to determine the actual temperature and salinity of the water sample. Time correction should be taken into account for all instruments in a serial plumbing system. The exact correction will depend on set-up and must be measured by the user. This correction step is critical in applying the correct temperature/salinity coefficients. A suggested method for assessing time delays is provided:

- Set-up instrumentation package as it will be deployed.
- Place plumbing intake hose in pure water.
- Once water is passing through all instruments, quickly move intake hose into raw seawater. This will provide an unambiguous signal in all instrumentation relative to pure water.
- The timing of the seawater signal for each instrument may then be used to assess flow delay through the package.

4. Laboratory Usage Procedure

Note – it is extremely important to thoroughly clean the instrument's windows and to completely remove bubbles from the sample tube. Dirty windows may lead to overestimations of c. Bubbles will produce high and erratic output voltages. Only use lenspaper to touch windows, as they are easily scratched. Isopropyl alcohol may be used as a lens cleaning solution.

Cleaning

- Remove the black plastic flow tubes by sliding the end sleeves toward the middle of the tube. Lift the flow tube out.
- Remove the O-rings.
- Wash the flow tube with a mild detergent.
- Rinse completely with water to ensure no soap residue is left inside the flow tube.
- Place the tube in a protected area where it can dry out completely.
- To reinstall, carefully replace the flow tube O-rings.
- Ensure the windows are clean and dry.
- Insert the flow tube into the meter, lining up the stainless steel cap screws with the grooves in the flow tubes. This will ensure that the feet on the ends of the flow tubes will not block the water flow. Slide the flow tube sleeves outward on both ends until the outside ring on the sleeve is flush with the C-Star body to secure the flow tube.

Setup

- Attach C-Star communications and power cable (provided with unit) to instrument and power supply/regulator. Be certain power leads are attached properly (consult user manual). Set voltage at approx 12V. Values higher than 15V will damage instrument.
- Attach output leads to voltmeter.

Dark Current Measurement

- Remove flow tube.
- Completely block the receiver. Multiple methods should be tried to achieve minimum transmission. In this test, placing a camera lens cap in front of the receiver lens and covering the C-Star with black cloth worked well.
- Record voltage. This is the V_{dark} value.
- Obtain at least 3 independent V_{dark} values for error estimation.

Reference Measurement

- Clean lens windows with isopropyl alcohol on lens paper by gently patting window. Do not use circular motions or apply pressure.
- Rinse lens with Milli-Q water.
- Attach flow tube securely, as described above. Caps may be placed on the intake/outflow ports to prevent entry of stray light. This was tested and found NOT to affect voltage readings.
- Fill flow tube with Milli-Q. This will serve as reference material. Alternatively, 0.2 or 0.7μm filtrate from a water sample can be used as a reference for the calculation of beam attenuation due to particles, c_p.
- De-bubble tube by gently tilting instrument and agitating.
- Record voltage. This is the V_{ref} value.
- Repeat to obtain at least 3 independent V_{ref} values for error estimation.

Sample Measurement

- Clean lens windows with isopropyl alcohol on lens paper by gently patting window. Do not use circular motions or apply pressure.
- Rinse lens with Milli-Q water.

- Attach flow tube securely, as described above.
- Fill flow tube with well-mixed water sample.
- De-bubble tube by gently tilting instrument and agitating.
- Record voltage. This is the V_{sig} value.
- Repeat to obtain at least 3 independent V_{sig} values for error estimation.

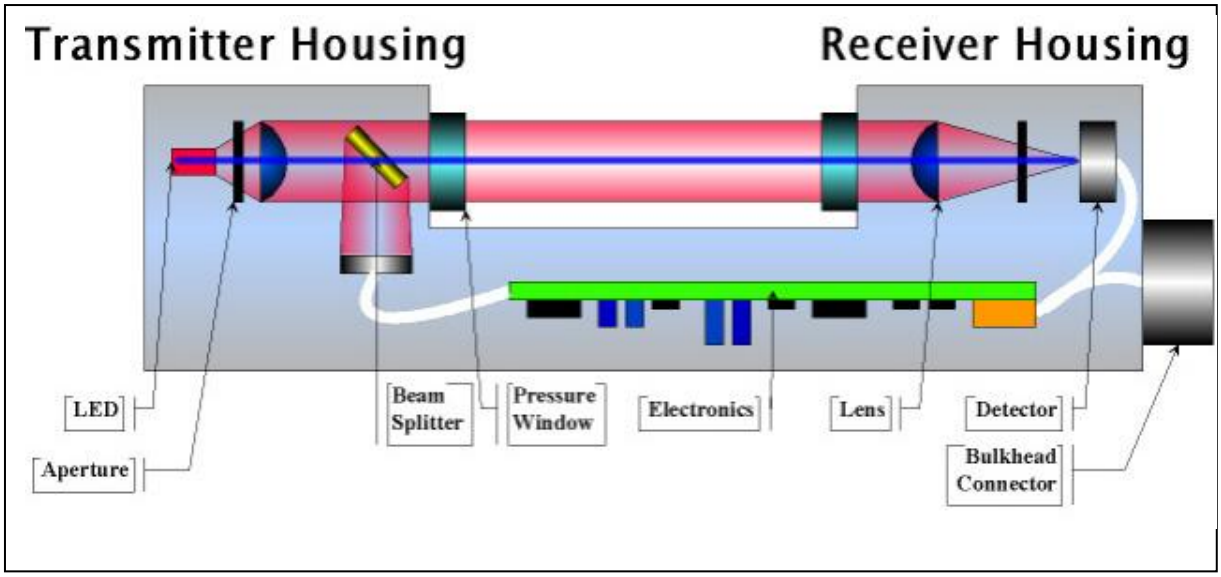

Figure 1. Schematic representation of the C-Star. Credit : WET Labs, C-Star user manual.

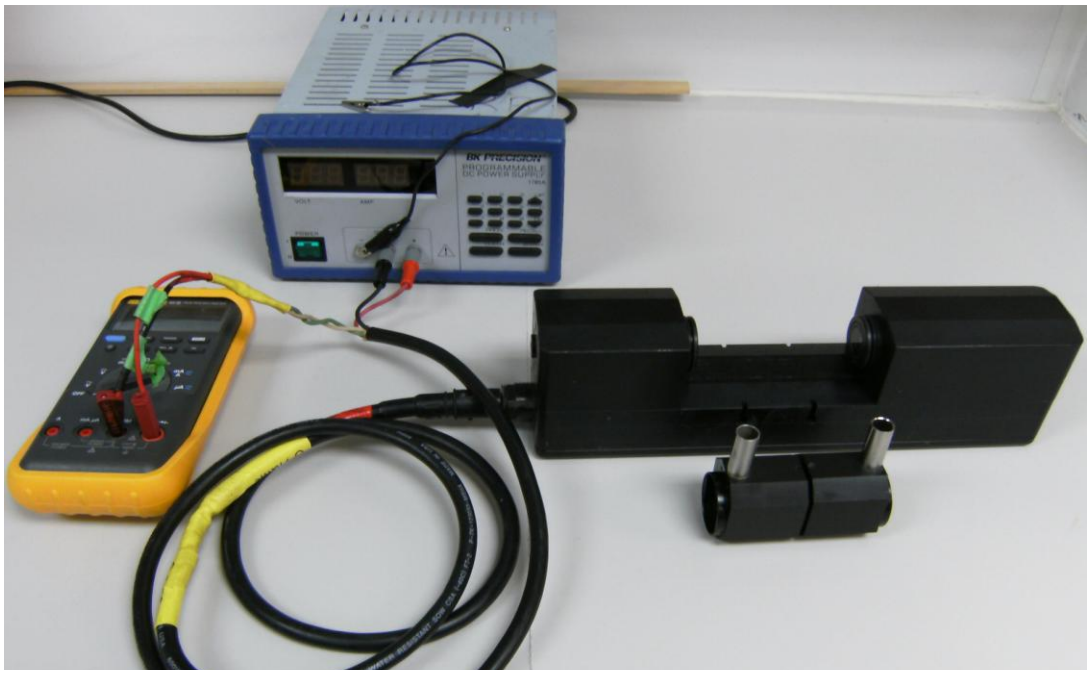

Fig 2. C-Star equipment set-up for laboratory measurements as described in the above procedure. Flow tube is not installed.

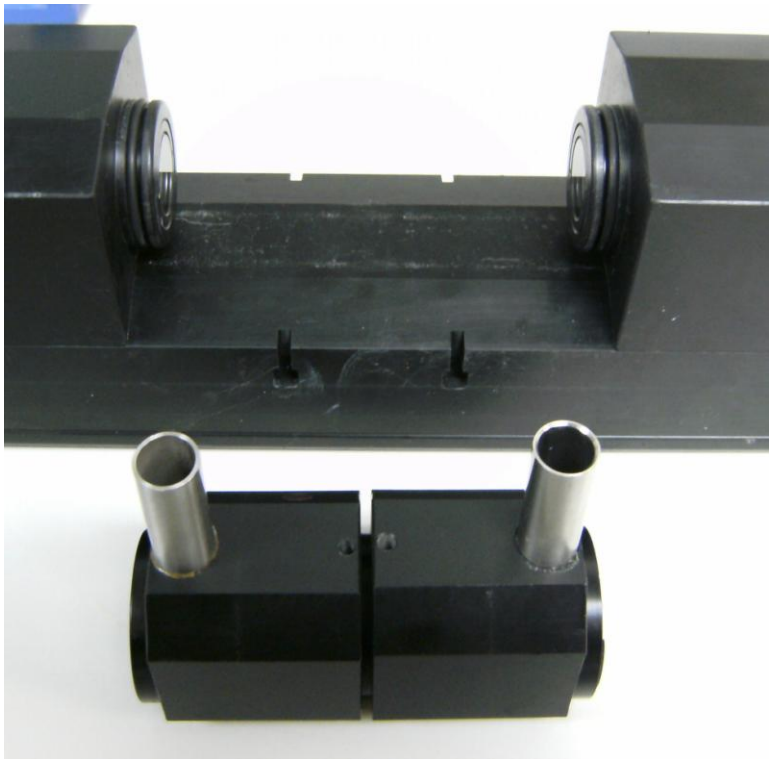

Fig 3. Close-up of C-Star detection path and source/receiver windows. Receiver is on left.

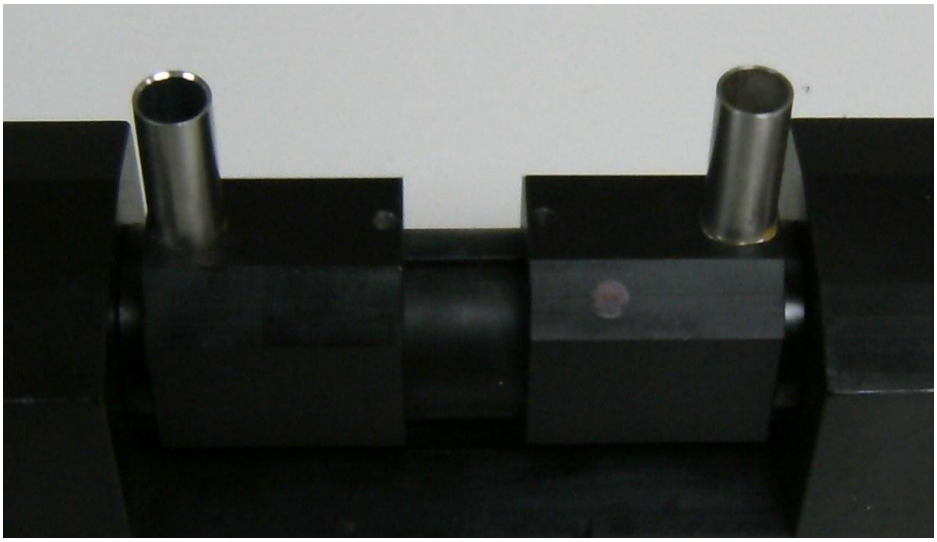

Fig 4. Close up of C-Star path with flow tube installed.

5. Results

For this test, 3 separate samples were measured for attenuation due to particulates. These samples were also analyzed using an ac-s (WET Labs) and a LISST 100X (Sequoia Sci.) for comparison. This data is presented below (Fig 4), with the raw voltage readings for clay sample provided (Table 1).

- Clay - 400 mg Arizona Test Dust added to 20L Milli-Q water. Final particle concentration: 0.02mg/ml. Milli-Q was used as a reference.
- Culture – Monoculture of *Thalassiosira weissflogii* maintained at Darling Marine Center. 0.2µm culture filtrate was used as a reference.
- Dock Water – Raw sample of Damariscota River Estuary Water. Collected at Darling Marine Center dock, July 15 2011. 0.2µm FSW was used as a reference.

V_{dark} (volts)	V_{ref} (volts)	V_{sig} (volts)	Tr (Vsig-Vdark) / (Vref-Vdark)	c (m^{-1})
0.056	4.58	2.12	0.46	7.87
0.056	4.56	2.04	0.44	8.22
0.055	4.58	1.90	0.41	8.98

Table 1. Clay sample voltage readings

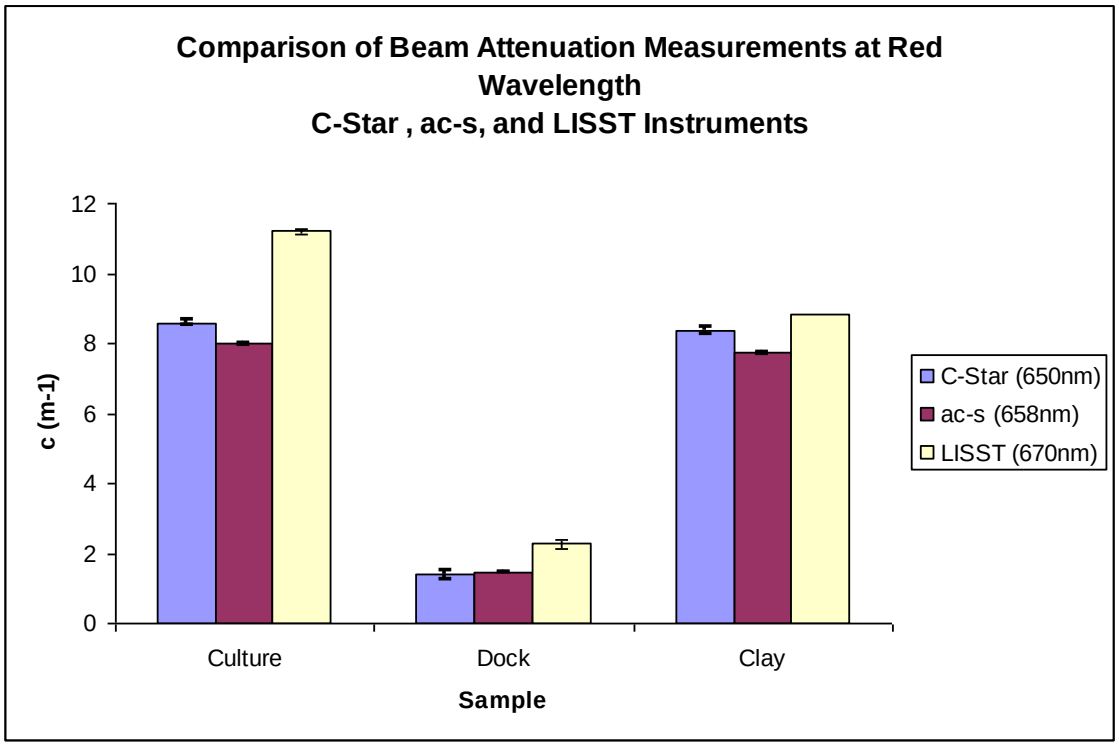

Fig 4. Beam attenuation (c) due to particulates. Measurements obtained using C-Star. Values obtained with ac-s and LISST instruments presented for comparison.

6. Discussion

The WET Labs C-Star transmissometer is a simple, effective instrument that provides beam attenuation measurements at a single wavelength. In this test, error was low and comparable to other instruments available. Disagreement between instruments is likely attributable to differing wavelengths and acceptance angles of the various instruments. C-Star instruments are available in several wavelengths depending on the desired application. The model used here has a reported nominal wavelength of 650nm, and is indicated for assessing c due to particulates and particulate dynamics. The ac-s provides attenuation for many wavelength values, and 658nm was used for this comparison. The LISST has a nominal wavelength of 670nm. Beam c was most similar between C-Star and ac-s.

Laser In-Situ Scattering and Transmissometry (LISST)

Section Guide

1. Introduction

The LISST-100X B instrument (figure 1) uses the technique of laser diffraction to obtain particle size-distribution (PSD) between 1.25 and 250 µm. It also records the optical transmission, pressure and temperature as supporting measurements. Instrument operation is based on Mie theory (Mie, 1908), which states that at small forward scattering angles, laser light diffraction by spherical particles is essentially identical to diffraction by an aperture of equal size (Fraunhofer approximation) (Agrawal and Pottsmith, 1994). The theory further states that the refractive index of particles has little or no effect on the distribution of light scattering (Agrawal and Pottsmith, 1994). The LISST measures forward scattered light transmittance at a single wavelength over a known path length (5 cm). The light source is a LED with a wavelength range of 660-670nm. Laser light scattering at 32 angles is the primary information that is recorded. This primary measurement is mathematically inverted to get the size distribution, and also scaled to obtain the Volume Scattering Function (VSF). The size distribution is presented as concentration ($\mu l.l^{-1}$) in each of 32 log-spaced size bins and the VSF as scattering (m^{-1} sr^{-1}).

LISST X 100 B is capable of resolving a particle size range of 1.25–250 μm. In this portfolio, data acquisition procedures and analysis are described. Particle volume distribution is estimated by determining the volume in each size class from:

$$PVC_i = (A_i d_i) / Cv \; PVV_{A,i}=(N_{A,i}d_i)/C_v \quad (1)$$

where $A_{,i}$ is the area in each size class i, d_i, is the diameter of that size and C_v is calibration value.

The appropriate values of C_v could be determined in a series of laboratory experiments.

Considering that LISST-100X assumes that particles are spherical, the particle number concentration (PNC_i) can be calculated from:

$$PNC_i = \frac{PVC_i}{(4/3)\pi(d_i/2)^3} \quad (2)$$

These calculations can be applied to estimate the concentration for one single species (cultures or natural assemblages) or for phytoplankton groups.

Figure 1: Lisst 100X (left) and his external battery (right) before deployment in Mediterranean Sea (Malika Kheireddine).

2. Lab measurement

Samples of clay and culture extracted from dock water (using 2 μm filter) are collected to determine the potential of LISST-100X B to detect size distribution. The procedures include two main parts: dark measurement and sample measurement.

2.1 Before acquisition

- Make sure LISST and Calibration chamber are thoroughly cleaned (Fig.2) with detergent and triple rinsed, and MQ water rinsed to minimize contamination.
- Install the calibration chamber into the LISST.

- From the LISST menu, select the “Collect Background scatter data” and then choose the factory background scattering file according to your instrument serial number. This file name should be like this “factory_zsc_xxxx.asc”.

New window will pop up and press on “Begin Collect” button. Then the LISST will automatically collect background data. Compare the factory background scattering ASCII file with the currently background scattering ASCII file. If they are in well agreement, then instrument is ready to measure real time data. If it is not acceptable, then collect background scattering data again with new sample of cleaned bubble free filtered water. After that if it still gives the same error message, then this instrument most probably suffer from alignment problem and make the necessary steps to realign this instrument.

Figure 2: Sensor part of Lisst 100X .

2.2 Measurement of sample

- Select your sample. It can be, for example, culture, sediment (clay) and dock water.
- Fill the sample chamber. Then, select “Open Real-Time Session” from the File menu. Choose the correct background scatter file and select an Output filename. A display will appear on the screen and click on “Timer-OFF” button. The button will be changed to “Timer –ON” and the LISST will automatically start to collect data.
- Press “Timer-ON” when sufficient water samples have been collected.
- When finished, close the main window to stop communication with the LISST.
- To convert the binary PSD to ASCII, select “convert the binary PSD to ascii” from the File menu and then open the file that you want to change and then select an Output file.

Table 1 shows the median size of each 32 size class that ranges logarithmically placed from 1.25 - 250 microns.

Table 1: Type B Instruments – 1.25 to 250 micron size range.

1.44	1.68	1.97	2.31	2.72	3.19	3.76	4.43
5.21	6.14	7.24	8.54	10.1	11.9	14.0	16.5
19.5	23.0	27.1	31.9	37.6	44.4	52.4	61.7
72.8	85.9	101	119	140	166	196	231

3. Data process

3.1 Process of raw data

Data that have been downloaded from the datalogger are in a raw binary file. The values in the raw data file are stored in the order shown in the table below.

Table 2: Raw Data Storage Format.

Elements	**Parameter**
1:32	Light intensity on detectors 1 through 32 that corresponded to 32 median angles for VSF measurements
33	Laser transmission Sensor
34	Battery voltage in raw counts
35	External Auxiliary input 1 (0 to 5V = 0 to 4096)
36	Laser Reference sensor
37	Pressure in raw counts
38	Temperature in units of 100ths of degrees C
39	(Day*100 + Hour) at which data taken
40	(Minutes*100 + Seconds) at which data taken

LISST measurements can be further processed in programming languages such as MATLAB or R. Pure water blanks or filtered sample blanks were taken before readings on different microsphere stocks. Raw LISST measurements consist of a set of 32 detector outputs, $sscat_i$, where i is the ring detector number. $sscat_i$ is post processed to subtract the pure water/filtered sample ring outputs ($zscat_i$) and for attenuation within the sample volume :

$$\csc at_i = (\frac{scat_i}{\tau} - zscat_i) \cdot dcal_i , \quad (3)$$

where $dcal_i$ is a set of manufacturer-supplied detector responsivity correction factors.

The zscat corrected scatter, $\csc at_i$, is then corrected for the area of each ring and for laser power in the measurement relative to the clear water measurement, giving the uncalibrated scattered power in each ring, $pscat_i$, from which, VSF can be calculated. Detailed information of LISST data process and calibration/validation can be found

in Slade and Boss, 2006. Appendix 1 is the major matlab code to derive pscat from raw data.

Data must be processed into particle size by the LISST-SOP program. Detailed processing steps including optional displays and procedures can be found from LISST -100 X User manual. (http://www.sequoiasci.com/products/part_LISST_100.aspx.)

The values in the LISST-SOP processed data file are stored in the order shown in the table below. Each sample is stored in one row. Table 3 gives the storage format of processed data from LISST-SOP software.

Table 3: Processed Data Storage Format.

Elements	**Parameter**
1:32	Volume concentration (in ul/l) for size class 1 through 32
33	Laser transmission Sensor
34	Battery voltage in calibrated units
35	External Auxiliary input 1 in calibrated units
36	Laser Reference sensor in calibrated units
37	Pressure in calibrated units
38	Temperature in calibrated units of degrees C
39	(Day*100 + Hour) at which data taken
40	(Minutes*100 + Seconds) at which data taken
41	Computed % Optical transmission over path
42	Computed Beam-C in units of 1/m

3.2 Transmittance and Beam attenuation

Transmittance (τ) is related to the beam attenuation coefficient c by the relationship:

$$\tau = e^{-cx} \qquad (4)$$

For filtered / pure water sample or unfiltered samples, the ratio of laser transmission to laser reference (rr) can be calculated from raw data filed : rr = zscat(33)/zscat(36).

Assuming the path-length (x) of filtered/pure water is zero:

$$\frac{rr\_sample}{rr\_blank} = \frac{e^{-cx}}{1} = \tau,$$

where c is beam attenuation.

Therefore, c can be calculated as:

$$c = -\log(\tau)/x. \quad (5)$$

4. Results

4.1 Particle size distribution

Comparisons of particle size distribution in volume (PVC) among clay, culture and dock water samples are shown in fig. 3 , fig. 4, fig. 5..

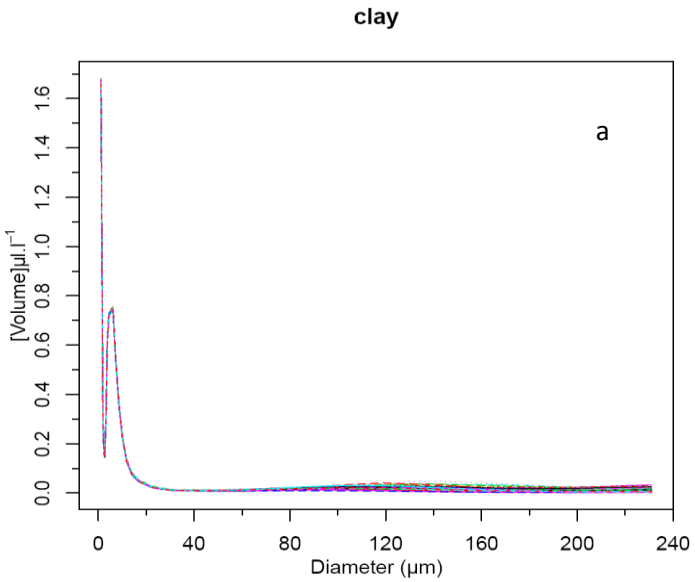

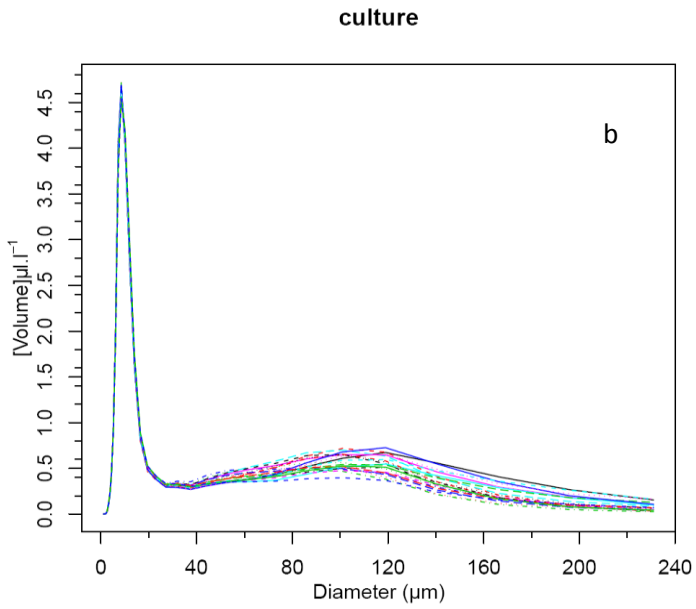

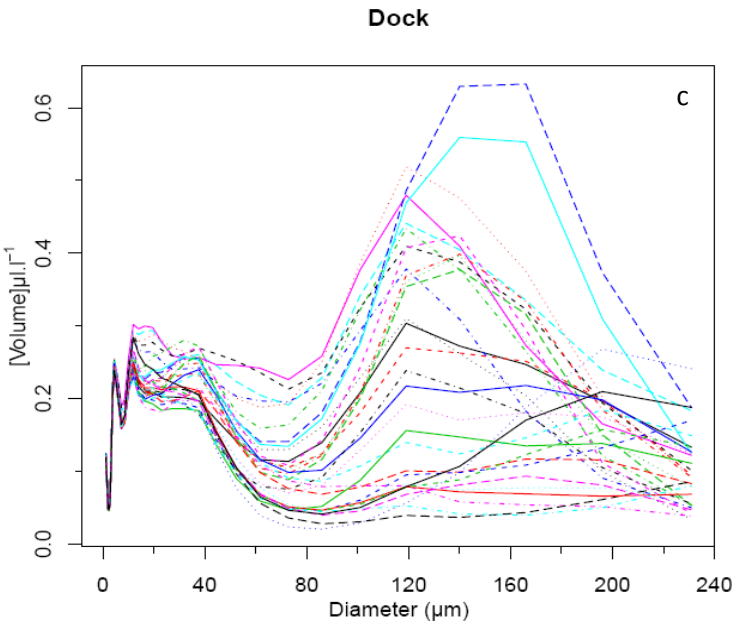

Figure 3: Particulate size distribution (PSD) for different samples (a, b, and c) with the LISST.

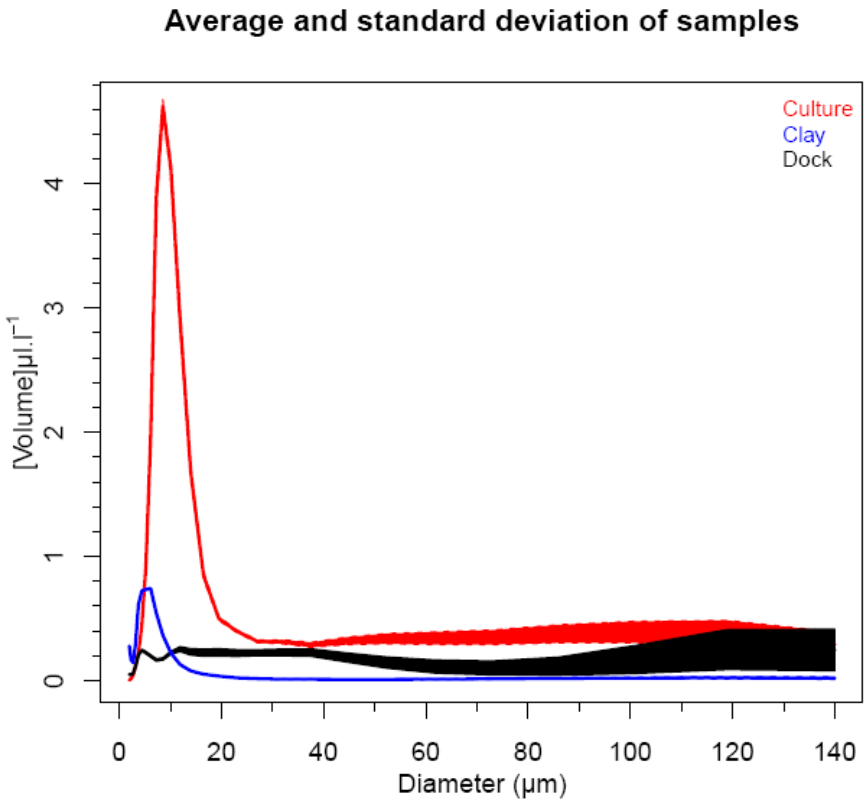

Figure 4: Average and standard deviation of PSD for Culture (red), Clay (blue) and Dock water (black).

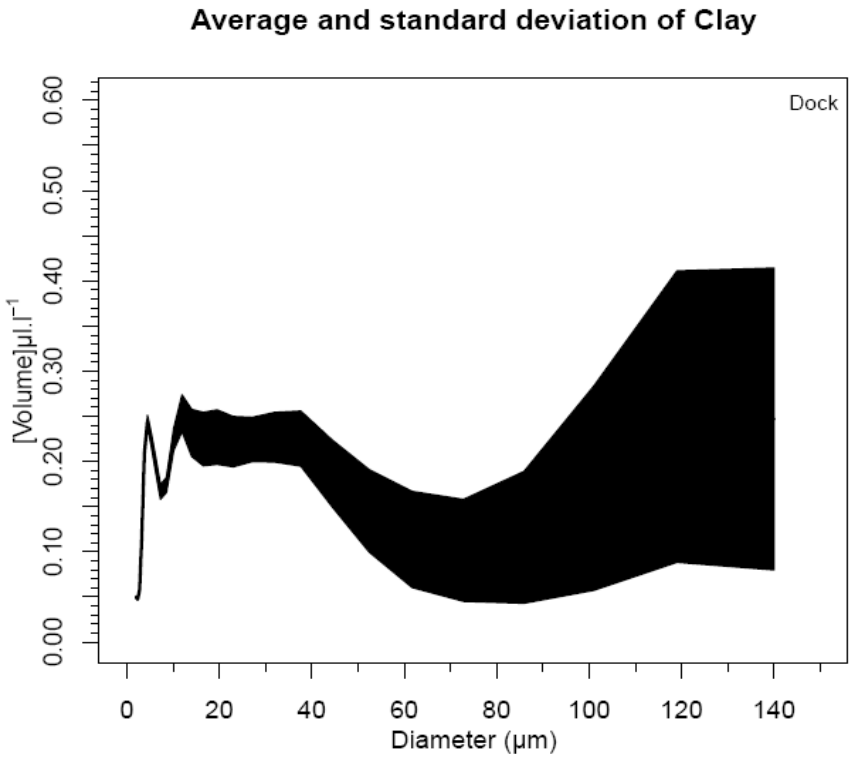

figure 5: Average and standard deviation of PSD Dock water.

The distribution of particle Number, N (D), PNC are calculated from the volume size distribution according to equation 2.The result is shown in figure 6.

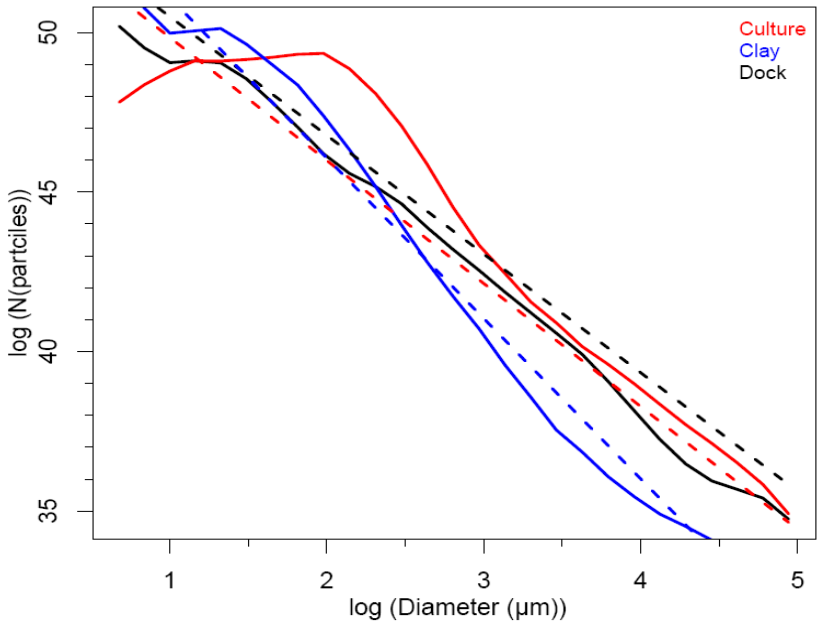

Figure 6: PSD in particle number for Culture (red), Clay (blue) and Dock water (black).

Because the particle shape is usually unknown, D is often represented as that of a volume-equivalent sphere. N (D) represents the differential distribution per unit size, also referred to as the density function of the PSD.

The general form of this relation (log (N) vs. log (D) can be used to describe an entire size distribution or selected portions:

$$N(D) = A^{-\gamma} \quad (6)$$

where γ is the slope distribution.

Values of γ reported for marine particle assemblages typically range between 3.5 and 4, but values outside of this range are not uncommon. The slope value is also likely to be sensitive to the range of the size distribution over which it is determined, as changes in slope as a function of size have been reported for marine particle assemblages.

Measurements of the PSD generally resolve only a limited portion of this size range, and no studies exist which have measured the PSD over the entire optically relevant size range. In particular, measurements of the PSD in the submicron range are rare and often controversial due to limitations of current techniques; despite the potential importance such particles are postulated to have on optical properties such as the backscattering coefficient.

The size distribution of these particles is important to the structure and functioning of aquatic ecosystems, such as it influences trophic interactions within the planktonic community. Particle size plays a strong role in determining the differential sinking rates of various particle types, and thus determines horizontal and vertical fluxes of materials within the water column.

4.2 Beam attenuation

Beam attenuation (c) calculated from equation 5 for LISST is shown in figure 7. The comparison of c calculated from the LISST with other two instruments, C Star and ACs are also shown in figure 7. As expected, clay and culture have higher beam attenuation value than dock water, yet LISST has much higher c value than the other two instruments. One possible reason is that for the smallest microspheres, scattering in the most near-forward angles is very low, and may lead to negative values of pscqt because of the variability caused by experimental uncertainty and electronic noise. In order to avoid negative pscat, the rings at which scatter magnitude is not sufficiently greater than the variability (half the difference between 84th and 16th percentiles) in zscat (blank sample) are discarded. The corrected beam attenuation value is shown in (Figure 8).

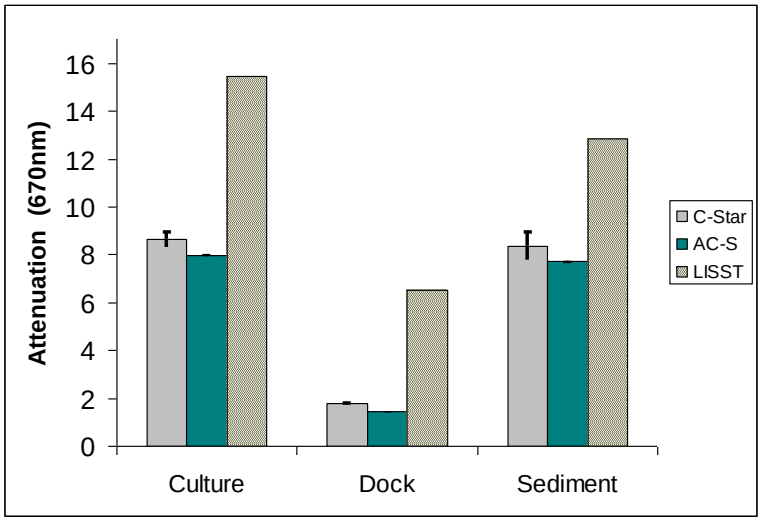

Figure 7: Beam attenuation comparison between three instruments: C-Star, AC-S, and LISST.

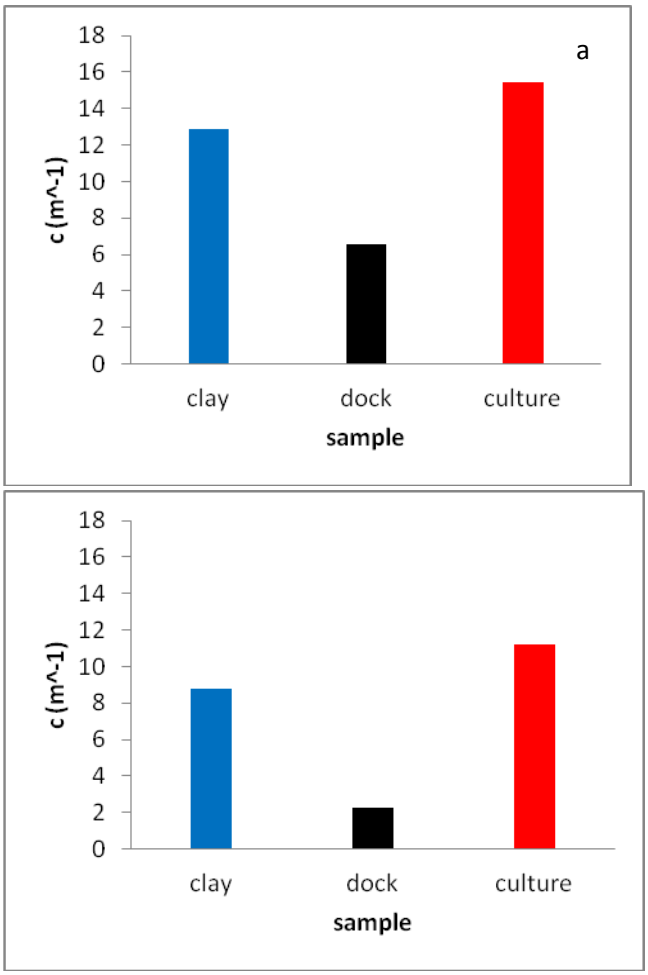

Figure 8: Beam attenuation (a) and with correction (b) for each sample.

5. References

Agrawal and Pottsmith, 2000 Y.C. Agrawal and H.C. Pottsmith, Instruments for particle size and settling velocity observations in sediment transport, *Mar. Geol.* **168** (2000), pp. 89–114.

Mie.G, "Beiträge zur Optik trüber Medien, speziell kolloidaler Metallösungen," Leipzig, *Ann. Phys.* **330**,377–445(1908).

LISST-100X User Manua. Version 4.6.2
http://www.sequoiasci.com/library/downloads/login.aspx

Slade WH, Boss E (2006): Calibrated near-forward volume scatteringfunction obtained from the LISST particle sizer. Optics Express 14: 3602–3615.

Appendix 1

```
function lisst = Process_LISST(rawdata, zsc_stdgain, ...
                    dcal, dias, m2, H, ...
                    is100x, pathl, theta0air, volconv)

% input:
% rawdata: LISST RAW data with 40 columns
% zsc_stdgain: The sample data used as blank. It can be a Sequoia-style single average of scans, or can be a log file taken on clean water (not corrected for any zscat). If a log file is specified, the std of that data is used; otherwise a set of default std (zscat) are used.
% dcal: "ringarea" file;


   % size of data file
   [ns,col] = size(rawdata);
   if col~=40
      error('Data matrix not 40 columns!')
   end

   % size of zscat
   zscat = zsc_stdgain(:)';
   if length(zscat)~=40
      error('Improper ZSCAT size!')
   end

   % Ringarea file provided by Sequoia
   dcal = dcal(:)';

   % LISST psd diameter bins
   dias = dias(:)';
   % If LISST is a 100X we need to divide the scattering by 10
   if strcmpi(is100x,'X')
```

```
        disp('**** Instrument is 100-X ****')
        rawdata(:,1:32) = rawdata(:,1:32)./10;
        % zscat(:,1:32) = zscat(:,1:32)./10  %.ASC zscat files are stored
        % in standard gain, NOT *10
    end

    MM = fix(rawdata(:,40)/100);
    SS = rawdata(:,40)-100*MM;
    DD = fix(rawdata(:,39)/100);
    HH = rawdata(:,39)-100*DD;
    timestamp = datenum(0,0,DD,HH,MM,SS);

    % First calculate transmission and attenuation
    % rr is ratio of water-transmitted to reference laser counts in clean water used to correct
transmission data
    rr = zscat(33)/zscat(36);
    % transmission and beam attenuation
    tau = rawdata(:,33)./rr./rawdata(:,36);
    cpg = -log(tau)/pathl;

    % Ring angle calculation (theta1 and theta2 are inner and outer ring angles IN WATER)
    theta_i = (200.^((0:32)/32)).*theta0air;
    %   theta_j = theta_i(2:33);
    %   theta_i = theta_i(1:32);
    theta_i = asin(sin(theta_i)./1.3308);
    theta = geomean([theta_i(1:32); theta_i(2:33)]);

    % "calibrated scatter" implies that we've corrected the raw scatter for the detector area
(determined based on geometry), zscat, dcal % (responsivity correction, aka ringarea file), and
attenuation
    % within the sample volume:
    % (1) first correct for attenuation (using tau) and subtract zscat...
    %     code in MatlabBundle.zip/nlia_func.m also has a z(36)/data(1,36) factor to correct for
drift in laser power; we make the correction later similar to vsfcode_new.m
    cscat = rawdata(:,1:32)./repmat(tau,1,32) -repmat(zscat(1:32),ns,1);
    % (2) correct for laser power (counts) in water (relative to zscat)
    cscat = cscat ./ repmat(rawdata(:,36)/zscat(36),1,32);
    % (3) correct for ring area cal
    cscat = cscat .* repmat(dcal,ns,1);

    % (4) apply analytic formulation for ring area (pscat has correct
    %  VSF shape) phi factor for ring area calculation
    phi = 1/6;
    pscat = cscat ./ repmat(pi*phi*pathl*(theta_i(2:33).^2-theta_i(1:32).^2),ns,1);

    % Inversion to psd as described in Sequoia App Note L006 (Rev 10/2006
    % Update: Correction is described in new MATLAB Processing article from Sequoia dated
30 Apr 2008

    VD = nan(ns,32);
```

```
    for ik=1:ns
        if mod(ik,1000)==0
            disp([num2str(ik) '/' num2str(ns)])
        end
       VD(ik,:) = nlia(cscat(ik,:),m2,H)/volconv;
    end


    % LISST vol psd returned by nlia is in uL/L
    Vp = (4/3)*pi*(dias./2).^3; % um^3
    Vp = Vp*1e-9; % converted to uL

    ND = VD./ repmat(Vp,size(VD,1),1); % #/L
    ND = ND ./ 0.001; % convert to #/m^3

    Ap = (pi/4)*(dias*1e-6).^2   % m^2
    AD = ND .* repmat(Ap,size(ND,1),1); % m^2/m^3

    lisst.timeraw = timestamp;
    lisst.cpg = cpg;
    lisst.theta = theta;
    lisst.cscat = cscat;
    lisst.pscat = pscat;
    lisst.dias = dias;
    lisst.AD = AD;
    lisst.ND = ND;
    lisst.VD = VD;

return
```

ac-9 and ac-s

Section guide

Determination of absorption and beam attenuation coefficient of particulate and dissolved material using ac-s and ac-9

1. Introduction

The ac-9 is a type of in-situ spectrophotometer that synchronously determines the spectral transmittance and spectral absorption of water over nine wavelengths; the light source is a collimated beam. The unit provides a method for determining the absorption, a (m^{-1}) and beam attenuation, c (m^{-1}) coefficients (Figure 1). The ac-9 has a 25-cm pathlength for effective measurement of the cleanest natural waters. The unit is also available in a 10-cm pathlength configuration (http://www.wetlabs.com/products/ac/acall.htm).

The ac-s offers almost an order of magnitude increase in spectral resolution of in-situ absorption and beam attenuation coefficients over the ac-9. The ac-s has the same flow-through system as the ac-9, same size, and superior stability. The ac-s employs a 25-cm pathlength for effective measurement of the cleanest natural waters. The light source features a linear variable filter with a collimated beam. The absorption tube has a reflecting surface and a large area detector, whereas the attenuation side has a non-reflective tube and a collimated detector. The instrument provides data at 79 wavelengths from 400–730 nm with 4 nm increments. Individual filter steps have a FWHM of 15.5 nm. The ac-s uses a Linear Variable Filter (LVF) to obtain its wavelengths.

Figure 1. ac-s (left) and ac-9 (right). (Wetlabs, Inc)

2. Data Measurements

Fundamentally, the methods for measuring $a(\lambda)$ and $c(\lambda)$ using ac-9 and ac-s are very similar. In this section the method has been provided step-by-step to calibrate the sensor using Mili-Q water in laboratory, measure $a(\lambda)$ and $c(\lambda)$ of total and dissolved materials both in the laboratory and deployment in the field (vertical profiling).

2.1. Calibration/blank

i. Clean the *a* and *c*-tubes by wetting lens paper with isopropyl alcohol or ethanol and pushing it through the tube with a tube with a smooth surface, e.g. plastic tubing. Make sure fingers do not touch side of lens paper that will come in direct contact with the tube.

ii. Clean the detector by wetting lens paper with isopropyl alcohol or ethanol and dabbing the lens paper along the detector surface. Mount the tubes on to ac-s or ac-9 unit. Connect instrument to Milli-Q flow-through tubing, power supply, and computer (Figure 2).

iii. Run ultrapure type-1 water from a system with a UV oxidizing cartridge through *a*-tube. Debubble by squeezing the connecting tubes and tilting the ac-s meter. When the reading is stabilized record data for 30 seconds and measure temperature of the water. (Temperature affects absorption and scattering).

iv. Repeat cleaning and runs until two MQ runs are +/- 0.005 m^{-1} from one another. "Debubbled" raw data will not fluctuate between runs.

v. Water calibrations should be done in orientation in which the meter will be deployed because a small variation in orientation of the instrument can affect the rotational plane of the filter wheel in the instrument and consequently affecting response of the instrument.

vi. Similar procedure is followed to calibrate the *c*-tube.

2.2. Filtered water in lab for $a_g(\lambda)$ and $c_g(\lambda)$

i. Run filtered sample (0.2 um) to obtain $a_g(\lambda)$.

ii. If there are several samples, start with the ones with lowest absorbance attenuation.

iii. Run filtered sample in *c*-tube to obtain $c_g(\lambda)$.

2.3. Unfiltered Water in Laboratory for a_t and c_t

i. Run unfiltered sample water through the *a*-tube to obtain $a_g(\lambda)$. If there are several samples, start with the ones with lowest absorbance attenuation.

ii. Run the same unfiltered sample in the c tube to obtain $c_g(\lambda)$..

iii. Re-run Milli-Q water as blank to re calibrate the sensor (post-calibration). Post calibration often provides information on if there has been any drift in sensor response (sensor drift).

iv. Clean tubes and detectors and let air dry overnight.

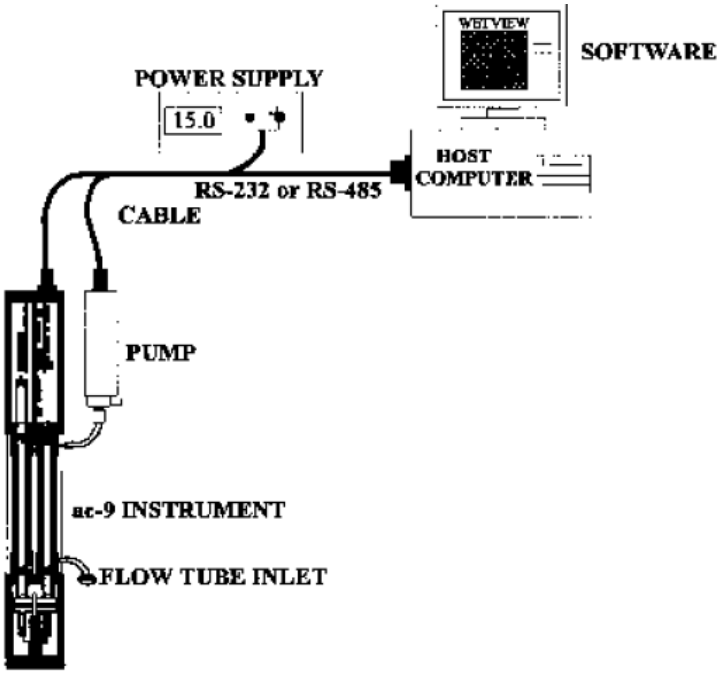

Figure 2. Typical ac-s/AC9 configuration. (Wetlabs).

2.4. Field Deployment to Measure $a_g(\lambda)$ and $c_g(\lambda)$

i. Run calibration (step I) in laboratory.
ii. Attach filter to intake tubing and make a cast

2.5. Field Deployment to Measure $a_t(\lambda)$ and $c_t(\lambda)$

i. Remove filter and do another cast.
ii. Re-run blank with Milli-Q.
iii. Clean tubes and detectors and let air dry overnight.

3. Data Processing

3.1. Data Processing for Laboratory Measurements

Total absorption and total beam-attenuation coefficient measurements from ac-s and ac-9 are corrected for temperature-salinity and scattering effects. The order of correction is provided in the following list.

Corrections to absorption and beam-attenuation coefficients :

i. Correct Milli-Q to same temperature as sample.

ii. Subtract MQ from sample.

iii. Subtract filtered from unfiltered.

iv. Scatter-correct the particle absorption spectrum.

3.1.1. Temperature and Salinity Corrections

Absorption coefficient of pure water is dependent on water temperature *T;* absorption coefficient of a seawater sample is dependent on both water temperature and salinity *S.* The difference between the water temperature *T* and the temperature of the pure water reference standard T_r changes the water-absorption baseline value $a_w(\lambda)$ and consequently affects the measured absorption $a_m(\lambda)$ and beam attenuation coefficients $c_m(\lambda)$. The reader is encouraged to read the NASA ocean optics protocol (Mueller *et al*., 2003) for a detailed explanation on the correction procedure. The temperature and salinity corrections are applied to measured absorption as below.

$$a_m^{TS}(\lambda) = a_m(\lambda) - \frac{\partial \mathbf{a}_w(\lambda)}{\partial \mathbf{T}}(T - T_r) - \frac{\partial \mathbf{a}(\lambda)}{\partial \mathbf{S}} S \qquad (1)$$

$$c_m^{TS}(\lambda) = c_m(\lambda) - \frac{\partial \mathbf{a}_w(\lambda)}{\partial \mathbf{T}}(T - T_r) - \frac{\partial \mathbf{c}(\lambda)}{\partial \mathbf{S}} S \qquad (2)$$

3.1.2. Scattering Correction

i. Spectrally varying Scattering Correction for ac-9:

$$c_m^{TS}(\lambda) = c_m(\lambda) - \frac{\partial \mathbf{a}_w(\lambda)}{\partial \mathbf{T}}(T - T_r) - \frac{\partial \mathbf{c}(\lambda)}{\partial \mathbf{S}} S \qquad (3)$$

ii. Spectrally varying Scattering Correction for ac-s:

Even a wavelength further into the near infrared can be used for ac-s:

$$a(\lambda) = a_{TS}(\lambda) - b(\lambda) * \frac{a_{TS}(730)}{b(730)} \qquad (4)$$

Where subscript TS denotes temperature-salinity corrected values of absorption coefficients.

3.1.3. Particulate Absorption Coefficients, $a_p(\lambda)$

Particulate absorption coefficients $a_p(\lambda)$ are measured by subtracting $a_g(\lambda)$ from $a_t(\lambda)$.

3.2. Data Processing for Field Measurements

i. Merge data in time with all other sensors (CTD), done by WETLabs WAP software. Align the ac-s data in time with the CTD (because water passes at different times through different sensors). Time delay is determined by aligning temperature features (e.g. thermocline) observed by CTD and NIR (~740nm) absorption wavelengths of the ac-s. The delay will be different for measurements with and without a filter.

ii. Subtract clean-water readings from both the filtered and unfiltered casts, corrected to match the aligned temp and salinity readings from the CTD.

iii. Bin data, such that you have at least 5-10 samples in each bin (so you can assume that the *a*- and *c* side of the ac-s are seeing the same water) this will be a function of package descent speed.

iv. Compare attenuation and absorption of the dissolved materials collected with a filter on the intake. If they are close (within $0.005 m^{-1}$) of each other, are smooth and have no red/infrared features resembling the temperature dependence of water absorption you are done. Otherwise fit the 700-750nm range to remove residual temperature effects. If dissolved absorption measured in the attenuation tube is significantly larger than that measured in the absorption tube you likely have a leak in your system and these data are not truly dissolved. You should have a smooth curve. If you have strong spectral features, you are likely experiencing problem with the calibration applied. If the features are between 710-750nm, you may still have residual temperature signal.

v. Obtain the particulate and dissolved absorption spectrum: Simultaneously scatter-correct and remove residual temperature effects from the absorption data collected without a filter on the intake, using a temperature offset solved by minimizing the temperature and scatter correction in the710-750nm range, following Slade et al. (2009) and Zaneveld et al.'s (1994) method 3 (bringing absorption to zero at 730nm and removing a spectrally varying offset proportional to the scattering spectra). If you

did well, the absorption between 720-750nm will be nearly zero, the chlorophyll peak, if present, will look canonical and values will be positive or not significantly different from zero at all wavelengths.

vi. Obtain the particulate and dissolved attenuation spectrum: Correct residual temperature effects in the attenuation data collected without a filter on the intake. You should have a smooth curve. If you have strong features, you are likely experiencing problems with the calibration applied. If the features are between 710-750nm, you may still have residual temperature signal.

vii. Compute particulate absorption and attenuation by removing the dissolved attenuation and absorption from the filtered cast.

4. Results

4.1. ac-s Measurements in Laboratory

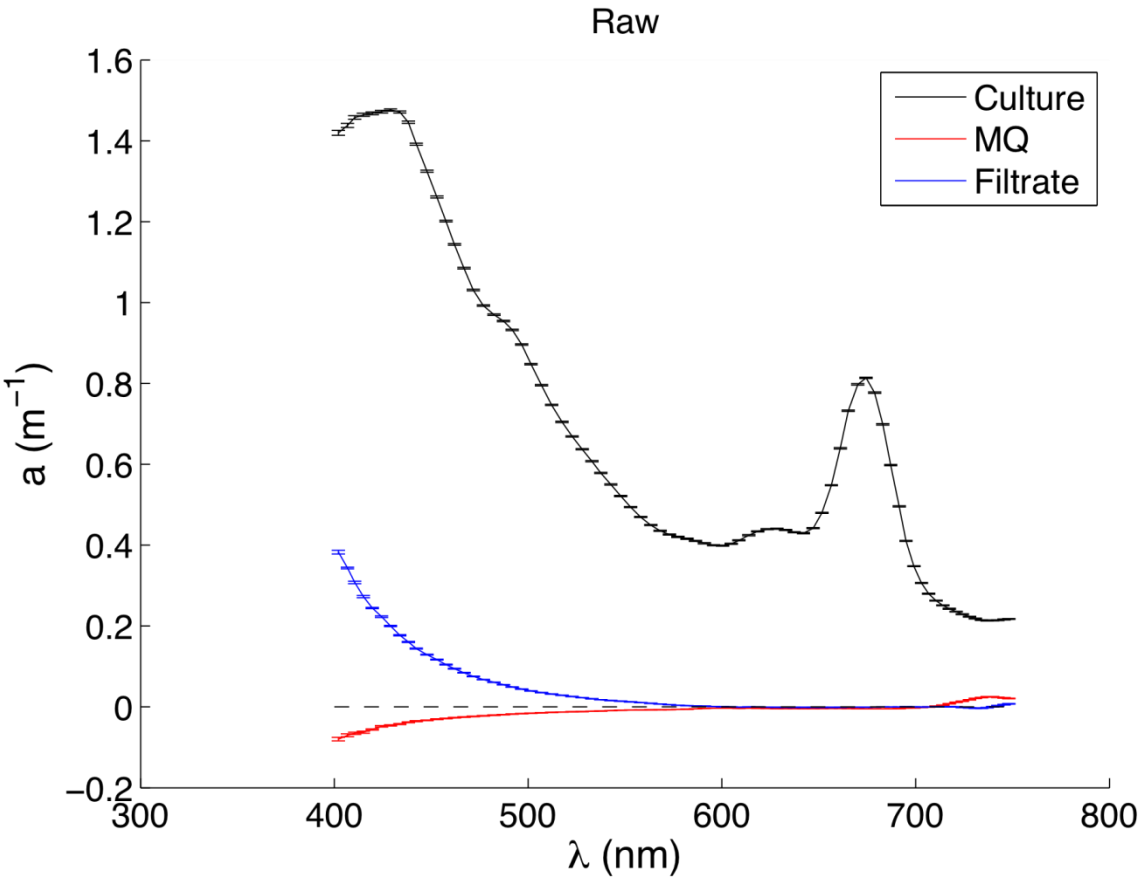

Figure 3. Uncorrected or raw $a_t(\lambda)$ (black line) and $a_g(\lambda)$ (blue line) values of the algal culture *Thalassiosira weissflogii*. Absorption by Mili-Q water as blank is also provided (red line).

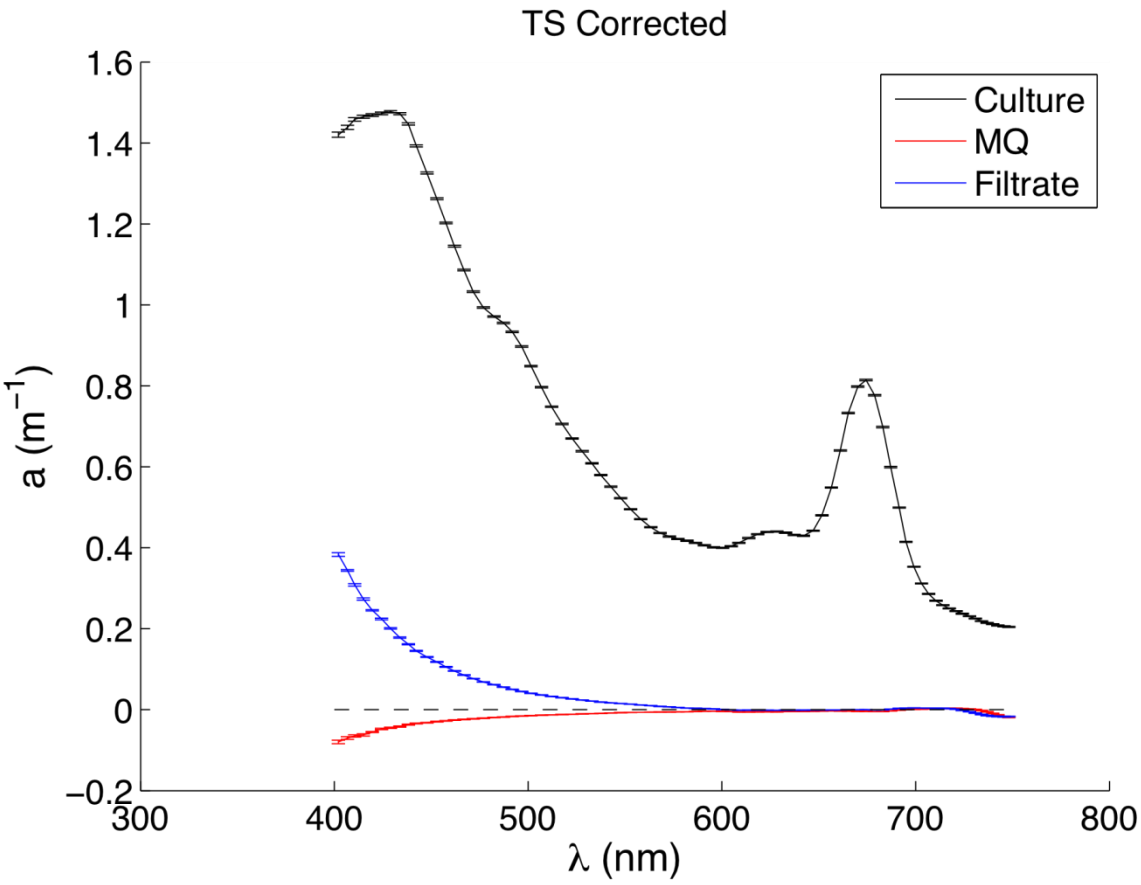

Figure 4. T/S corrected $a_t(\lambda)$ (black line) and $a_g(\lambda)$ (blue line) values of the algal culture *Thalassiosira weissflogii*. T/S corrected absorption by Mili-Q water as blank is also provided (red line).

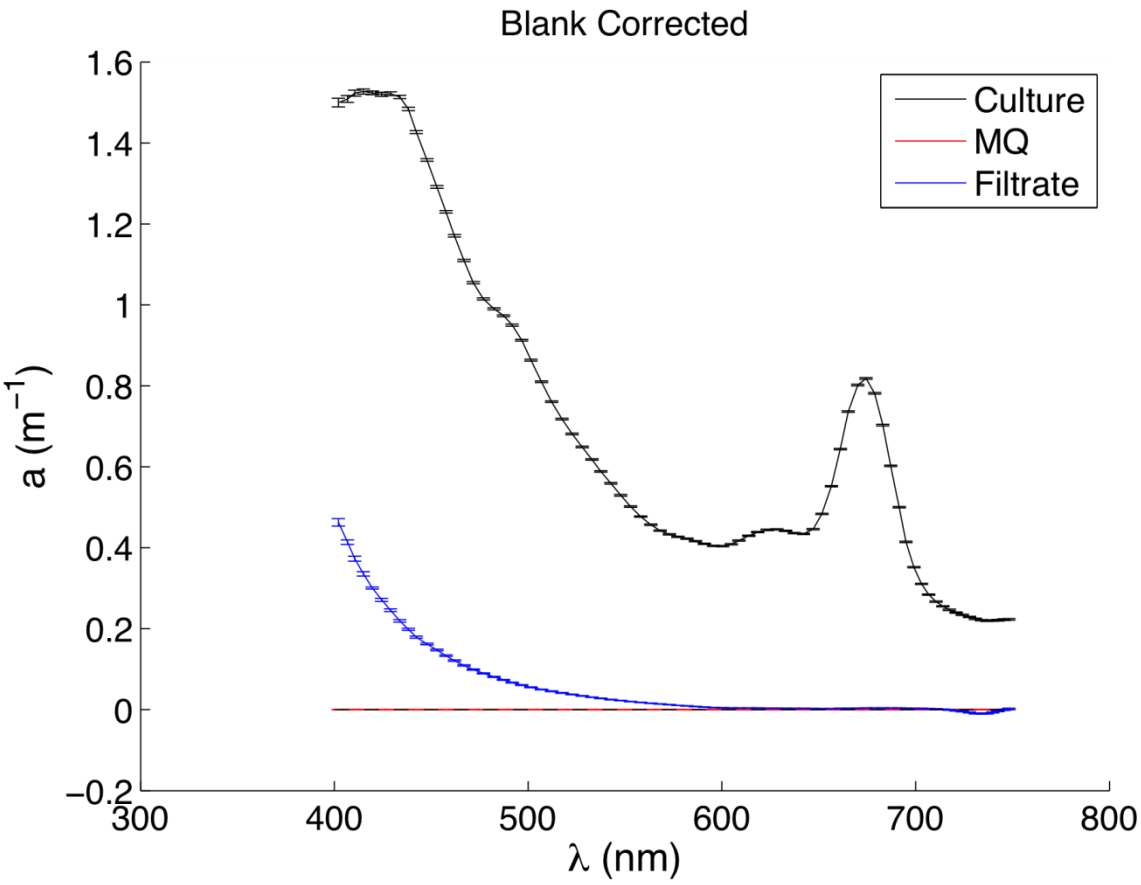

Figure 5. Blank (MQ) subtracted $a_t(\lambda)$ (black line) and $a_g(\lambda)$ (blue line) values of the algal culture *Thalassiosira weissflogii*. Blank subtracted absorption by Mili-Q water as blank is also provided (red line).

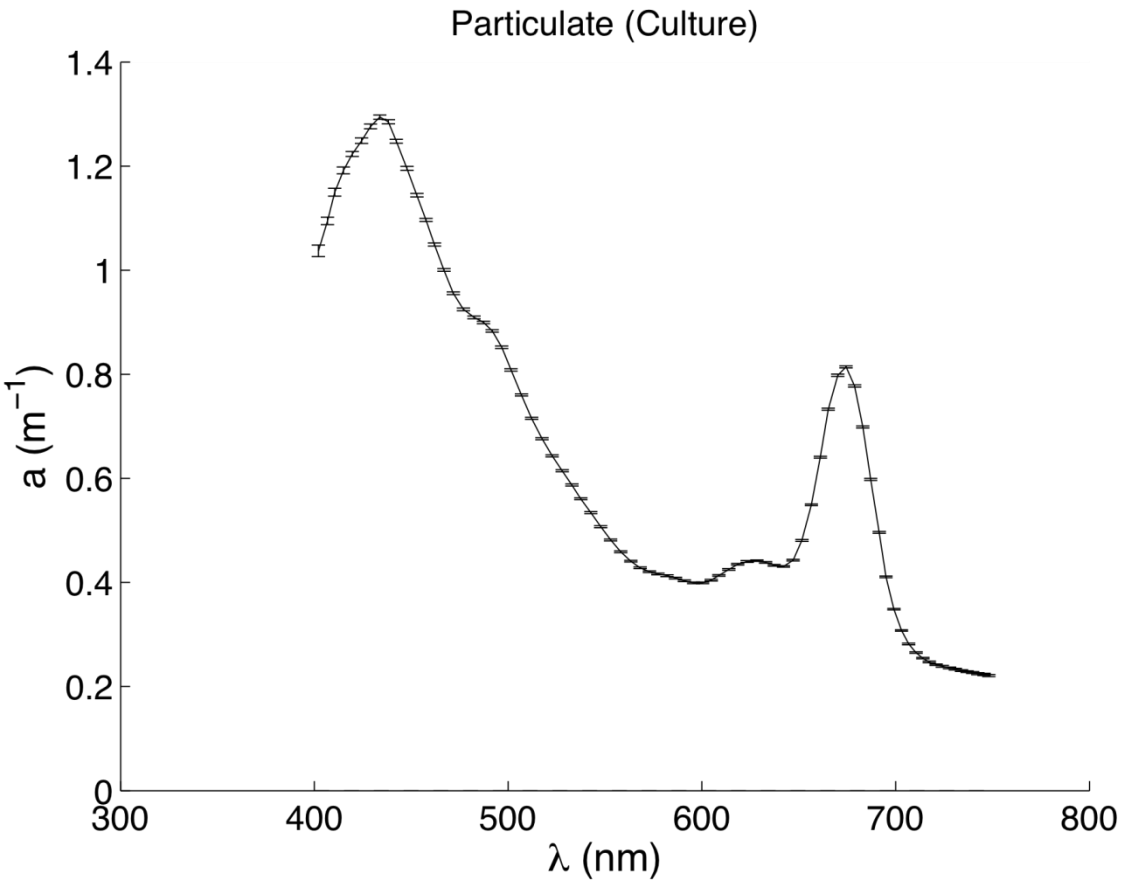

Figure 6. Particulate absorption spectrum, $a_p(\lambda)$ of the algal culture, *Thalassiosira weissflogii*, was calculated by subtracting $a_g(\lambda)$ from $a_t(\lambda)$.Notice the high values in the Near-Infrared wavelength range due to scattering.

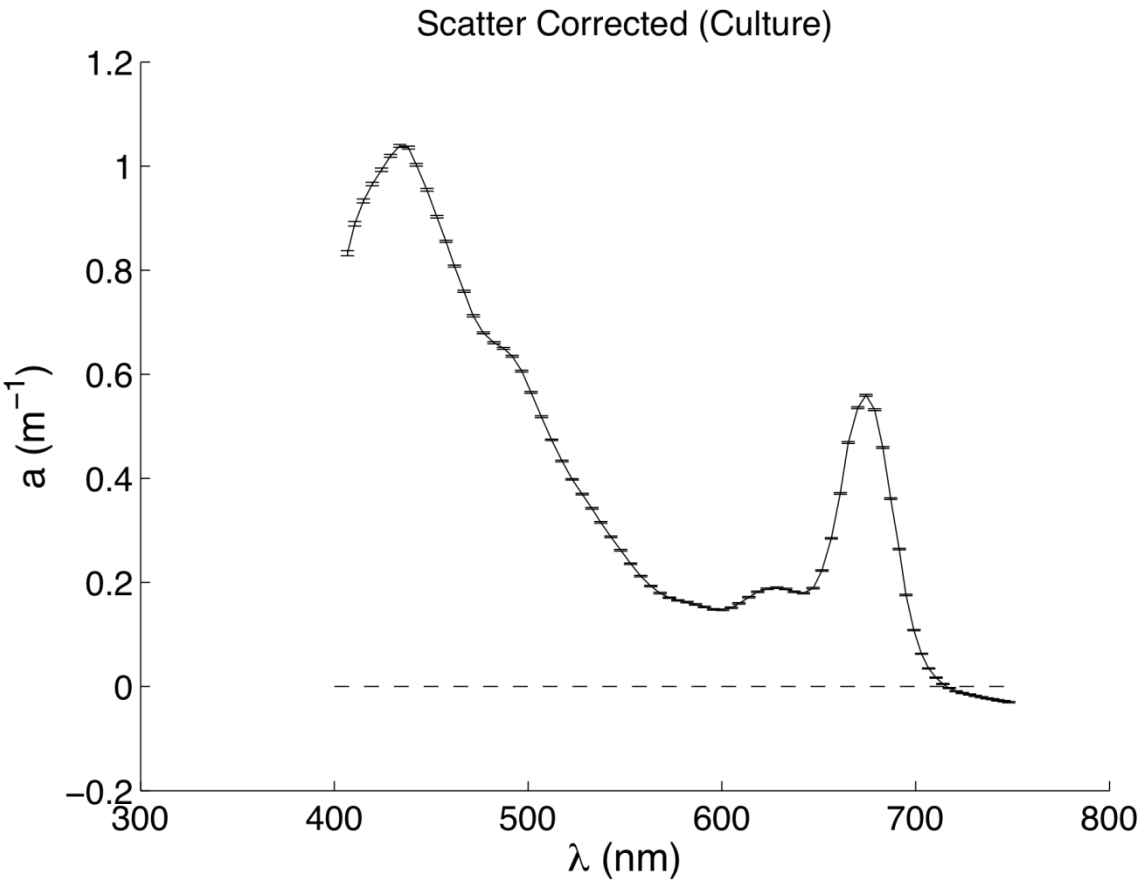

Figure 7. Spectrally based scattering correction was applied to the $a_p(\lambda)$ spectrum. Note that scatter correction show a negative offset in the Near-Infrared wavelength range. An iterative correction of residual temperature is likely required.

4.2. Field Sampling Results

Cruise samples from Gulf of Maine (GOM) were collected with an ac-s loaded in a frame with an attached pump for flow-through measurements. Two repeated casts were done-1) with a filter attached to the intake tubing for measurements of absorption and beam-attenuation coefficients of dissolved matter, $a_g(\lambda)$ and $c_g(\lambda)$, and 2) without any filter attached to measure the total absorption and beam-attenuation coefficients, $a_t(\lambda)$ and $c_t(\lambda)$.

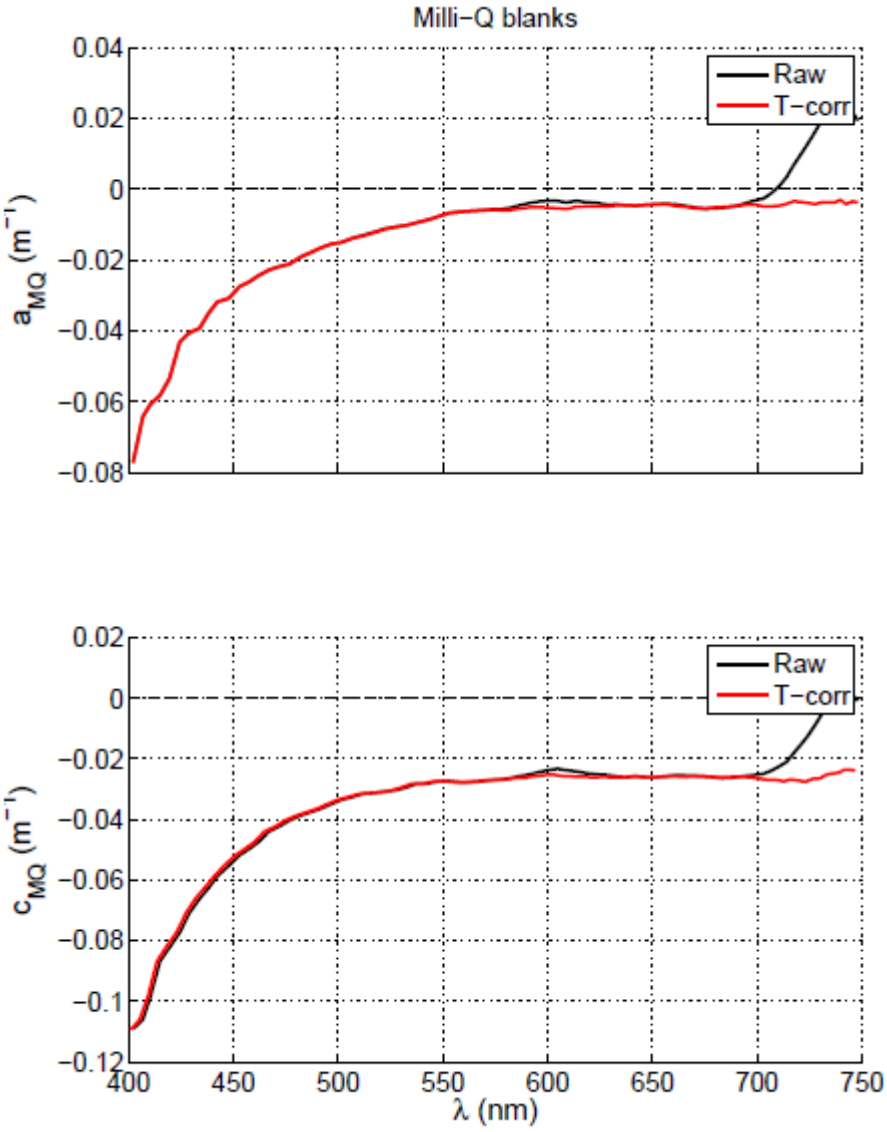

Figure 8. Milli Q temperature corrected a (top panel) and c (bottom panel).

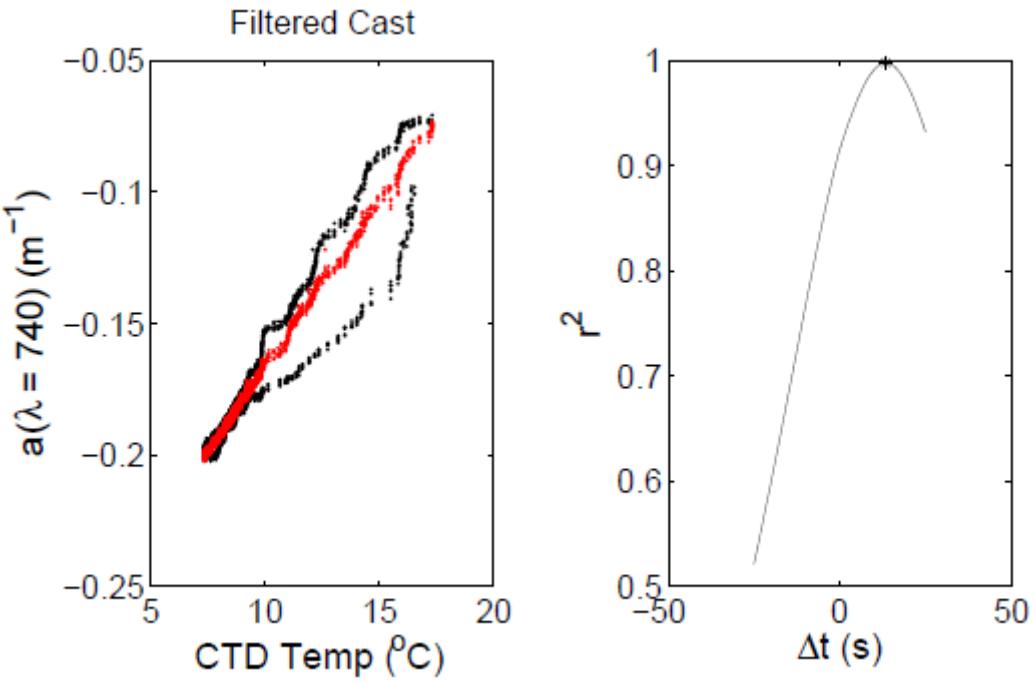

Figure 9. Left panel: Difference between corrected (red) and uncorrected (black) for filter lag. Right panel is correlation between temperature and absorption a (740) as a function of the pump lag. Time lag maximizes the correlation between the CTD temp and a (740). The black lines represent the up and down casts. On the way down (upper black line), the actual temperature (CTD thermostat) responds earlier than a (lambda = 740) to the decreasing temperature because of the time lag caused by the filter. On the upcast (lower black line), the CTD temp reads warmer temperatures than the time-lagged ac-s.

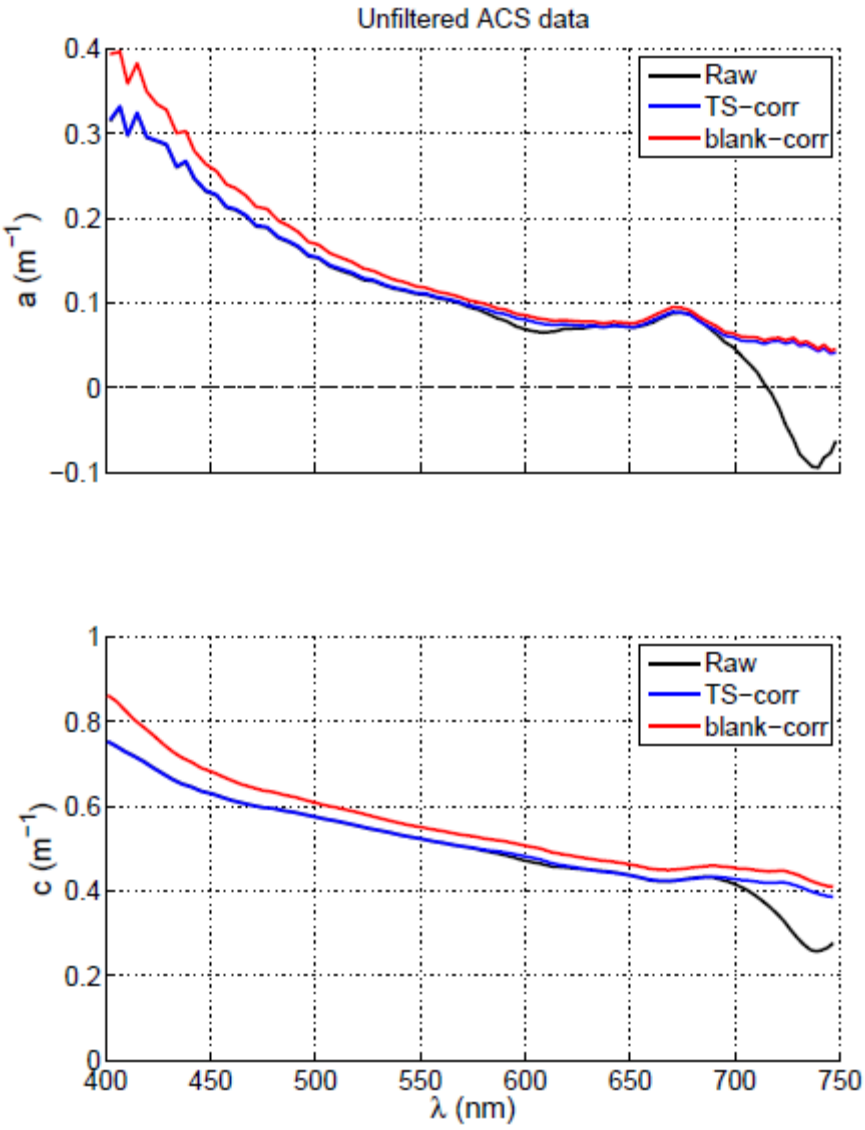

Figure 10. Unfiltered raw, blank subtracted and T/S corrected $a_t(\lambda)$ (top panel) and $c_t(\lambda)$ (bottom panel).

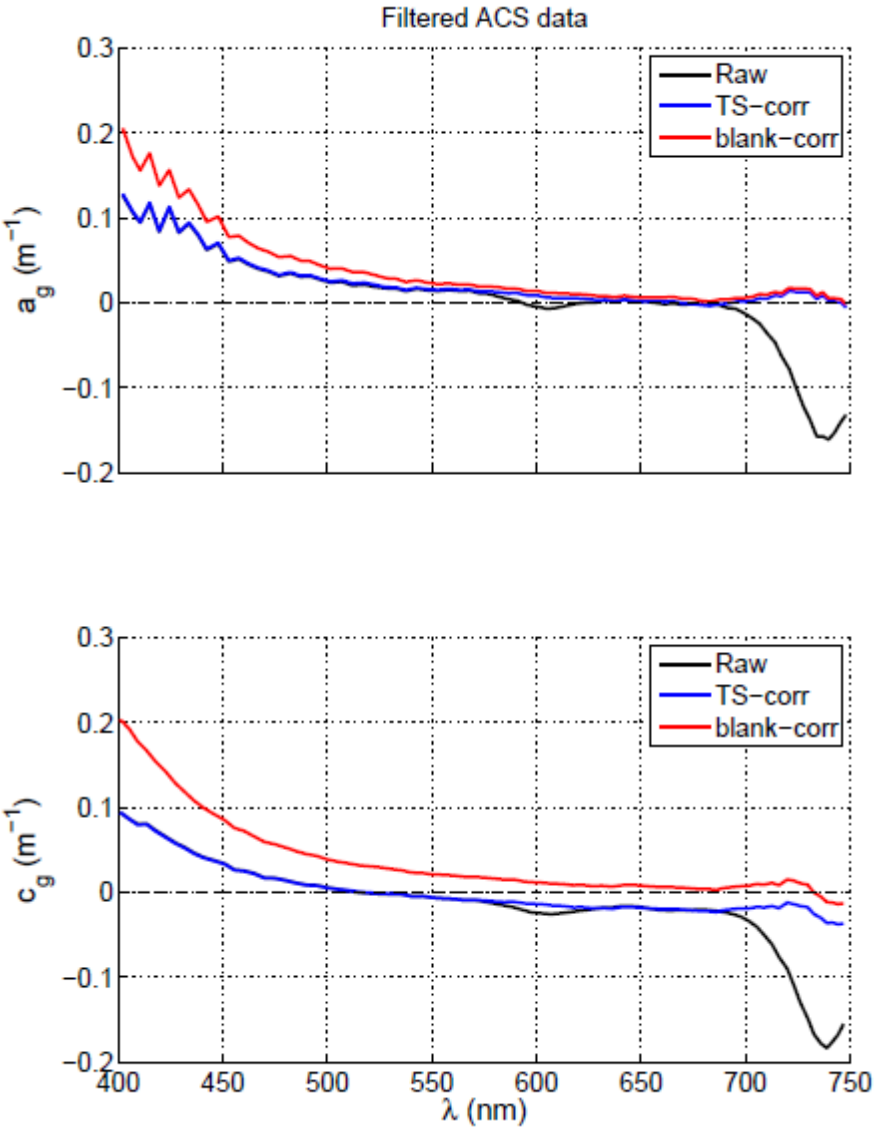

Figure 11. Filtered raw, blank subtracted and T/S corrected $a_g(\lambda)$ (top panel) and $c_g(\lambda)$ (bottom panel). Note the effect of imperfect residual temperature effect in red line on the $c_g(\lambda)$ plot.

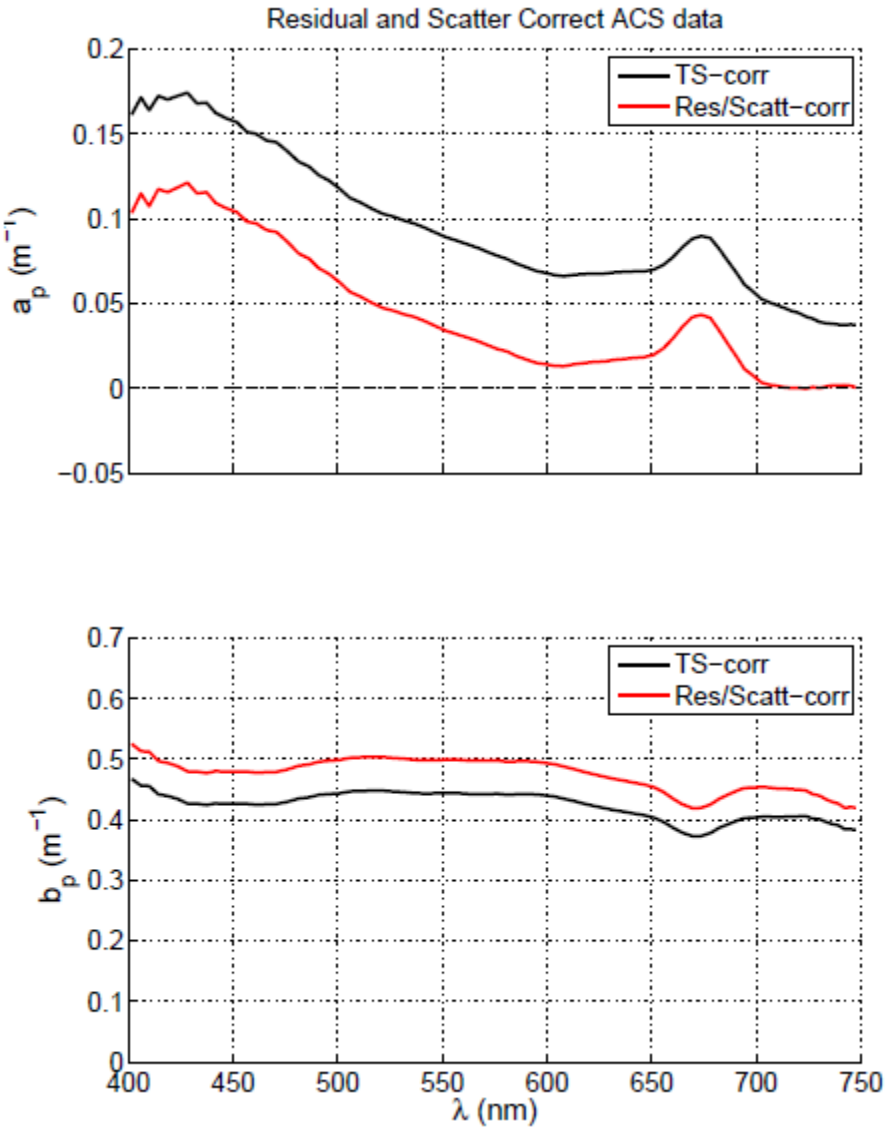

Figure 12. Filtered T/S and residual- and scatter-corrected a_p (top panel) and raw and blank corrected b_p (bottom panel).

BB9 Scattering Meters

Section guide

1. Instrument Description

The BB9 is an instrument manufactured by WET Labs that measures the volume scattering function (β, m^{-1} sr^{-1}) at nine wavelengths at a nominal angle of 117 degrees. The BB9 holds three BB3 instruments, and each of them measures backscattering at three different wavelengths (Figure 1.1).


a


b

Figure 1.1. a) ECO-BB9 instrument showing the three BB3s. b) BB3 detail. Colored circles are LED sources and adjacent black circles are the corresponding detectors.

Source lights are 9 LEDs at 412, 440, 488, 510, 532, 595, 650, 715, 880 nm (read section 3 for details on LED sources), and for each source there is a detector. Source beam and acceptance detector intersect at 117^{o}, because signal measured here is less determined by the type and size of materials in the water and more determined by the concentration of the materials (Boss and Pegau, 2003, BB9 user's guide) (Figure 1.2).

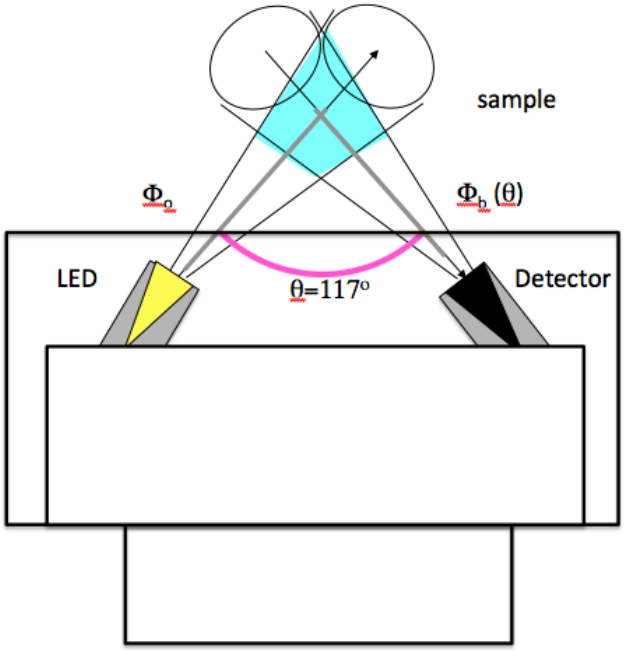

Figure 1.2. Schematic diagram of LED source and detector angle. Position of sample is shaded in blue.

The BB9 instrument raw output is in counts, collected at a sample rate of 1 Hz, which is then converted (as described in section 4) to volume scattering coefficients, $\beta(\theta,\lambda)$ with units of m^{-1} sr^{-1}, where θ is angle and λ is wavelength. The backscattering coefficient, $b_b(\lambda)$ can be estimated from $\beta(\theta,\lambda)$ by integrating over the backward hemisphere. The user should be aware that in water with high absorption, $\beta(\theta,\lambda)$ and $b_b(\lambda)$ will be under-estimated unless they are corrected for absorption along the path length of the BB9. This bias can be corrected if spectral measurements of the absorption coefficient are made, for example using a WET Labs AC-9 or AC-S (refer to section 4).

Links:
- User's guide:
www.**wetlabs**.com/products/pub/eco/**bb9**k.pdf

- Instrument specifications:
www.**wetlabs**.com/products/pub/specsheets/**bb9**sse.pdf

2. Data Measurement

2.1 Calibration

WET Labs performs factory calibrations on all BB9 instruments and provides a calibration sheet with scale factors and dark counts that allow conversion of raw counts to $\beta(117°, \lambda)$. Dark counts are measured by covering the sensors with black tape and immersing them in water. Scale factors are calculated by performing a series of BB9 measurements on a range of

concentrations of non-absorbing beads with known optical properties. Measurements of beam attenuation, *c*, are taken by another instrument and assumed to be equal to total scattering *b*, which is then converted to $\beta(117°, \lambda)$ using the known phase function of the beads at 117° (i.e. the ratio of $\beta(117°, \lambda)$ to $b(\lambda)$).

Dark counts are known to change with instrument setup, and can easily be measured in the field by covering sensors with black tape in the same manner. Therefore it is recommended that dark counts be measured in the same environment and setup in which measurements are made. In the case of a field study, at least one full cast should be made to test for effects of pressure, temperature or power supply fluctuations on dark counts.

Scale factors are more difficult to measure in the lab and therefore WET Labs calibrations are generally used. However, instrument response will change with time and possible biofouling, so it is recommended that the BB9 is sent to WET Labs for calibration before and after any major field deployment. After field deployment, a calibration should be requested both before and after cleaning, to account for the effect of any biofouling.

2.2 Physical Set Up

The BB9 instrument requires a power supply for the LEDs and electronics as well as a connection to a computer equipped with either a terminal program or WET Labs ECOView software. A test cable with a 6-socket connector is attached on the instrument side, while on the other side a cable split is used to connect to a 7-15V DC regulated power source (via battery leads) and the host computer (via a serial port).

The instrument must be securely mounted on its deployment hardware, without damaging the exterior casing. When launching the instrument do not forget to remove the plastic caps from the sensors and replace them as soon as the instrument is out of the water. The instrument should also be aligned so that light from the LED sources will not impinge on any part of the deployment hardware, as this will affect the sensor output.

(Please consult User's Guide for a detailed explanation of instrument set up).

2.3 Procedure

The BB9 begins measurements as soon as it is powered (note that when mounted with e.g. a DH4, recording can be scheduled or manually started) with a sample rate of 1 Hz. The instrument outputs raw data as counts ranging from 0 to 4120. Using a terminal emulator (such as HyperTerminal) networked to the instrument via the host computer's serial port, the user can capture raw data for subsequent processing. Data files are usually stored as delimited text files and can be imported into a range of numerical analysis applications including among others MS Excel or MATLAB.

Before any measurements are made, the sensor faces should be flushed with pure water and, if necessary, a soap solution. Acetone or other solvents should <u>not</u> be used to clean the sensor faces, as the sensor faces are composed of ABS plastic and optical epoxy which have the potential to be dissolved. After cleaning, the sensor faces should be gently patted dry with lens paper.

As noted in Section 2.1, take dark readings by placing black tape over each sensor. These 'dark counts' will allow for a subsequent subtraction of the instrument's baseline reading in the absence of light. (For a more detailed discussion on dark counts, please consult Section 4.1).

After the dark readings are taken, sample measurements can be made. Sample measurements can be made in the laboratory (e.g. as discrete samples at the bench top) or in the field (e.g. as continuous water column profiles). For laboratory measurements, samples should be analyzed (if possible) in order of increasing concentration. Take triplicate measurements of each sample to allow for a subsequent calculation of the measurement variance. After each sample, the sensor faces can be cleaned and an additional filtrate measurement should be made. Finally, after each sampling session, the instrument should be rinsed thoroughly, dried and stored in clean, dry conditions.

Simultaneous measurements of temperature and salinity should also be made in order to calculate the contribution of seawater to the scattering measurement. If absorption is likely to be high, spectral absorption measurements should also be taken, for example with an AC-9 or AC-S, to correct for absorption along the path length of the instrument. It is often assumed that dissolved matter does not contribute to backscattering. However, nonzero backscattering has been measured for seawater passed through a 0.2 µm filter (Dall'Olmo et al., 2009). Subsequently, if the goal is to obtain *particulate* backscattering, it is best to measure filtered as well as unfiltered samples if possible. This may be possible in a benchtop experiment or flow-through system, but is not for a profile. Measurement of filtered samples not only allows the quantification and subtraction of any scattering by dissolved matter, but, if taken frequently, also improves estimates of b_{bp} by accounting for instrument drift, poor estimates of dark counts, and poor estimates of scattering by seawater.

2.4 Particle Concentration Data

Backscattering measurements are often used as proxies for particle concentration, as a strong linear relationship between b_{bp} and particle concentration (e.g. particulate organic carbon concentration or total suspended mass concentration) is often observed in marine environments. In order to convert BB9 measurements into particle concentration measurements, discrete samples should be taken along with backscattering measurements for different levels of particle concentrations. The relationship between b_{bp} and the concentration of the particle assemblage of interest can then be obtained by comparing the particle concentrations of each discrete sample and their corresponding BB9 backscattering estimates. The discrete samples should be analyzed for particle concentration and then compared with their corresponding BB9 measurements in order to establish the relationship between b_{bp} and concentration for the particle assemblage of interest. In the lab, samples can be taken directly from the tank, ideally from the same level where the BB9 is located. In the field, samples can be taken from a Niskin bottle, which should be attached to the same cage as the one containing the BB9 if possible. If the bottle sample and BB9 measurements are not taken simultaneously it is preferable to match the bottle sample with the BB9 reading taken at the same density. This will not necessarily be at the same depth, as internal waves can move water vertically between casts, or between upcast and downcast.

3. Verification of LED Output Wavelengths

Ancillary data is necessary to determine possible variations in the instrument LED output spectra compared to the reported factory BB9 wavelengths. Variations between the actual and reported band center wavelengths and Full Width Half Maximum (FWHM) are important to measure in order to further understand the uncertainties in the instrument measurements.

Radiometric measurements of each of the nine LEDs are performed to evaluate variations in the actual and reported band centers. These measurements are collected by placing a radiometer approximately 1 cm from the face of the LED of interest for 10 seconds. The collected spectra are then averaged and compared to the LED band centers reported by Wetlabs.

This example uses a Satlantic HyperOCR radiometer (see chapter entitled "Hyperspectral Radiometers", pg 116) to measure the sources of the LEDs reportedly at 412, 440, 488, 510, 532, 595, 650 and 715 nm and an ASD Fieldspec HandHeld radiometer (See http://support.asdi.com/Document/Documents.aspx for further information) for 880 nm (Figure 3.1). Measurements show that the peaks (maximum wavelength) at 412, 488, 510, 532, 595 and 880 nm are actually shifted towards the blue and peaks at 440, 650 and 715 towards the red relative to the reported band centers (Figure 3.1). The radiometer measurements also highlight variations in the full width half maximum (FWHM) between the LEDs (Table 3.1). These measured variations are specific to the BB9 and radiometers used in this particular experiment and only represent the spectral output of the LED. The radiometric measurements are not representative of the end spectral response of the detector because they do not account for the effects of the BB9 detector and filter. Because this comparison is based on accessory measurements, the user must also be aware of uncertainties introduced by the radiometer itself. Ideally the radiometric measurements should be collected directly after the radiometer has been factory calibrated.

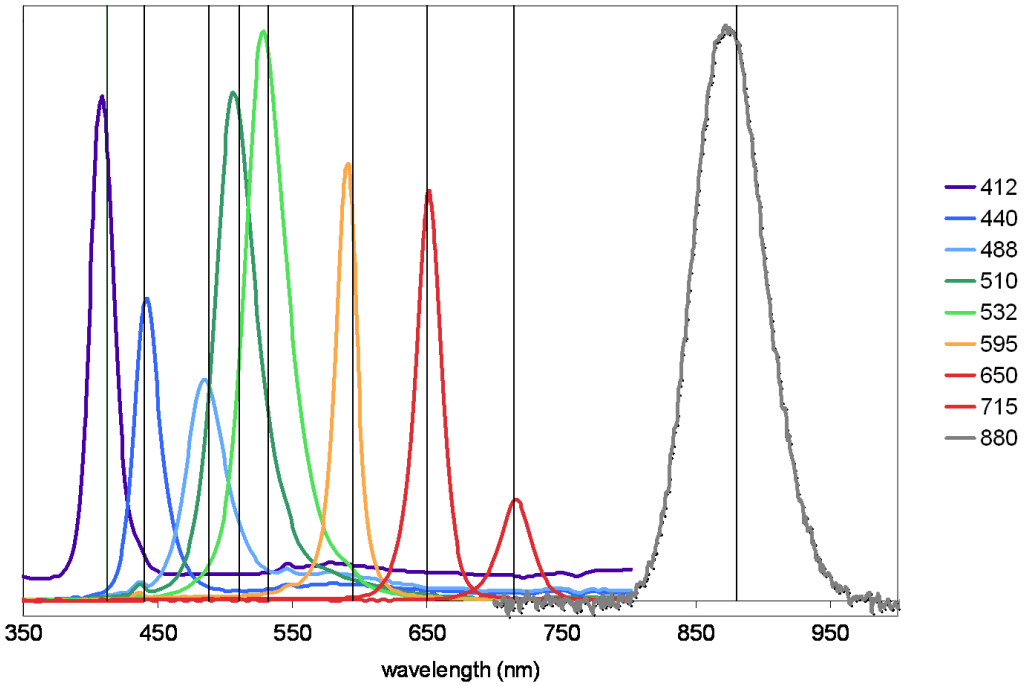

Figure 3.1 LED output spectra measured by a Satlantic HyperOCR (412, 440, 488, 510, 532, 595, 650 and 715 nm) and an ASD (880). Variations in the radiometer based LED output spectra (color curves) and reported band peaks (grey vertical lines) are evident for all bands.

Table 3.1 Comparison between factory and measured band center wavelengths, difference between the two wavelengths, full width half maximum (FWHM) and the low and high FWHM wavelengths.

Factory (nm)	Measured (nm)	Difference	FWHM	low	high
412	409	3	21	397	418
440	442	-2	24	430	454
488	485	3	38	468	506
510	505	5	36	490	526
532	529	3	37	512	549
595	592	3	17	581	598
650	652	-2	22	640	662
715	715	0	28	702	730
880	872	8	91	831	922

4. Data Processing

Cruise data

A BB9 profile that was taken under the following conditions will be used as an example to show the steps in processing BB9 data.
Date: July 20, 2011
Time: 15:31 GMT
LAT: 43° 44.9 N
LON: 69° 29.9 W
Cloud cover: 5%
Wind Speed: 3 knots

The BB9 was set in an IOP package (Figure 4.1), which includes an AC-S for measuring attenuation and absorption coefficients, a CTD measuring temperature, salinity, pressure, conductivity, and density, a Chlorophyll fluorometer and a CDOM fluorometer. Raw counts from the profile are shown in Figures 4.2 and 4.3.

Figure 4.1. Profiling package containing the BB9. Sensor faces are pointed downward at bottom of cage.

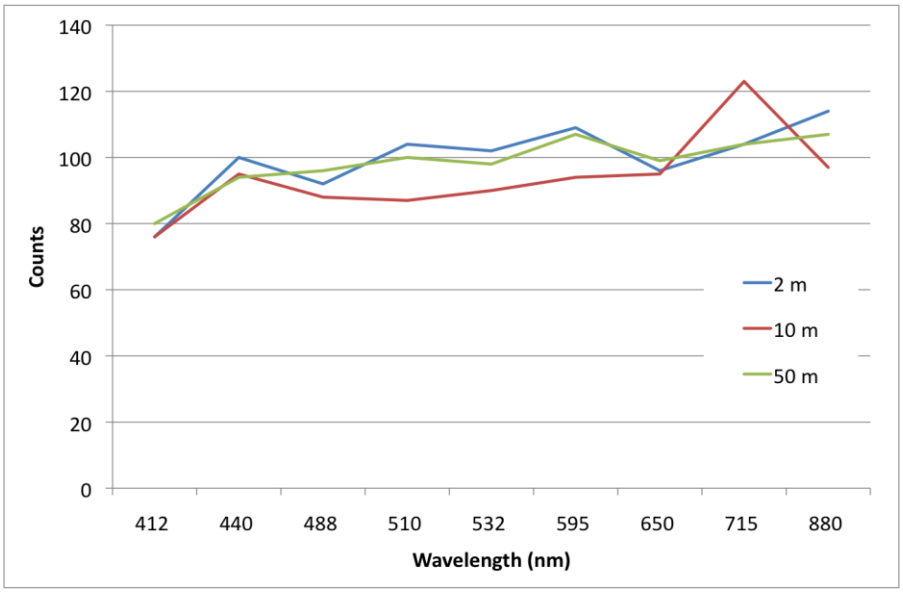

Figure 4.2 Raw output of the BB9 at all wavelengths and three depths.

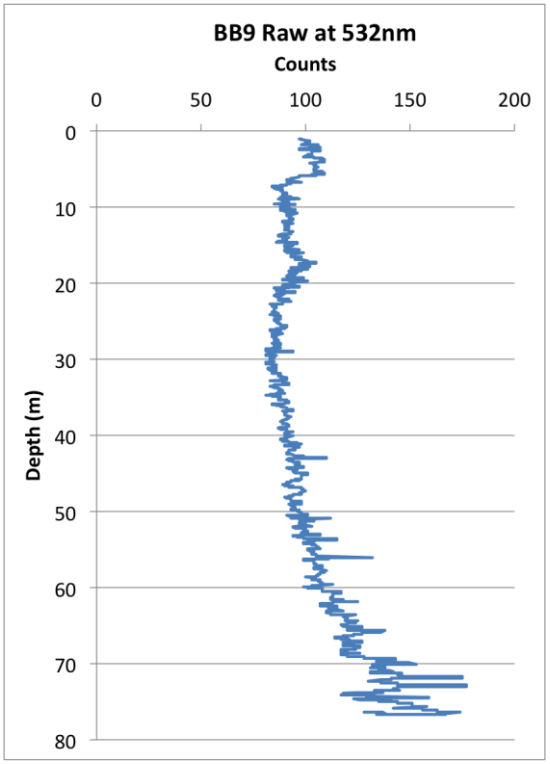

Figure 4.3. Raw output of a single BB9 wavelength (532 nm) vs. depth (m) during the downcast of a vertical profile.

Summary of data processing steps
Five steps are necessary to convert raw counts into the particulate backscattering coefficient $b_{bp}(\lambda)$.

Step 1. Subtract dark counts
Step 2. Convert to $\beta(117°)$ using scale factor
Step 3. Correct for absorption
Step 4. Subtract β_{sw} to obtain β_p
Step 5. Convert to b_{bp}

4.1 Dark Counts

Dark counts are the raw counts that the BB9 reports when the sensor is blocked so that it receives no light. Dark counts must be measured and subtracted separately for each of the 9 sensors associated with the 9 wavelengths. Dark counts are provided by the manufacturer in the calibration document for each wavelength. However, dark counts can vary with time and according to instrument setup, so it is best to measure them yourself in the same setup used to measure the sample of interest. Dark counts can be measured by completely covering the sensors with black tape (ensure that when removing the tape no glue remains).

Table 4.1 shows a comparison of dark counts measured in three ways for the same BB9: 1) dark casts taken in the field, 2) measured in a laboratory sink, and 3) factory dark counts. For dark casts taken in the field (Cast1, Cast2 and Cast3), medians and standard deviations are shown for the entire cast. For these casts no significant trend with depth and/or time has been observed. Both medians and standard deviations of the dark counts are higher for the three dark casts than for the factory dark. Differences range from 3 at high wavelengths to 16 at low wavelength exceeding the standard deviations of the dark counts. Standard deviations of dark counts measured in the lab sink are even higher, and median values differed widely at some wavelengths from both factory and field counts. These results highlight the strong dependence of dark counts and instrument precision on instrument setup. The very high standard deviations in the lab sink suggest the possibility of a grounding problem (e.g. the light of the sensor reaches the side and/or the bottom of the water container). However, the dark counts measured during the three dark casts are consistent within one standard deviation. For this reason we chose the average dark count of the three dark casts as the appropriate dark count to subtract from the BB9 profile.

Table 4.1. Median dark counts (± standard deviation) for three dark casts taken on two days, one dark time series taken in a lab sink and the factory dark counts and scale factors.

λ (nm)	Cast1	Cast2	Cast3	mean from 3 casts	lab sink	Factory Dark	Casts - factory	Factory scale factor (m^{-1} sr^{-1} $count^{-1}$)
412	52±8.6	49±7.4	48±6.1	50	53±17.49	34±0.7	16	2.26E-05
440	57±3.1	55±3.9	55±2.4	56	84±66	47±0.6	9	2.17E-05
488	55±3.1	52±1.9	52±1.7	53	53±53	44±0.9	7	1.98E-05
510	57±2.8	56±2.4	57±2.3	57	57±10	52±0.8	5	1.77E-05
532	54±1.3	55±1.0	55±0.9	54	72±26	50±0.7	4	1.62E-05
595	54±1.2	55±1.4	55±1.0	55	61±31	50±0.9	5	1.29E-05
650	53±2.0	52±3.0	52±2.5	52	53±9	46±1.2	6	1.08E-05
715	53±1.1	53±1.3	53±1.0	53	50±26	50±1.8	3	9.04E-06

4.2 Scale Factor and how to Calculate β

Each wavelength has a scale factor associated to it provided in the factory calibration document of the instrument. Beta for each wavelength is then calculated as follows:

$$\beta(\theta) = (\text{signal measured - dark}) * \text{scale factor} \qquad \text{Eq. 4.1}$$

cruise: we calculated β using Eq. 4.1. with the mean dark counts shown in Table 4.1. and scale factors provided by the factory, which are also displayed in Table 4.1.

4.3 Absorption (and Scattering) Correction

In any instrument measuring β(θ), light can be absorbed or scattered on its path from the source to the sample volume to the detector (see Figure 1.2 for schematic). Absorption along the path length will decrease the amount of scattered light that reaches the detector. Additionally, backward or side scattering can decrease the amount of emitted light that reaches the sampling volume and decrease the amount of scattered light that travels from the sample volume to the detector. These effects are minimized thanks to the very short path length of 3.91 cm from light source to sample volume to detector. However, for very high particle and/or colored dissolved matter concentrations, this effect can become important, and should be corrected for.

4.3.1 Absorption Correction

If the absorption coefficient of particles and dissolved matter is known (e.g. through AC-9 or AC-S measurements), the effect of absorption along the path length can be corrected using Eq. 4.2, where L is the path length in meters and a is the absorption coefficient due to particles and dissolved material in inverse meters.

$$\beta(\theta)_{corrected} = \beta(\theta)_{measured} e^{La} \qquad \text{Eq. 4.2}$$

It should be noted that pure water absorption, assumed to be constant, should *not* be included in the correction because its effect should already be accounted for in the factory calibrated scale factor. Fig. 4.4 shows the magnitude of the pathlength correction factor (e^{La}) vs. the absorption of particulate and dissolved matter (a_{pg}) for the BB9 (L = 0.0391 m). A ~5% correction is necessary at a = 1.25 m^{-1} and a ~10% correction is necessary at a = 2.5 m^{-1}. At a < 0.1, the correction factor is < 0.5% and therefore considered as negligible. For the cruise, we applied an absorption correction using a_{pg} obtained from an AC-S (mounted on the same cage as the BB9). The calibrated values of β(117°) are shown before and after the absorption correction in Figures 4.5 and 4.6. The effect of this correction is minimal. Note that we could not measure absorption at 880nm with the AC-S, subsequently the corrected β is missing at this wavelength.

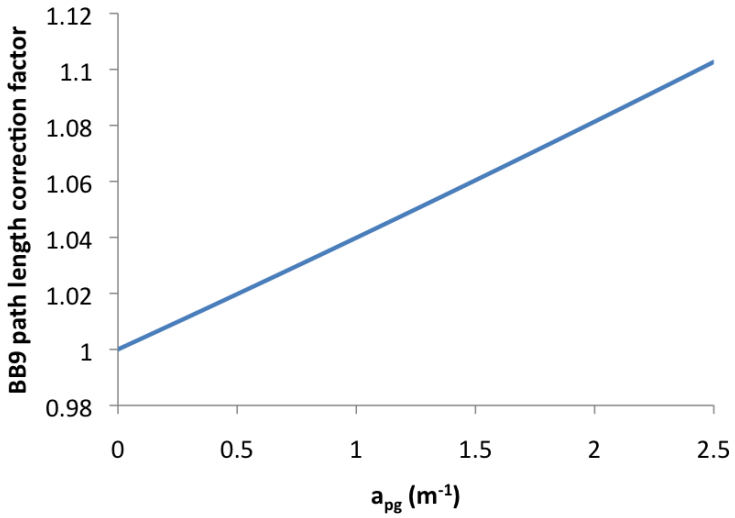

Figure 4.4. Correction factor e^{La} required to compensate for absorption in the path length of the BB9, vs the absorption coefficient due to particulate and dissolved matter. This figure is derived from Eq. 4.2, using the BB9 path length of 3.91 cm.

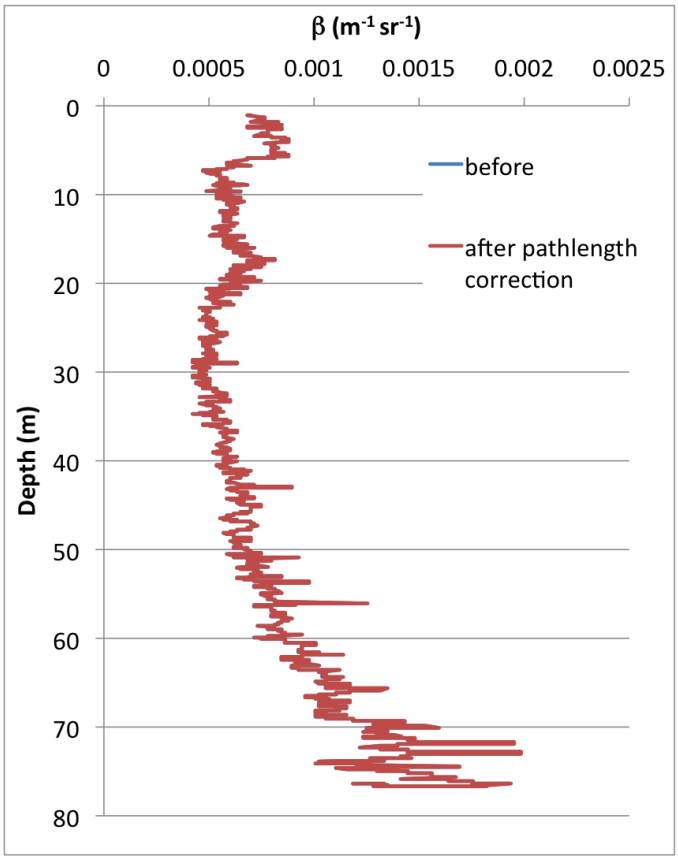

Figure 4.5. Beta calculation vs. depth before and after pathlength absorption correction. Data displayed corresponds to the 532 nm channel only.

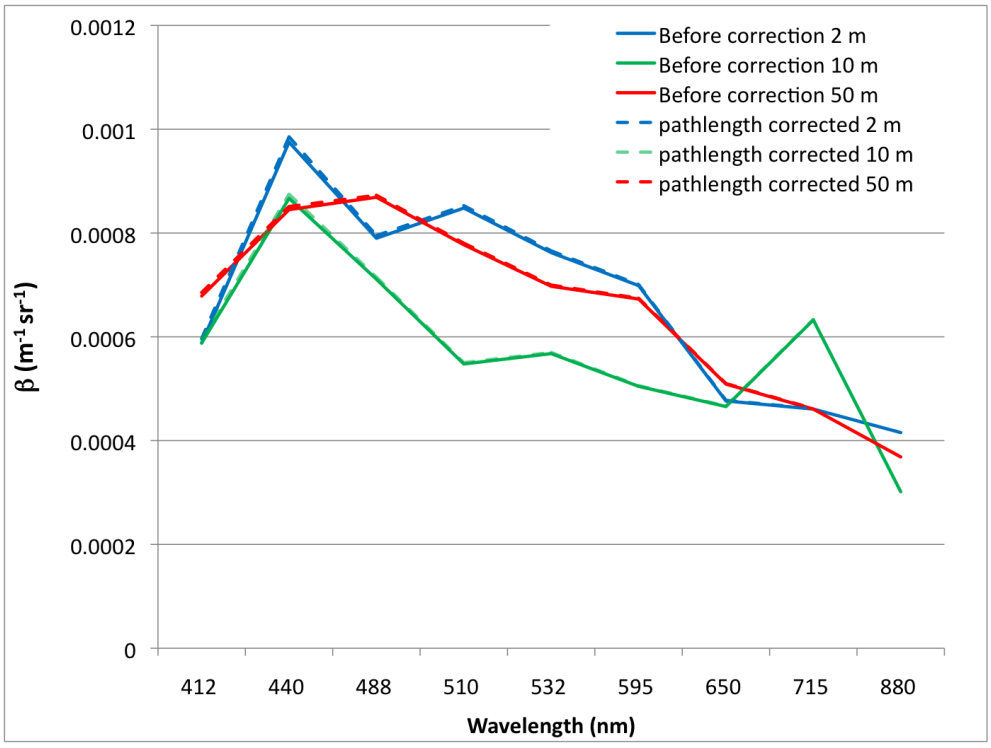

Figure 4.6. Beta calculation vs. wavelength before and after pathlength and absorption correction. Data displayed corresponds to three different depths (2, 10, 50 m, respectively).

4.3.2 Scattering Correction

It is less certain what is the appropriate way to correct for the effect of scattering within the instrument path on estimates of $\beta(\theta)$. Near forward scattering should have minimal effect on instrument readings. Side and backward scattering should be roughly proportional to $\beta(\theta)$, so their effects should increase at higher $\beta(\theta)$, producing a non-linear relationship between $\beta(\theta)$ and raw instrument counts. However, WET Labs calibrations show a high degree of linearity ($R^2 > 0.99$; see BB9 manual). This suggests that the effect of scattering in the path length is very small, at least within the range of *b* measured in the WET Labs calibrations (typically from ~0.05 m^{-1} to 2-4 m^{-1}). Any effect that *does* occur in this range will be partially incorporated in the WET Labs scale factor, and therefore the manufacturer does not recommend any scattering correction. If *b* exceeds the range used in the WET Labs calibration, a combined scattering and absorption correction may be necessary, and would take the form of Eq. 4.3, where ε is the fraction of scattered light that is lost from the BB9 path (consisting of backward and sideways scattering). This equation was not used on the data presented here. Instead, only the absorption correction (Eq. 4.2) was used.

$$\beta(\theta)_{corrected} = \beta(\theta)_{measured} e^{L(a+\varepsilon b)} \qquad \text{Eq. 4.3}$$

4.4 Calculation of β_{sw} and Water Correction

The particulate scattering $\beta_p(\theta)$ is obtained by subtracting the scattering by pure seawater, $\beta_{sw}(\theta)$, from the total measured scattering $\beta(\theta)$ (Eq. 4.4). Implicit in this equation is the assumption that colloids and other dissolved matter do not scatter light. As mentioned in Section 2.3, this assumption can be tested by measuring filtered water, but this is difficult in a profile setup and therefore Eq. 4.4 is used for the cruise data presented in the present document.

$$\beta_p(\theta) = \beta(\theta) - \beta_{sw}(\theta) \qquad \text{Eq. 4.4}$$

Zhang et al. (2009) have developed a theoretical algorithm for estimating scattering due to seawater (β_{sw}), based on the temperature, salinity, and depolarization ratio. See Appendix for Matlab code used to implement this algorithm. We estimated β_{sw} according to Zhang et al. (2009) for the 9 wavelengths of the BB9, for θ=117, with a depolarization ratio of 0.039 and the temperatures and salinities measured by the CTD (attached to the same cage as the BB9). We then subtract β_{sw} from the absorption and pathlength corrected β, using Eq. 4.4., and obtain β_p at angle 117. Estimates of $\beta(117°)$ before and after the subtraction of $\beta_{sw}(117°)$ are shown in Figures 4.7 and 4.8.

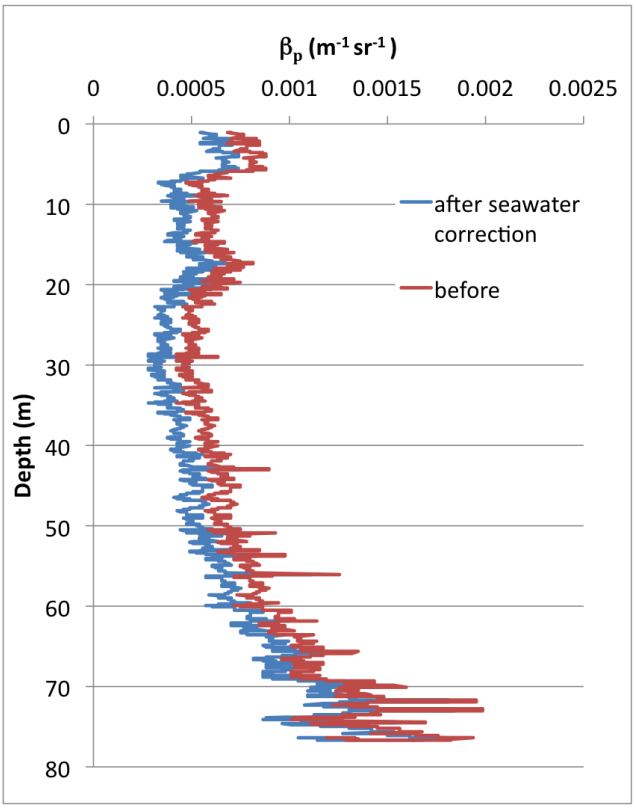

Figure 4.7. Beta calculation vs. depth before and after seawater correction. Data displayed corresponds to the 532 nm channel only.

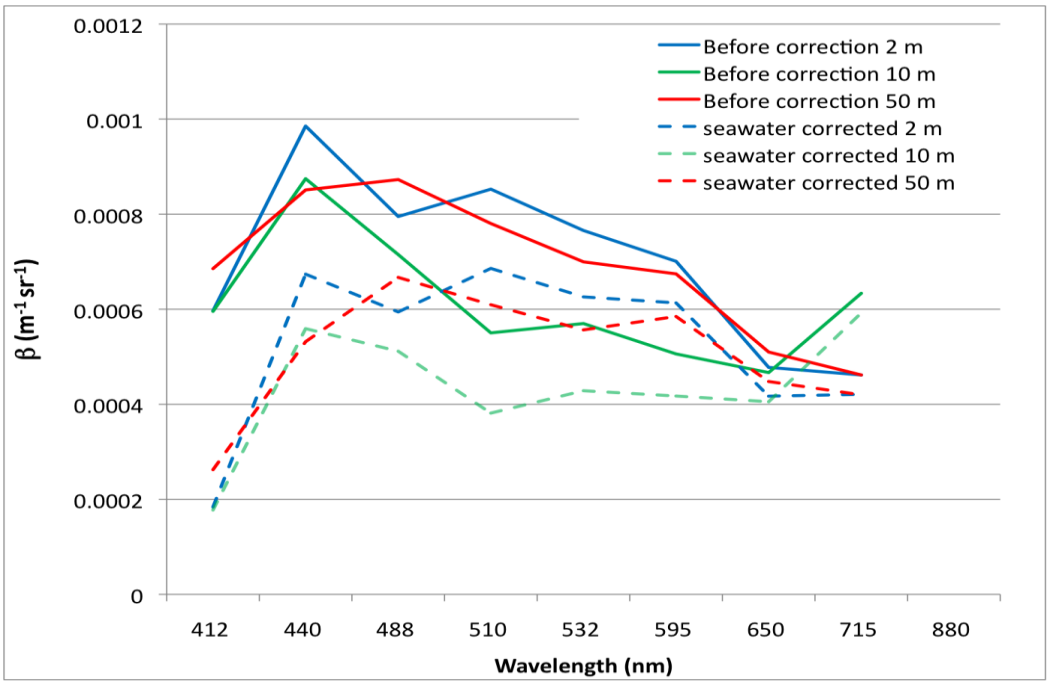

Figure 4.8. Beta calculation vs. wavelength before and after beta seawater correction. Data displayed corresponds to three different depths (2, 10, 50 m, respectively).

4.5 Conversion to b_{bp}

Particulate VSF from a single angle can be converted to particulate backscattering ($\mathbf{b_{bp}}$) by multiplying by 2π and a dimensionless factor (χ) (Eq. 4.5):

$$b_{bp} = 2\pi\chi\beta_p(\theta) \qquad \text{Eq. 4.5}$$

The χ factor is angle-dependent; some estimations for χ can be found in e.g. Boss and Pegau (2001) and Sulivan and Twardowski (2009). In this particular case, we used χ = 1.1 for the angle 117° (Boss and Pegau, 2001). However, it should be noted that work is being done to revise both χ factors and centroid angles in WET Labs scattering instruments (Sullivan et al., submitted manuscript). Estimates of b_{bp} calculated using Eq. 4.5 are presented in Figures 4.9 and 4.10. The profile data in Figure 4.10 are bin averaged at 1 m intervals.

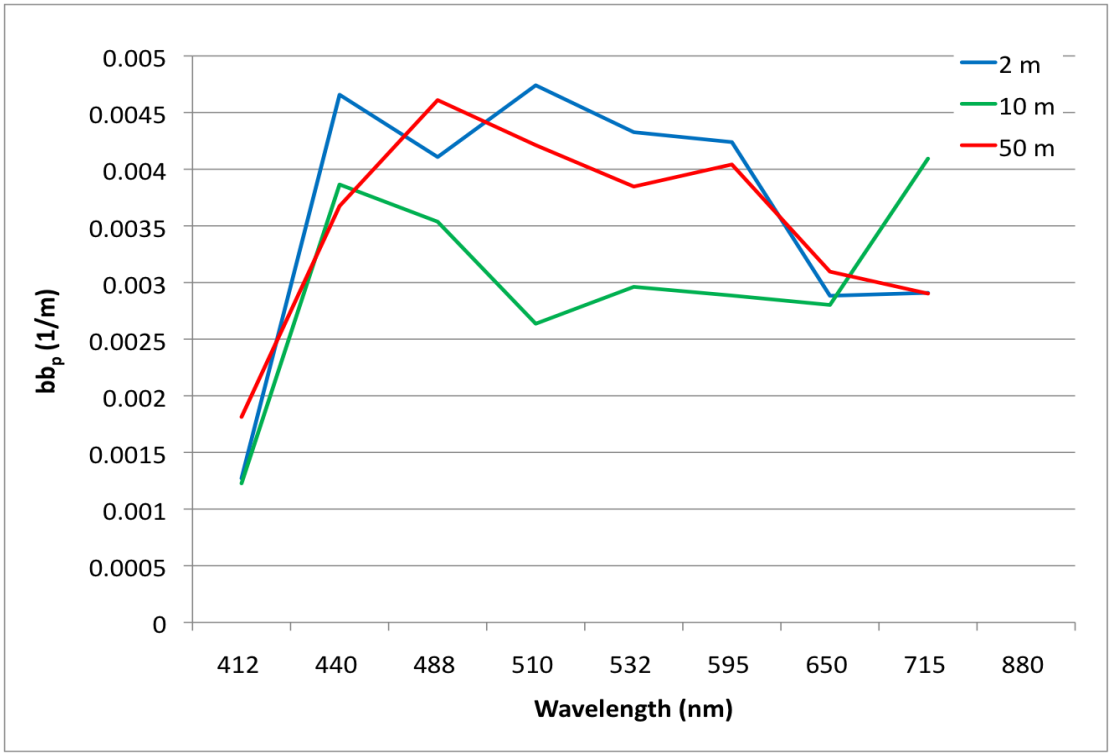

Figure 4.9 Particulate Backscattering (b_{bp}) vs. wavelength. Data displayed corresponds to three different depths (2, 10, 50 m, respectively).

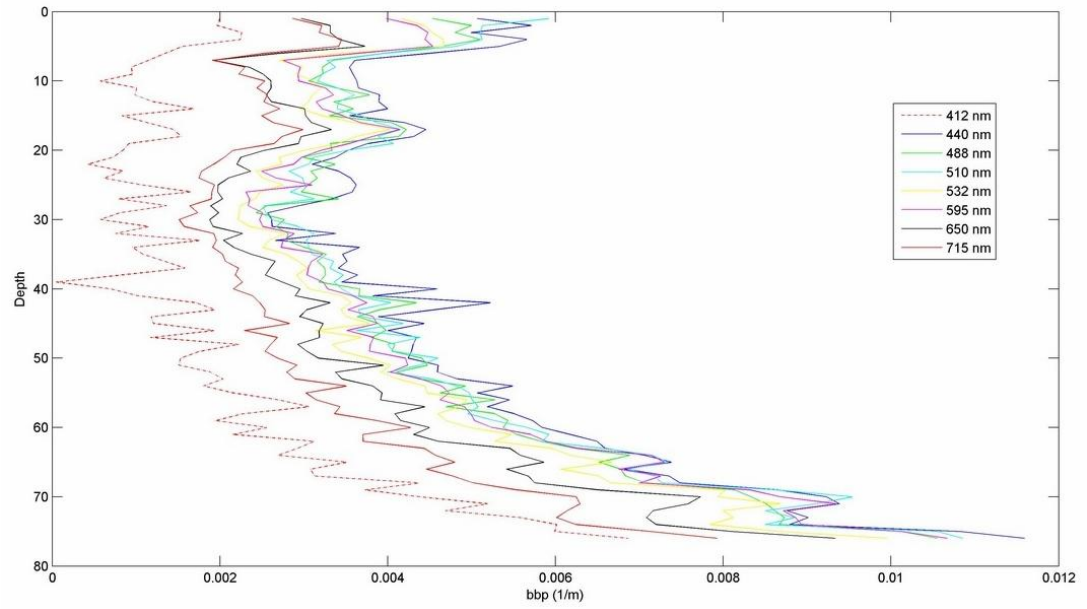

Figure 4.10. Particulate Backscattering (bbp) vs. depth (m) for cast 1. Each color corresponds to one of the BB9 channels.

5. Data Results and Interpretation

5.1 b_{bp} and Rrs

Backscattering is approximately related to Rrs according to Eq. 5.1 (e.g. Morel and Prieur, 1977; Gordon, 1994)

$$R_{rs} \propto b_b / (b_b + a) \qquad \text{Eq.5.1}$$

A primary goal of collecting the cruise data presented here is to obtain closure between, on the one hand, remote-sensing reflectance (*Rrs*) modeled from in-situ IOPs based on the above equantion and using the radiative transfer software Hydrolight, and, on the other hand, *Rrs* estimated from in-situ radiometric measurements. To this end, accurate b_{bp} measurements are vital, given the relationship in Eq. 5.1. Please refer to the chapter on closure (pg 155) for the results of this exercise and the chapter on hyperspectral radiometers (pg 116) for discussion of radiometric quantities and *Rrs*.

5.2 Proxy for particle concentration

A strong relationship often exists between particle concentration and b_{bp} in the ocean. However, this relationship can vary with particle type. Subsequently, in order to use b_{bp} as a quantitative proxy for particle concentration, discrete measurements of particle concentrations such as particulate organic carbon concentration or total suspended mass concentration are necessary. Such measurements were not taken on this cruise, so we can only discuss patterns in relative particle concentration.

Backscattering is moderately high in the top 5 m and from 15-20 m (Fig. 4.10), most likely indicating high plankton concentrations in the surface mixed layer and at a sub-surface layer. Absorption data from an AC-9 mounted together with the BB9 indicate high phytoplankton

absorption in this sub-surface layer, suggesting that the higher backscattering here is caused by a higher concentration of phytoplankton. Backscattering also increases with depth (Fig. 4.10), likely caused by increasing concentrations of particles re-suspended from the bottom, which is at approximately 90 m depth.

5.3 Backscattering ratio

A profile of the backscattering ratio is obtained by dividing the b_{bp} data reported here by the b_p data derived from the AC-S (see chapter on AC-S, pg 73). As shown in Figure 5.1, backscattering ratio increases from about 0.0075 near the surface, where phytoplankton likely dominate, to more than 0.03 at 90 m deep, where mineral particles likely dominate. These results are consistent with both theoretical and empirical results showing that backscattering ratio is correlated with the index of refraction, which is low for phytoplankton (~1.02) and higher for inorganic particles, and tends to increase monotonically with depth in shallow waters (Boss et al., 2004).

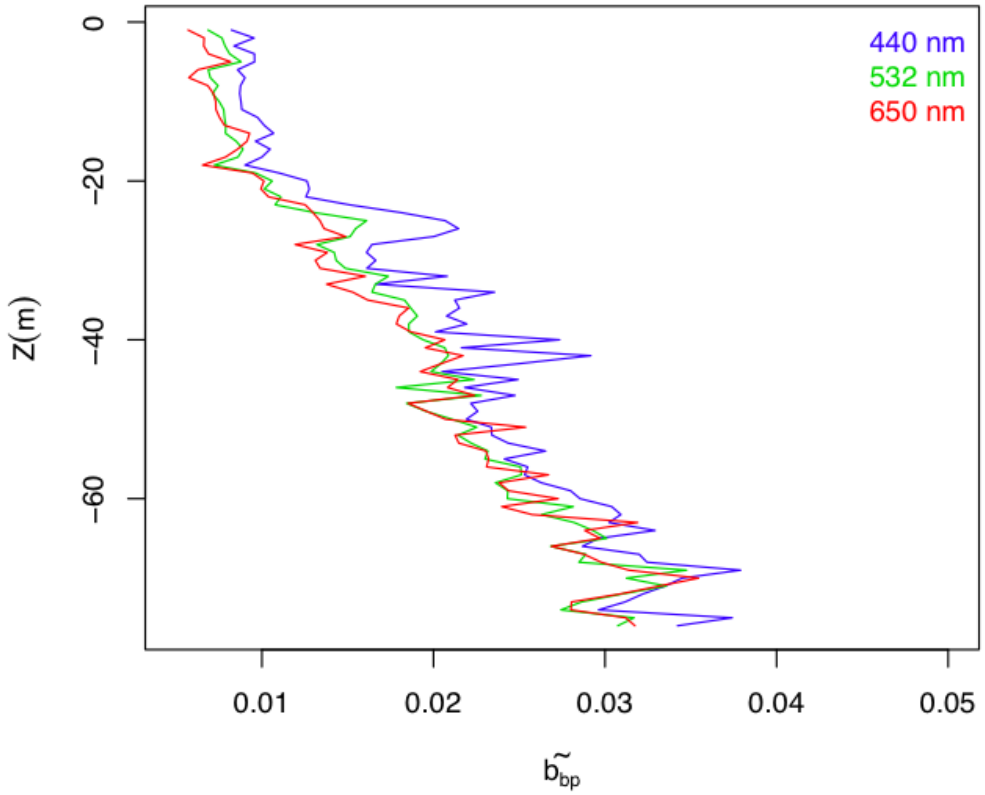

Fig. 5.1. Backscattering ratio vs. depth, calculated from the ratio of b_{bp} from the BB9 and b_p from the AC-S. The three colors represent different wavelengths (440, 532, and 650 nm), showing little spectral variation.

5.4 Backscattering spectral slope

Theoretical studies have indicated that for homogeneous spherical particles, a power law of the type $b_{bp}(\lambda) \propto \lambda^{-\eta}$ can be fitted to the b_{bp} spectra, and the spectral slope η is inversely related to particle size (Wozniak and Stramski, 2004). Attempts to validate this relationship for marine particles have shown mixed results. One study of phytoplankton cultures found no relationship between η and particle size (Whitmire et al., 2010). A field study of suspended sediments did show a relationship between spectral b_{bp} and particle size, but the relationship was variable and not always present. Also, the b_{bp} spectra often did not fit a power law (Slade et al., 2010).

We calculated η by fitting a the power law function in Eq. 5.2 to the b_{bp} spectrum at each depth.

$$b_{bp}(\lambda) = a * (\lambda/420)^{-\eta} \qquad \text{Eq.5.2}$$

Backscattering at 412 nm was excluded from the fit because it appeared anomalously low and did greatly reduced the fit of the power law function. The profile of η is shown in Fig. 5.2 (blue line) along with the c_p spectral slope γ (red line).

The c_p spectral slope γ is expected to behave in a similar way as η, based on theoretical results (Boss *et al.*, 2001b), and γ has been somewhat better validated than η as a proxy for particle size (Kitchen *et al.*, 1982; Boss *et al.*, 2001a; Slade and Boss, 2010). We calculated γ in the same way as η (using an equation analogous to Eq. 5.2) from AC-S data. The two spectral slopes agree within the wide 95% confidence intervals of η (Fig. 5.2; pale blue lines) and share some features, including a dip at the deep chlorophyll maximum at ~18 m and a decrease near the bottom, indicating the possibility of larger particle sizes at these locations. Only in the top 10 m do the two slopes diverge significantly.

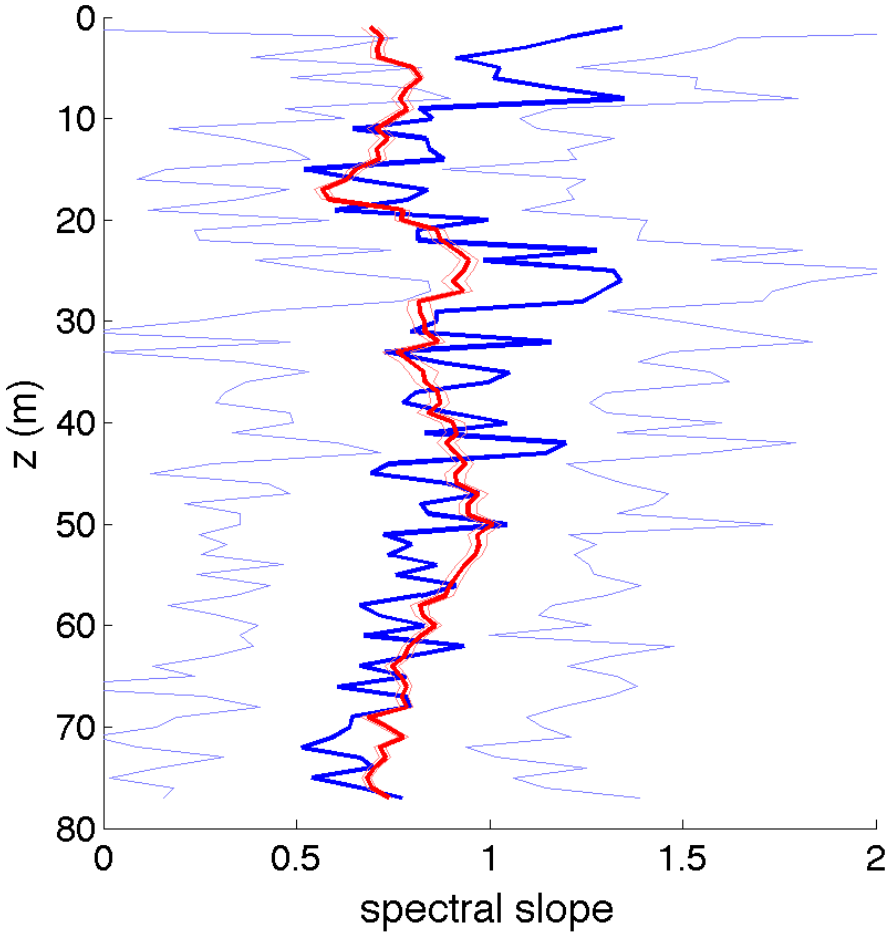

Fig. 5.2 Particulate backscattering spectral slope parameter η (dark blue line) bounded by 95% confidence intervals (light blue lines). Particulate beam attenuation spectral slope γ (red line), derived from the AC-S, is also included for comparison.

References:

Boss, E., Pegau, W.S., Gardner, W.D., Zaneveld, J.R.V., Barnard, A.H., Twardowski, M.S., Chang, G.C., Dickey, T.D., 2001a. Spectral particulate attenuation and particle size distribution in the bottom boundary layer of a continental shelf. Journal of Geophysical Research-Oceans 106 (C5), 9509-9516.

Boss, E., Twardowski, M.S., Herring, S., 2001b. Shape of the particulate beam attenuation spectrum and its inversion to obtain the shape of the particulate size distribution. Applied Optics 40 (27), 4885-4893.

Boss, E. and W. S. Pegau. 2001. "Relationship of light scattering at an angle in the backward direction to the backscattering coefficient," *Applied Optics*, 40(30):5503–5507.

Boss, E., W. S. Pegau, M. Lee, M. Twardowski, E. Shybanov, G. Korotaev, and F. Baratange. 2004. Particulate backscattering ratio at LEO 15 and its use to study particle composition and distribution, J. Geophys. Res., 109, C01014, doi:10.1029/2002JC001514.

Gordon, H.R. 1994. "Modeling and simulating radiative transfer in the ocean. Chapter 1 in *Ocean Optics*", R.W. Spinrad, K.L. Carder and M.J. Perry [eds], Oxford.

Kitchen, J.C., Zaneveld, J.R.V., Pak, H., 1982. Effect of particle size distribution and chlorophyll content on beam attenuation spectra. Applied Optics 21 (21), 3913-3918.

Morel, A. and L. Prieur. 1977. Analysis of variations in ocean color, *Limnology and Oceanography*, **22**, 709-722.

Slade, W., Boss, E., 2010. Spectral attenuation and backscattering as indicators of particle size distribution. Ocean Optics XX, Anchorage, AK.

Sullivan , J. M., and M. S. Twardowski. 2009. "Angular shape of the volume scattering function in the backwards direction". *Applied Optics*, 48(35):6811–6819.

Sullivan, J.M., Twardowski, M., Zaneveld, J.R., Moore, C. "Measuring optical back-scattering in water". *Light Scattering Reviews*, vol. 7. Praxis Publishing Ltd, submitted for publication.

Whitmire, A.L., Pegau, W.S., Karp-Boss, L., Boss, E., Cowles, T.J., 2010. Spectral backscattering properties of marine phytoplankton cultures. Optics Express 18 (14), 15073-15093.

Wozniak, S. B., and D. Stramski (2004), Modeling the optical properties of mineral particles suspended in seawater and their influence on ocean reflectance and chlorophyll estimation from remote sensing algorithms, Appl. Opt., 43, 3489–3503, doi:10.1364/AO.43.003489.

Zhang, X. D., L. B. Hu, and M. X. He. 2009. "Scattering by pure seawater: Effect of salinity", *Optics Express*, Vol. 19, No. 7

Appendix: Matlab code for calculating β_{sw}

```
function [betasw,beta90sw,bsw]= betasw_ZHH2009(lambda,Tc,theta,S,delta)
% Xiaodong Zhang, Lianbo Hu, and Ming-Xia He (2009), Scatteirng by pure
% seawater: Effect of salinity, Optics Express, Vol. 17, No. 7, 5698-5710
%
% lambda (nm): wavelength
% Tc: temperauter in degree Celsius, must be a scalar
% S: salinity, must be scalar
% delta: depolarization ratio, if not provided, default = 0.039 will be
% used.
% betasw: volume scattering at angles defined by theta. Its size is [x y],
% where x is the number of angles (x = length(theta)) and y is the number
% of wavelengths in lambda (y = length(lambda))
% beta90sw: volume scattering at 90 degree. Its size is [1 y]
% bw: total scattering coefficient. Its size is [1 y]
% for backscattering coefficients, divide total scattering by 2
%
% Xiaodong Zhang, March 10, 2009


% values of the constants
Na = 6.0221417930e23 ;   %  Avogadro's constant
Kbz = 1.3806503e-23 ;          %  Boltzmann constant
Tk = Tc+273.15 ;       %  Absolute tempearture
M0 = 18e-3;              %  Molecular weigth of water in kg/mol


error(nargchk(4, 5, nargin));
if nargin == 4
        delta = 0.039; % Farinato and Roswell (1976)
end


if ~isscalar(Tc) || ~isscalar (S)
        error('Both Tc and S need to be scalar variable');
end


lambda = lambda(:)'; % a row variable
rad = theta(:)*pi/180; % angle in radian as a colum variable


% nsw: absolute refractive index of seawater
% dnds: partial derivative of seawater refractive index w.r.t. salinity
[nsw dnds] = RInw(lambda,Tc,S);

% isothermal compressibility is from Lepple & Millero (1971,Deep
% Sea-Research), pages 10-11
% The error ~ +/-0.004e-6 bar^-1
```

```
IsoComp = BetaT(Tc,S);


% density of water and seawater,unit is Kg/m^3, from UNESCO,38,1981
density_sw = rhou_sw(Tc, S);

% water activity data of seawater is from Millero and Leung (1976,American
% Journal of Science,276,1035-1077). Table 19 was reproduced using
% Eq.(14,22,23,88,107) then were fitted to polynominal equation.
% dlnawds is partial derivative of natural logarithm of water activity
% w.r.t.salinity
dlnawds = dlnasw_ds(Tc, S);


% density derivative of refractive index from PMH model
DFRI = PMH(nsw);  %% PMH model

% volume scattering at 90 degree due to the density fluctuation
beta_df = pi*pi/2*((lambda*1e-9).^(-4))*Kbz*Tk*IsoComp.*DFRI.^2*(6+6*delta)/(6-
7*delta);
% volume scattering at 90 degree due to the concentration fluctuation
flu_con = S*M0*dnds.^2/density_sw/(-dlnawds)/Na;
beta_cf = 2*pi*pi*((lambda*1e-9).^(-4)).*nsw.^2.*(flu_con)*(6+6*delta)/(6-7*delta);
% total volume scattering at 90 degree
beta90sw = beta_df+beta_cf;
bsw=8*pi/3*beta90sw*(2+delta)/(1+delta);
for i=1:length(lambda)
        betasw(:,i)=beta90sw(i)*(1+((cos(rad)).^2).*(1-delta)/(1+delta));
end



function [nsw dnswds]= RInw(lambda,Tc,S)
% refractive index of air is from Ciddor (1996,Applied Optics)
n_air = 1.0+(5792105.0./(238.0185-1./(lambda/1e3).^2)+167917.0./(57.362-
1./(lambda/1e3).^2))/1e8;


% refractive index of seawater is from Quan and Fry (1994, Applied Optics)
n0 = 1.31405; n1 = 1.779e-4 ; n2 = -1.05e-6 ; n3 = 1.6e-8 ; n4 = -2.02e-6 ;
n5 = 15.868; n6 = 0.01155;  n7 = -0.00423;  n8 = -4382 ; n9 = 1.1455e6;


nsw =
n0+(n1+n2*Tc+n3*Tc^2)*S+n4*Tc^2+(n5+n6*S+n7*Tc)./lambda+n8./lambda.^2+n9./lamb
da.^3; % pure seawater
nsw = nsw.*n_air;
dnswds = (n1+n2*Tc+n3*Tc^2+n6./lambda).*n_air;
```

```
function IsoComp = BetaT(Tc, S)
% pure water secant bulk Millero (1980, Deep-sea Research)
kw = 19652.21+148.4206*Tc-2.327105*Tc.^2+1.360477e-2*Tc.^3-5.155288e-5*Tc.^4;
Btw_cal = 1./kw;


% isothermal compressibility from Kell sound measurement in pure water
% Btw = (50.88630+0.717582*Tc+0.7819867e-3*Tc.^2+31.62214e-6*Tc.^3-0.1323594e-
6*Tc.^4+0.634575e-9*Tc.^5)./(1+21.65928e-3*Tc)*1e-6;


% seawater secant bulk
a0 = 54.6746-0.603459*Tc+1.09987e-2*Tc.^2-6.167e-5*Tc.^3;
b0 = 7.944e-2+1.6483e-2*Tc-5.3009e-4*Tc.^2;


Ks =kw + a0*S + b0*S.^1.5;


% calculate seawater isothermal compressibility from the secant bulk
IsoComp = 1./Ks*1e-5; % unit is pa


function density_sw = rhou_sw(Tc, S)


% density of water and seawater,unit is Kg/m^3, from UNESCO,38,1981
a0 = 8.24493e-1;  a1 = -4.0899e-3; a2 = 7.6438e-5; a3 = -8.2467e-7; a4 = 5.3875e-9;
a5 = -5.72466e-3; a6 = 1.0227e-4;  a7 = -1.6546e-6; a8 = 4.8314e-4;
b0 = 999.842594; b1 = 6.793952e-2; b2 = -9.09529e-3; b3 = 1.001685e-4;
b4 = -1.120083e-6; b5 = 6.536332e-9;

% density for pure water
density_w = b0+b1*Tc+b2*Tc^2+b3*Tc^3+b4*Tc^4+b5*Tc^5;
% density for pure seawater
density_sw = density_w
+((a0+a1*Tc+a2*Tc^2+a3*Tc^3+a4*Tc^4)*S+(a5+a6*Tc+a7*Tc^2)*S.^1.5+a8*S.^2);


function dlnawds = dlnasw_ds(Tc, S)
% water activity data of seawater is from Millero and Leung (1976,American
% Journal of Science,276,1035-1077). Table 19 was reproduced using
% Eqs.(14,22,23,88,107) then were fitted to polynominal equation.
% dlnawds is partial derivative of natural logarithm of water activity
% w.r.t.salinity
% lnaw = (-1.64555e-6-1.34779e-7*Tc+1.85392e-9*Tc.^2-1.40702e-11*Tc.^3)+.....
%        (-5.58651e-4+2.40452e-7*Tc-3.12165e-9*Tc.^2+2.40808e-11*Tc.^3).*S+.....
%        (1.79613e-5-9.9422e-8*Tc+2.08919e-9*Tc.^2-1.39872e-11*Tc.^3).*S.^1.5+.....
%        (-2.31065e-6-1.37674e-9*Tc-1.93316e-11*Tc.^2).*S.^2;
```

```
dlnawds = (-5.58651e-4+2.40452e-7*Tc-3.12165e-9*Tc.^2+2.40808e-11*Tc.^3)+.....
        1.5*(1.79613e-5-9.9422e-8*Tc+2.08919e-9*Tc.^2-1.39872e-11*Tc.^3).*S.^0.5+.....
        2*(-2.31065e-6-1.37674e-9*Tc-1.93316e-11*Tc.^2).*S;


% density derivative of refractive index from PMH model
function n_density_derivative=PMH(n_wat)
n_wat2 = n_wat.^2;
n_density_derivative=(n_wat2-1).*(1+2/3*(n_wat2+2).*(n_wat/3-1/3./n_wat).^2);
```

Hyperspectral Radiometers

Contributing authors (in alphabetical order by last name): Nathan Briggs, Haidi Chen, Apurva Dave, Fernanda Henderikx Freitas, Clemence Goyens, Courtney Kearney, Leanne Powers, Sara Rivero, Ryan Vandermeulen

Section Guide

1. Introduction

1.1 Overview

An important application of field radiometric measurements is the determination of apparent optical properties (AOPs) in the ocean. To this end, Satlantic Inc. has developed hyperspectral sensors that measure both irradiance (HyperOCR-I) and radiance (HyperOCR-R) in the visible and Near-InfraRed (350-800 nm) range at 3.3 nm spectral resolution. These sensors can be deployed in a variety of instrument configurations, such as the HyperSAS, HyperTSRB and HyperPro, each of which allows for a different combination of above- and below-water radiometric measurements. For the HyperSAS configuration, the radiance and irradiance sensors are mounted on an above-water platform. For the HyperTSRB, the sensors are deployed at the sea surface on a buoy, measuring irradiance above the water and radiance below the water. For the HyperPro, the sensors are deployed on a subsurface platform that profiles through the water column. Depending on the scientific objective of the user, one configuration may be preferable to another. Note, however, that deploying the three instruments simultaneously is highly valuable for data closure.

Sections 2-4 in this chapter provide detailed descriptions of the setup, deployment and data processing for each system. For all instruments, it is assumed that data is logged using Satlantic's SatView software and then run through Satlantic's SatCon software before the processing described in this document. SatCon applies factory calibrations and creates text files for both "light" and "dark" readings. Section 5 discusses methods of calculating AOP's and other derived quantities from the processed data and address instrument closure. Throughout this document, the discussion and figures (particularly in section 5) will focus on field data collected in the Gulf of Maine during July 2011. The details of the field data are given below:

Date and time:	15:31 GMT, July 20, 2011
Location:	Lat: 43° 44.9 N; Lon: 69° 29.9 W
Sky state:	clear sky, bright sun, 5% cloud cover
Sea state:	very calm, wind speed 3 knots

1.2 User references

Descriptions of Satlantic's radiometric sensors and instrumentation, as well as links to user manuals and system brochures, can be found online at Satlantic's website (http://www.satlantic.com/products.asp?CategoryID=1). Links to the user manuals are also provided below:

HyperOCR sensors:
http://www.satlantic.com/documents/808354_HyperOCROperationManualSAT-DN-249RevC.pdf

HyperSAS:
http://www.satlantic.com/documents/236460_HyperSASManual.pdf

HTSRB:
ftp://ftp.satlantic.com/pub/manuals/HyperTSRB.pdf

HyperPro:
ftp://ftp.satlantic.com/pub/manuals/HyperPro.pdf

1.3 Notation

Throughout this document the following notations are used:

(*0*+) – measurement right above the sea surface.

(*0*-) – measurement right below the sea surface.

Ed – down-welling irradiance (irradiance has units of W m^{-2} nm^{-1} or similar).

Es – also down-welling irradiance but measured above water (as on HyperSAS).

Eu – upwelling irradiance.

Lu – upwelling radiance (radiance has units of W m^{-2} sr^{-1} nm^{-1} or similar).

Lw – water-leaving radiance. May also be referred as *Lu(*0+) in the literature. *Lw* can be calculated by calculating the transmission of ***Lu(0-)*** through the sea surface.

Lt – (on HyperSAS) sea-surface radiance measured at a certain angle θ (See Figure 2.1).

Li – (on HyperSAS) sky or indirect radiance measured at a certain angle θ (See Figure 2.1)

Rrs – Remote-sensing reflectance defined as the ratio of *Lw* or *Lu(*0+) to Ed (sr^{-1}).

PAR – Photosynthetically available radiation (usually integrated across visible spectrum) (µmol quanta m^{-2} s^{-1}).

K – diffuse attenuation coefficient (m^{-1}).

R – reflectance defined as the ratio of *Eu* to *Ed* (unitless).

Q – upwelling radiance distribution defined as the ratio of *Eu* to *Lu* (sr).

ρ – Fresnel reflectance factor; alternatively from Mobley (1999): "the proportionality factor that relates the radiance measured when the detector views the sky to the reflected sky radiance measured when the detector views the sea surface." In practice, ***ρ*** is used to estimate *Lw* from the HyperSAS measured *Li* and *Lt* (see section 2).

ϕ – azimuthal angle (with respect to the sun).

θ – zenith angle.

2. HyperSAS

The Satlantic, Inc HyperSAS is a Hyperspectral Surface Acquisition Remote Sensing System for above-water measurements of ocean color. The main purpose of the instrument is to obtain high-precision, high-resolution hyperspectral measurements of water-leaving spectral radiance and downwelling spectral irradiance.

2.1. Components and assembly procedure

Refer to the user manual for set-up and calibration. The HyperSAS should be securely clamped (e.g. with the mounting frame proposed by Satlantic) to the platform where the measurements will be collected (e.g. a dock or boat). The mounting frame proposed by Satlantic lets the user adjust the zenith angle (θ) of the sea-surface radiance (Lt) and sky radiance (Li) sensors as well as the azimuth angle (ϕ) of the entire instrument suite by rotating the entire configuration (Fig. 2.1.). Mobley (1999) recommends using a zenith angle of 40° for the Lt and Li sensors and an azimuth angle of 135°. This minimizes sun glint and decreases dependence on the wind speed. As mentioned by Santlantic's manual, this set-up ensures that Lw will dominate the Lt signal. The Fresnel reflectance factor (ρ) used to estimate the water leaving radiance from the measured radiances Li and Lt (see further in section 2.2. for more details about ρ), depends on the viewing angles, θ and ϕ. Consequently, it is crucial to record the viewing angles with high accuracy during the deployment of the instrument or to keep these angles as constant as possible. For example, if the HyperSAS is mounted on a boat, boat rotation should be minimized to retain ϕ at 135.

The Ed sensor should be pointed towards zenith as given in Figure 2.1. In addition to the three sensors, the Network Hub (device that provides power to the sensors and can be used to provide optional pitch and roll data) has to be mounted on the frame with the red arrow labels pointing up such that the pitch and roll angles are valid. Note that on an iron ship the measured pitch and roll angles may be incorrect as the magnetic field of the iron ship may have an effect on the magnetic compass of the instrument. It is therefore highly recommended to have additional GPS measurements and accurate angle measurements! Measurements may be useless if the angles have not been measured accurately and subsequently the data not corrected properly.

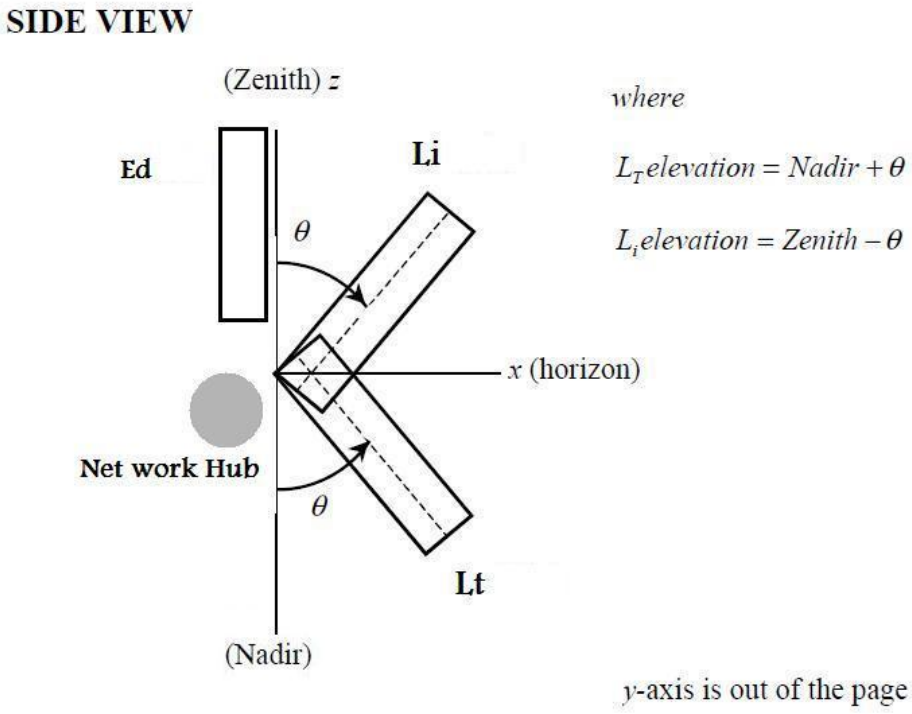

Figure 2.1. SAS coordinate system of HyperSAS (based on conceptual scheme in the 236460_HyperSASManual.pdf).

The lenses of the radiance sensors should be cleaned prior to use with an appropriate lens paper. Also note that the cable that is plugged into the back of the two radiance sensors and the network hub must be in the proper orientation. Sensors might receive power but not communicate with the computer if the cables are not properly plugged into the sensors. Therefore make sure that the network hub is connected with the middle cable-end while the two external cable-ends are connected to the sensors (any of them). Also, it is crucial to ensure that the down-looking radiance sensor is not blocked during deployment, for example by leaning underneath the field of view of the sensor (*Lt*).

2.2 Measurements and data processing

2.2.1 Measurements

While deployed, the shutter within each sensor will close periodically and record dark values, which can be used for the dark correction during processing (referred later as dark measurements recorded during light measurements). When the sensors have power, a clicking noise associated with the dark shutter opening and closing should be heard.

2.2.2 Data processing

Step 1 – Subtract Dark Readings:

Two files are created for each sensor, one containing all dark measurements (containing a "D" in the title) and one containing all light measurements (with an "S" or "s" in the title). The first column of each file contains the three-digit instrument ID number and the year and time the data are recorded are located in the two last columns. Use the Matlab code 'read_hyproSAS.m' (Appendix 1) and 'read_OCR2.m' (Appendix 2) to read the '.dat' files. The former lists and reads all the files and calls the latter which pairs and subtracts the dark measurements from the light measurements. Note that before the dark measurements are subtracted from the light measurements, the code first interpolates the dark measurements to the time scale of the light measurements.

Step 2 – Interpolate to a single set of wavelengths:

After the dark measurements have been subtracted from the light, the light measurements should be interpolated to the wavelengths of one instrument. In order to avoid data creation (often resulting from incoherent interpolations), light measurements should be interpolated to the wavelengths of the shortest spectrum. In the present study this coincides with the wavelengths of the *Ed* sensor.

Step 3 – Quality control of timeseries:

The purpose of this step is to visualize the data over time in order to identify any inconsistent data that should be deleted from the data set. By inconsistent we mean data with significant jumps or drops in time. These might result from, for instance, blocking the light sensor while measuring (creating shade over the measured surface) or sudden changes in ϕ (e.g. due to boat movements). Changes in ϕ might be corrected by varying ρ over time. However, this requires very accurate ϕ records while collecting measurements. Nevertheless, even very hard working students realize that keeping accurate ϕ records is a very difficult task! Figure 2.2 shows how *Lt*, *Li* and the ϕ of the sensors (uncalibrated because of the effect of the iron ship on the magnetic field and subsequently the compass) varies over time compared to *Ed*. *Lt* and *Li* show sudden drops and bumps corresponding to variations in the platform direction while *Ed* shows a constant increasing slope (the sky is getting brighter during measurement deployment). Subsequently, the ratio of *Lu* over *Ed* will not be normalized to changes in light intensity, which highlights the importance to filter the data set.

Step 4 – Align sensors in time:

Since the three sensors used all have different integration times, the variation in the sensor to sensor time stamp must be addressed in order to calculate *Rrs*. The user has three options: 1) calculate the median value of the data (e.g. Figure 2.3); 2) linearly interpolate the data in time; or 3) bin the data to a common time scale. Remember, if the data are interpolated, avoid creating 'new' data by interpolating to the data set with the coarsest temporal resolution.

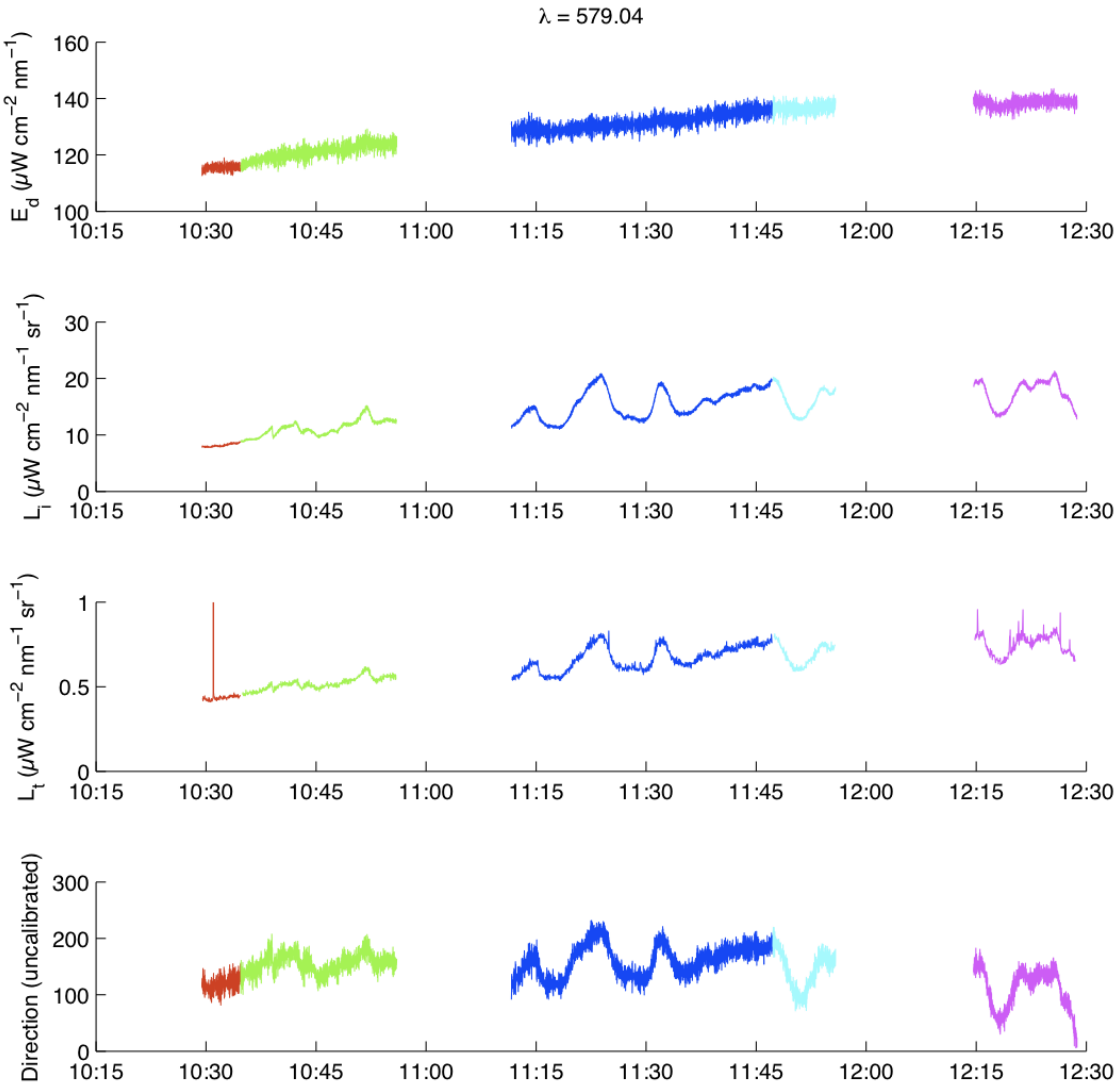

Figure 2.2. A time series of radiance, irradiance and direction variations over time for five different HyperSAS deployments over a 2 hour span in the the Gulf of Maine in July 2011. Each color represents a different deployment. Radiometric data is reported for λ = 579 nm.

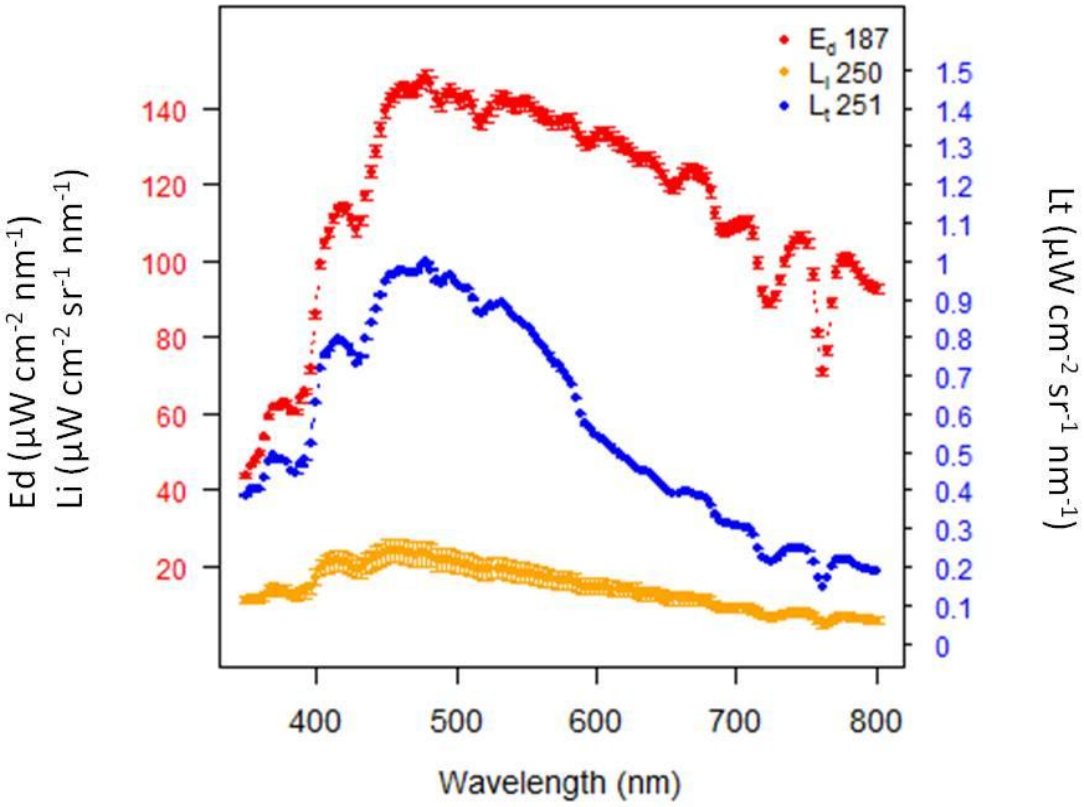

Figure 2.3. Spectra of Li, Lt and Ed after subtracting the dark measurements and taking the median values of each time series.

Step 5 (Optional) – correct Lw for zenith angle:

An additional correction can be made in order to account for possible effects of the viewing angle for *Lt* measurements. Because the *Lt* sensor measures the sea-surface radiance at a certain angle, subtracting the sea-surface reflectance (ρLi) will still produce an estimate of *Lw* at that viewing angle. Since the HyperSAS *Ed* sensor is zenith-directed, the *Rrs* estimates require water leaving radiances directed towards zenith. Therefore a correction can be applied to the angled *Lw* value to transform it into a zenith-directed *Lw*. *Lw* intensities are known to increase with greater zenith angle, especially in highly turbid waters, so this correction would be expected to lead to a decrease in *Lw* values and, consequently, in the *Rrs* estimate.

In order to investigate the effect of zenith angle on the HyperSAS *Lt* data reported here, we used the observed IOP profiles to run the radiative transfer software Hydrolight, which output the full angular *Lw* distribution. The effect of zenith angle was different at different wavelengths, with a maximum difference of 2% between Lw (ϕ=135°, θ=0°) and Lw(ϕ=135°, θ=45°) at λ = 385 nm.

3. HTSRB

The Hyperspectral Tethered Spectral Radiometer Buoy (HyperTSRB or HTSRB) (Figure 3.1) from Satlantic is a hyperspectral radiometer especially designed to measure downwelling spectral irradiance right above the sea surface (*Ed*) and upwelling spectral radiance 60 cm below the sea surface (*Lu*(-60 cm)). These data are used to estimate *Rrs* (remote sensing reflectances) at the sea surface.

Figure 3.1 Satlantic HTSRB (owned by the Darling Marine Center, University of Maine). Note the yellow buoy responsible to stabilize the instrument and to avoid shadowing of the sensor under water. Ed sensor is located on the top, Lu sensor is located on the bottom.

3.1 Deployment and Data Acquisition

The HTSRB deployment scheme is designed to measure radiometric quantities at a distance from the vessel in order to minimize vessel contamination in the light field (Figure 3.2). Prior to deployment, lens paper should be used to clean the lenses of the radiometer. The instrument is tethered to the vessel and should be at a constant distance from the ship. Satlantic Inc. recommends that the instrument stabilizes in the water for at least 20 minutes before data gathering.

Upwelling radiance (*Lu*) at a depth of 60 cm and downwelling irradiance (*Ed*) data are recorded over a user-defined time frame. Dark counts are subtracted from the main data internally by the instrument, so no further calibration is necessary (provided the factory calibration is current).

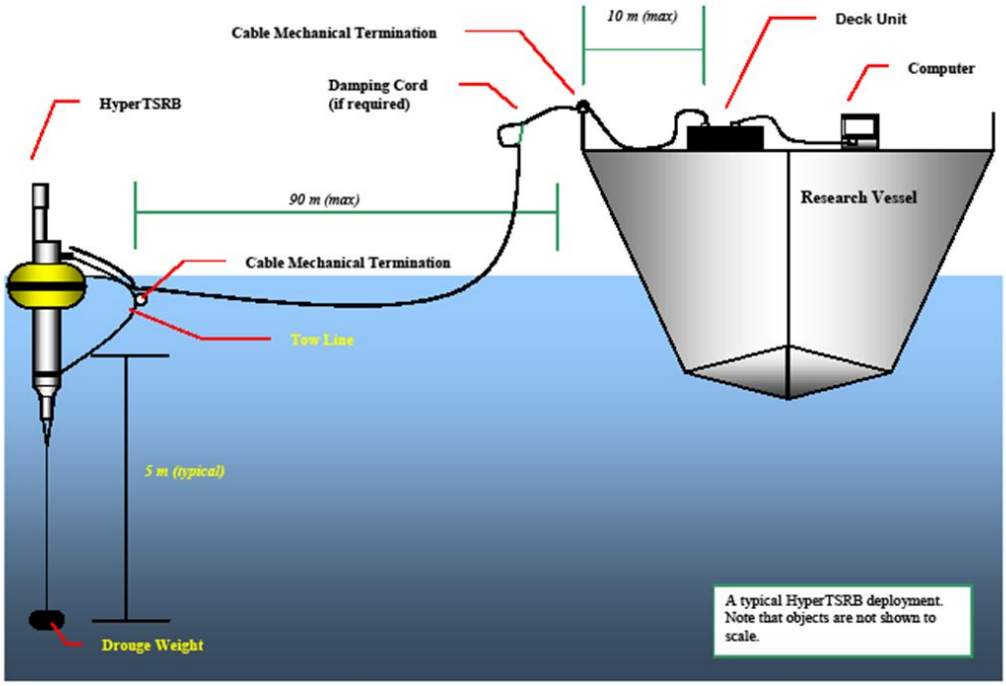

Figure 3.2 HTSRB deployment schematic. A distance between the boat and the instrument is necessary to avoid shadowing and contamination of the light field (Fig source: HyperTSRB manual R6.1).

The *Lu* sensor points down in the water and the *Ed* sensor points towards the sky in air. Note: even though most buoys have a drogue weight, rough sea surfaces can result in tilt of the instrument and therefore affect the quality of the measurements (there is no tilt sensor within the instrument).

3.2 Calibration

All HyperTSRB sensors are factory calibrated. The user should ensure that the HTSRB data acquisition software (SatView, see link to website in reference) is provided with the most recent optical calibration file before collecting data. As optional outputs, SatView provides both raw binary data and already calibrated and dark-corrected radiance and irradiance data (*Lu* and *Ed*), so there is no need for further calibration by the user.

4. HyperPro

4.1. Description of Instrument

Satlantic's free-falling optical profiler consists of a profiling frame that can serve as a platform for Satlantic's multispectral and hyperspectral radiometers. The field data included in this report were obtained using hyperspectral radiometers (See Section 1.0). The profiler itself is equipped with pressure and tilt sensors that are used to monitor its descent rate and angle. Besides profiler mode, a flotation collar can be mounted on the profiler frame to allow the unit to operate in 'buoy' mode and provide surface measurements. The buoy mode is briefly explained in Section 4.2.3. The profiler is connected to a shipboard host computer and power supplied via a single cable that acts as a combined mechanical and electrical tether. Satlantic's SatView software is installed on the host computer and provides real-time, interactive data logging and display.

4.2 Data Measurement

4.2.1 Physical Set-up and Procedure

Additional equipment required include a DC power source (normally a 12V battery), a computer with a free serial communications port, instrument calibration files and data acquisition and processing software (e.g. *SatView*, *SatCon*). Instrument body, computer and battery should be connected to the deck unit. Components and cables should be connected with care making sure that both ends are free of dirt, that they are properly aligned with the connector pins before final connection, and that the locking sleeve is tight.

Since radiometers can be detached from the body it is important to measure and document the distance between the radiometer sensors and the pressure sensor to account for the depth offset; especially if the instrument is being used alternately as buoy and profiler.

Other general recommendations include making sure that the instrument is not being shadowed by the boat and making sure that there is good communication between instrument and computer before deployment. It is important to use the lock that secures the cable to the main body of the instrument to prevent damage in the connections due to pulling. It is also helpful to take notes on wind speed and cloud cover while the instrument is recording.

All HyperPro measurements should be combined with measurements from a reference radiometer, a separate instrument that is mounted high on the ship's structure to measure the downwelling irradiance during the cast. The measurements from the reference account for changes in the subsurface light field due to variations in cloud cover.

4.2.2 Calibration

All sensors on the HyperPro are factory calibrated by Satlantic. The user should ensure that SatView is using the most recent optical calibration file before collecting data. To do this in SatView, create a data log/file for your cruise and add the sensors you are using with the most recent calibration files. Be aware that calibration files (.CAL) for each sensor are packaged as Satlantic Instrument Package (.SIP) files. Add the package files into Satview, not individual calibration files. Ideally, sensors should be calibrated before and after use in major field/sampling events.

4.2.3 Buoy Mode

For near surface measurements of upwelling radiance (*Lu*) and irradiance (*Eu*) attach a flotation collar (provided by Satlantic) to the profiler system and turn the irradiance sensor to face downward (Figure 4.1). Try to attach sensors at the same level. The Operation Manual states that these measurements can be made as little as 5 cm below the surface. In order to correct for the distance the sensor is below the surface, measure the distance between the waterline and where both sensors lie beneath the surface. These measurements are important because reflectance (*R*) and remote sensing reflectance calculations (*Rrs*) are based on radiance and irradiance measurements in air at the sea surface.

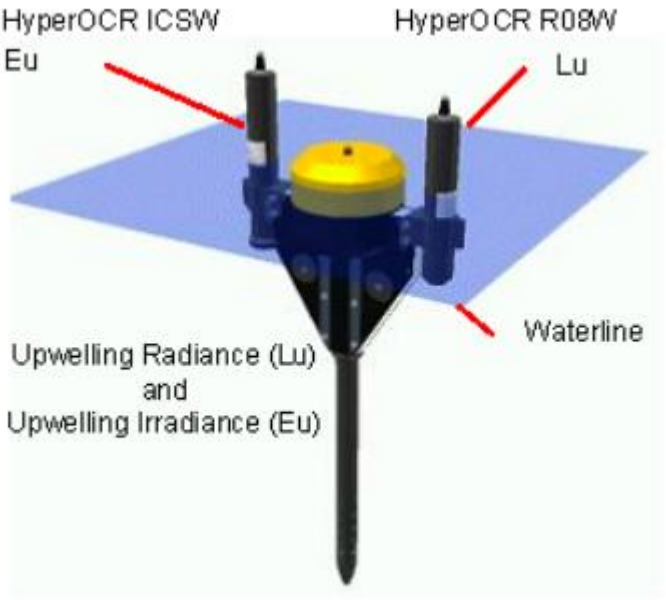

Figure 4.1. Diagram of HyperPro set-up for operation in buoy mode (Operation Manual For: Profiler II Document Number: SAT-DN-00223 Rev I, available from the Manufacturer's website)

Try to keep the instrument away from the boat to prevent interference with ship shadow. Additionally, try to match data collection times with casts of other radiometers and additional instruments. After data collection, make sure to look at the time series of each cast in order to check for fluctuations in the data. Make sure to note times when the instrument is too close to the boat and the sky conditions are variable. Remove any data that is compromised before processing an entire time series.

4.2.4 Profiling mode

A HyperPro profile starts when the instrument has reached a distance of 5-10 m off the ship stern (Figure 4.2.). The instrument is then released and falls at an approximately constant rate in the water column while collecting data. The descent can be stopped anytime by pulling the cable. This technique avoids disturbances caused by the shadow of the ship and allows for measurements with minimal tilts (less than 5° over most of the profile). The cable may extend over the field of view of the irradiance sensor, but the small diameter of the cable minimizes any negative effects on the measured light field. The addition of a temperature and if possible a conductivity sensor, provides a good description of some water column properties. The most important aspect during data collection is to prevent the cable from ever coming under tension, because even brief periods of tension can adversely affect the vertical orientation and descent velocity of the profiler.

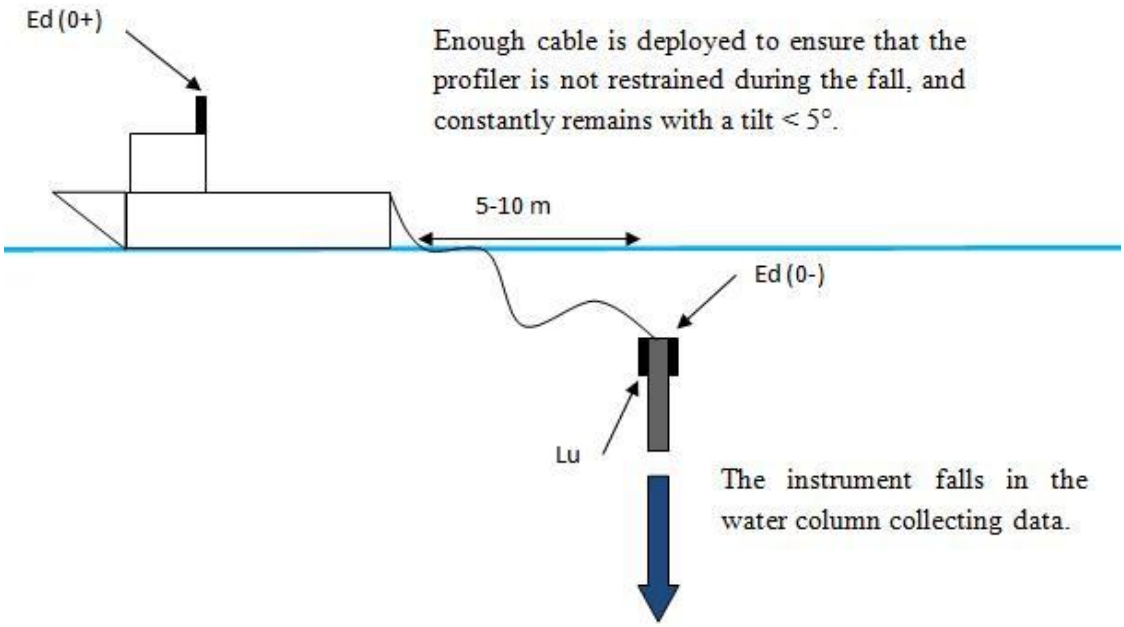

Figure. 4.2. - Scheme of the HyperPro deployment

4.3 Processing of Raw Data

4.3.1 Raw Data Outputs

RAW data include 8 sub-files: header file; tilt/pressure file; reference irradiance (*Es*) light/dark, downward irradiance (*Ed*) light/dark profile, upward radiance (*Lu*) light/dark profile. File suffixes are listed in Table 1.

Table1. HyperPro file information

File Suffix	**Sensor Type**	**notes**
HED	Reference /SAS	dark-frame file
HSE	Reference /SAS	light-frame file
PED	Hyperpro Ed	dark-frame file
HPE	HyperPro Ed	light-frame file
PLD	Hyperpro Lu	dark-frame file
HPL	HyperPro Lu	light-frame file
HEADER	HyperPro ancillary	pressure tare info
MPR	HyperPro ancillary	tilt/ pressure/ time data file

4.3.2 Dark Correction

Usually HyperPro data is dark corrected with the values obtained from shutter darks. Shutter darks are continuously recorded during the measurements by occluding the input fiber with an optical shutter, typically after every five light samples. HyperPro raw data dark correction is carried out in the following steps (refer to Appendix 2 for Matlab codes):

1. Discard light frame data collected before the first or after the last dark frame data.
2. Interpolate shutter darks as a function of measurement time to match the number of dark and light data measurements.
3. Correct light data using shutter darks:

$$Lu = Lu_{light} - L_{Dark}$$

$$Ed = Ed_{Light} - Ed_{Dark}$$

$$Es = Es_{Light} - Es_{Dark}$$

4.3.3 Pressure Tare Correction

Pressure sensors often have a small offset value that will change with atmospheric pressure (Figure 4.3). The offset is removed by a pressure tare. This value is stored in the header records when the data is collected. Pressure tare is taken when the *Ed* sensor is located at the surface of the water. This measurement is a combination of the atmospheric pressure and the pressure of the water column from the surface to the pressure sensor. To calculate the depth of our *Ed* measurements we need to subtract this pressure tare value.

To calculate *Lu* depth we have to take into account the offset between the *Ed* radiometer and the *Lu* sensor. The pressure value at *Lu* is calculated by subtracting the pressure tare value from the measured pressure values, as calculated for *Ed*, and then adding the distance between the *Lu* sensor head and the *Ed* sensor head. (i.e. *Lu* "Distance to Surface").

Note: When using this pressure tare mode it is very important that you do not specify a value other than zero for 'Distance to Pressure' for any sensors.

Pressure *Ed* = Measured Pressure - Pressure Tare

Pressure *Lu* = Measured Pressure - Pressure Tare + Distance to Surface (*Lu*)

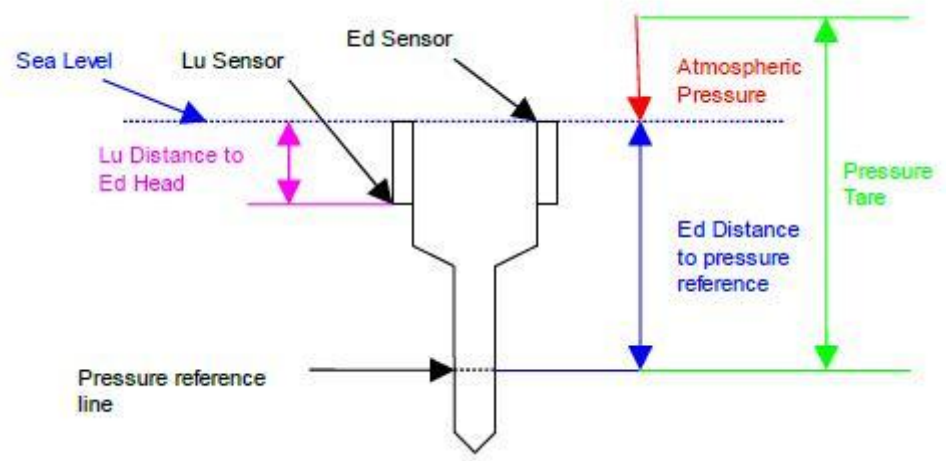

Figure 4.3. Conceptual schematics between different radiance, irradiance and pressure sensors on the profiler.

4.3.4 Tilt Correction

HyperPro measurements can be edited to remove any tilt contaminated records. Tilt information can be found in the MPR file. In MPR file, Tilt(X) and Tilt(Y) is the instrument deviation angle (in degree) from nadir view. A tilt threshold (5° for example) is used and the data records whose tilt angles are larger than the threshold in either X direction or y direction are removed. Figure 4.4 shows how, in the present study, the tilt data is removed from the dataset.

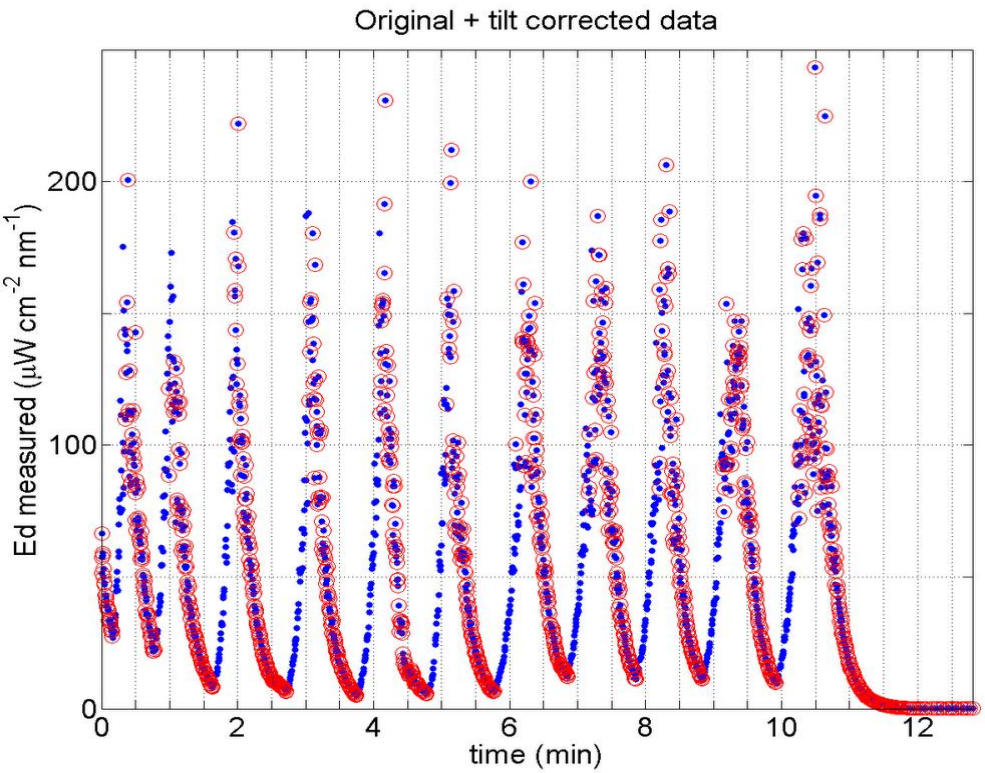

Figure 4.4. Ed(z) data from a multi-profile cast. Blue dots indicate all measurements as a function of time, while red circles surround measurements that passed the tilt correction (i.e. measurements that were made while sensor tilt in the x and y directions was less than 5 degrees). The plot clearly shows that the majority of high-tilt measurements were made during the upcasts. This is consistent with the expectation that the profiler should be stably nadir-oriented as it descends under its own weight, but tilted as it is pulled back up to the surface and towards the boat.

4.3.5 Pressure Coordinate and Spatial Binning

For the HyperPro profiler, the spatial coordinates are based on pressure. Pressure data for *Ed*, *Lu*, and *Es* are interpolated from pressure sensor based on common coordinate (time) in each '.dat' file. The interpolation method used for both Profiler and Reference instruments is 'linear'.

Each cast can be recorded as one or multiple profiles. A complete profile includes one down-cast and one up-cast. Distinct profiles are delineated by separation point (i) based on pressure profile. Separation point (i) is defined as:

$$\text{diff(Pressure(i-1))} < 0;\ \text{diff(Pressure(i+1))} > 0;\ \text{diff(time)} > 0$$

where *diff* is the derivative operator.

For each profile, data is spatially binned and averaged and two bin intervals (0.2 m and 1.0 m) are used (Figure 4.5). At each bin, averaged *Ed* and *Lu* across all profiles are calculated and two mega bin profiles (0.2 and 1 m bins) are derived.

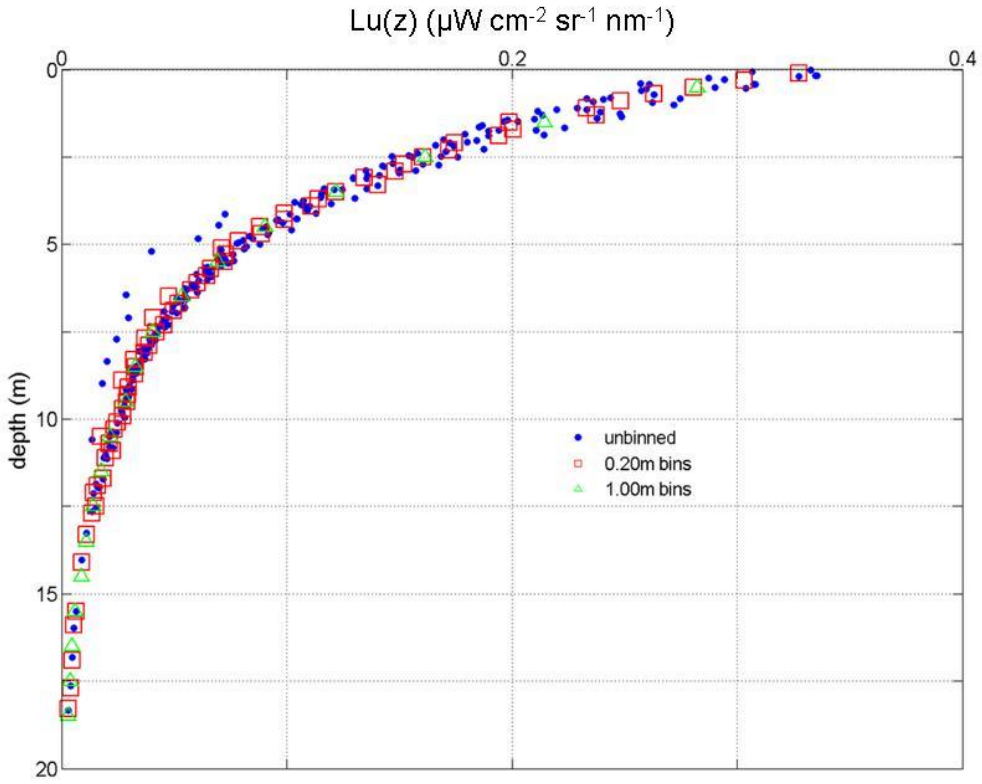

Figure 4.5. Vertical profile of upwelling radiance (Lu) as a function of depth. Blue circles indicate original measurements, while the open red and green markers show data binned at 0.2 m and 1.0 m intervals, respectively.

5. Analysis of processed radiometric data

After the raw radiometric data are processed, the user can determine a range of other quantities. This section describes calculations for photosynthetically available radiation (PAR), the diffuse attenuation coefficient (K), remote sensing reflectance (*Rrs*) and other quantities.

5.1 Photosynthetically available radiation (PAR)

PAR is a measure of the number of photons available for photosynthesis by chlorophyll. Units of PAR can be expressed as quanta cm^{-2} s^{-1} and is estimated using the following equation:

$$PAR = \int_{400nm}^{700nm} \frac{h}{\lambda c} \mathbf{E_d(}\lambda) d\lambda$$

λ - wavelength

h - Plank's constant 6.625x 10^{-34} Js

c - speed of light $3x10^8$ m s^{-1}

Ed(λ) -Downwelling spectral irradiance (mW cm^{-2} nm^{-1})

Before calculating PAR, the Ed(z) profile is normalized to the time-mean of surface irradiance (*Es*, as measured from the SAS). This minimizes the effects of high frequency variability in the light field due to clouds. The Trapezoidal Rule can be used to do numerical integration from 400 to 700 nm in order to derive the PAR profile.

5.2 Attenuation coefficient, K

The diffuse attenuation coefficient (*K*) is an apparent optical property that is useful for characterizing how light is naturally attenuated with depth as a result of the inherent optical properties of the water. As such, *K* is essential for estimating water leaving radiance in the absence of direct measurements since it allows for estimation and extrapolation of radiance values. *K* can be computed from radiometric profiles, as made using the HyperPro system. There are several methods of computing *K* from HyperPro data, but computational techniques will remain constant, regardless of whether the user is deriving *Kd* (*K* based on downwelling irradiance (*Ed*)) or *KLu* (*K* based on upwelling radiance (*Lu*)). The following section describes four methods of deriving *Kd* for three wavelengths. The four methods are as follows:

- K1 = $\frac{1}{<E>} \times \frac{Ed_2 - Ed_1}{Z_2 - Z_1}$

- K2 = $\frac{\ln Ed_1 - \ln Ed_2}{Z_2 - Z_1}$

- K3 = Linear fitting to ln *Ed*(z)

- K4 = Nonlinear fitting to *Ed*(z)

Open raw or binned data with data analysis tool, such as Microsoft Excel or Matlab.

Method K1 --> Use equation K1 to find *dEd/dz* at each bin interval. Take the mean of these computed values over the entire water column, or over the depth range you wish to compute *K*. The mean is your *K* value.

Method K2 --> Use equation K2 to find *d ln(Ed) /dz* at each bin interval. Take the mean of these computed values over the entire water column, or over the depth range you wish to compute *K*. The mean is your *K* value.

Method K3 --> Take the natural log of *Ed* at each bin interval. Using a scatter graphing function, plot ln(*Ed*) as a function of depth over the desired depth range. Add a linear trendline, and show the equation on the chart. The slope of the regression is your *K* value.

Method K4 --> The desired end product is the slope of the non-linear least squares fit to *Ed* as a function of depth (z). This value will be your *K* value. In Matlab, the user can use a non-linear least squares minimalization function such as *fminsearch*.

NOTE: in Microsoft Excel, fitting an exponential curve to *Ed* as a function of depth does not output a true least-squares fit. The user must use the 'solver' function. For instructions on how to load the Solver add-in, follow this link.

STEP 1

In order to use the solver function in Microsoft Excel, first create a 'model' for each $Ed(\lambda)$ profile. The model will be a perfect exponential curve that uses an approximate K value as a slope, and is essentially your least-squares fit. Create this curve by retaining the $Ed(\lambda,0-)$ value, and calculating $Ed(\lambda)$ for each depth below using the following equation:

$$Ed(\lambda,z) = Ed(\lambda,0-)\, e^{-kz}$$

NOTE: The *K* value used in this equation should reference a cell value, as this will be a dynamic number that will be changed by the solver in order to create the least-squares fit. In other words, make sure that as the cell containing the *K* value is changed, the model will adjust accordingly.

STEP 2

Calculate the standard deviation between the model and original data set at each binned-depth interval. Calculate STDEV for each wavelength. This is the target cell that will be minimized using the solver function.

STEP3

Call up the Solver add-in. The following pop-up should appear:

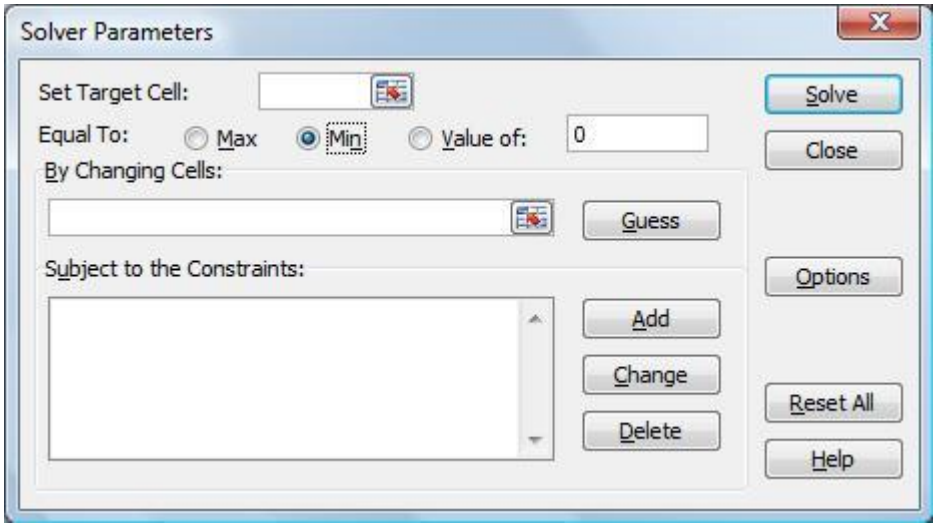

In the *Set Target Cell* edit box, select the STDEV cell for a wavelength, calculated in STEP 2. By selecting MIN, the solver will attempt to minimize the value of the deviations by changing the value of *K* in the model. In the *By Changing Cells* edit box, select the cell containing the initial *K* value that was used to compute the model. Click the SOLVE button. The solver will then compute the value of *K* that returns the closest fit of the model to your data. The resulting value is $K(\lambda)$ using a non-linear least squares fit model.

5.2.1 Comparison of Methodology

The four methods of calculating *Kd* were compared across three wavelengths (443, 555, and 670 nm) and PAR. The results are shown in Figure 5.1. There is good agreement between methodologies in the lower wavelengths, but there are some discrepancies in the red wavelengths and PAR. There is a similar pattern for *KLu*, as shown in Figure 5.2.

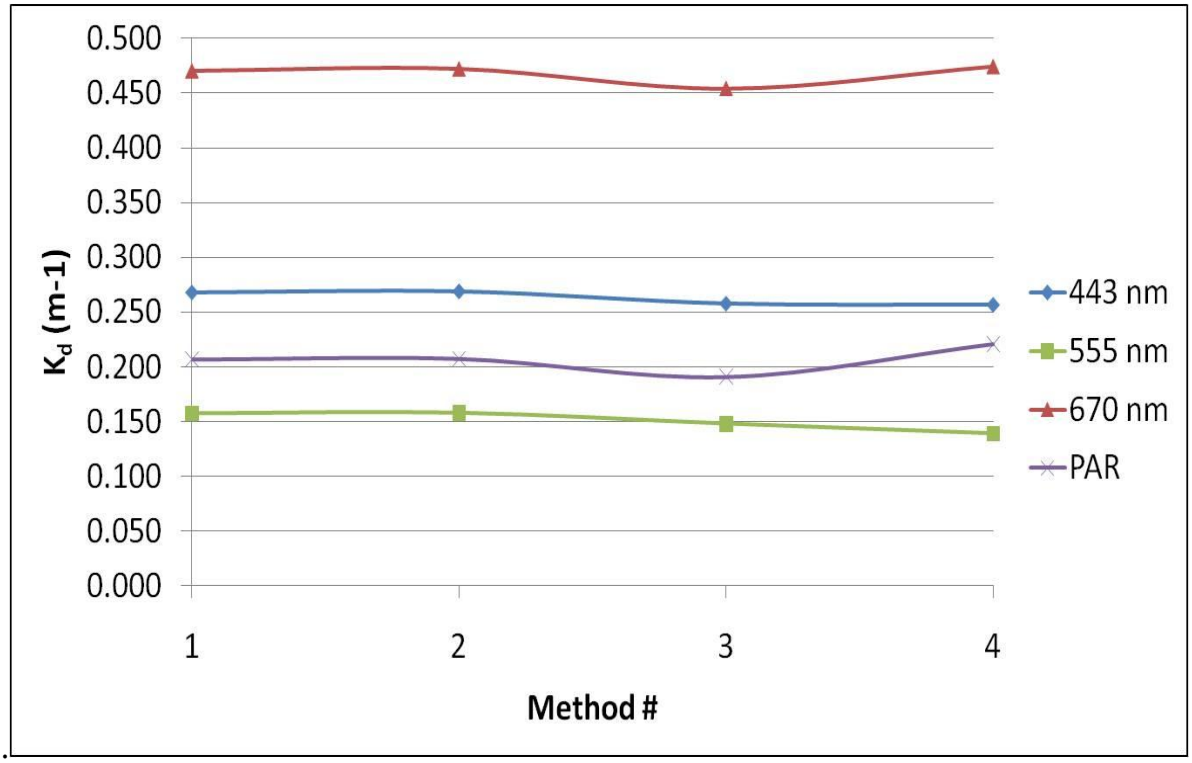

Figure 5.1 - Comparison of methods for calculating Kd

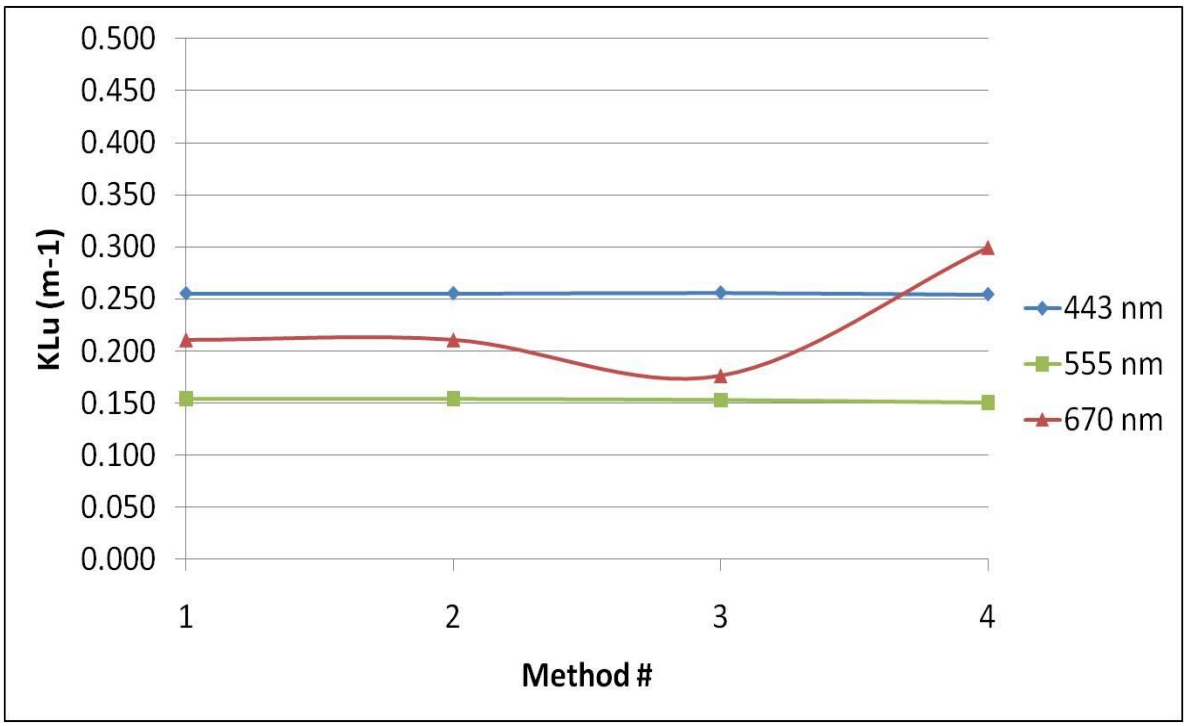

Figure 5.2 - Comparison of methods for calculating KLu

5.3 Remote sensing reflectance, *Rrs*

Calculation of remote sensing reflectance requires values for upwelling radiance that has been transmitted through the surface (*Lw* or *Lu(*0+)) and the downwelling irradiance above the surface (*Ed* or *Es*). Since each instrument configuration described here provides a different combination of above- and below-water radiance and irradiance measurements, processed data from each of the three systems are analyzed distinctly.

5.3.1 HyperSAS

The HyperSAS system makes direct measurements of *Ed*, *Li* (sky radiance) and *Lt* (sea-surface radiance). Since Lt incorporates both upwelling radiance and surface-reflected radiance, the first step of the analysis is to determine what the reflected portion is and remove it. To do this, multiply *Li* by the Fresnel reflectance factor (ρ) and then subtract this product from *Lt*. The "standard" value for the reflectance factor is 0.028 (2.8%), but a different value may be more appropriate given different sky conditions. There are several ways to define the appropriate ρ or to verify the validity of the estimated rho value:

1. Mobley (1999) and Mobley et al. (2005) provide a ρ table and give a complete overview about how to estimate the appropriate ρ as a function of the viewing angles (θ and ϕ) and the wind speed.
2. The validity of the estimated ρ can also be verified using Hydrolight.
3. Assuming that remote sensing reflectance is null in the NIR (which might not be true in some cases, in particular in CASE 2 waters) the user might also prefer to estimate ρ by minimizing the following cost function:

$$\chi = \sum_{\lambda=750}^{800} \{(Lt_\lambda - \rho Li_\lambda)/Ed_\lambda\}$$

Figure 5.3 shows the importance in determining the right ρ. Indeed a too high/low ρ will underestimate/overestimate *Rrs*.

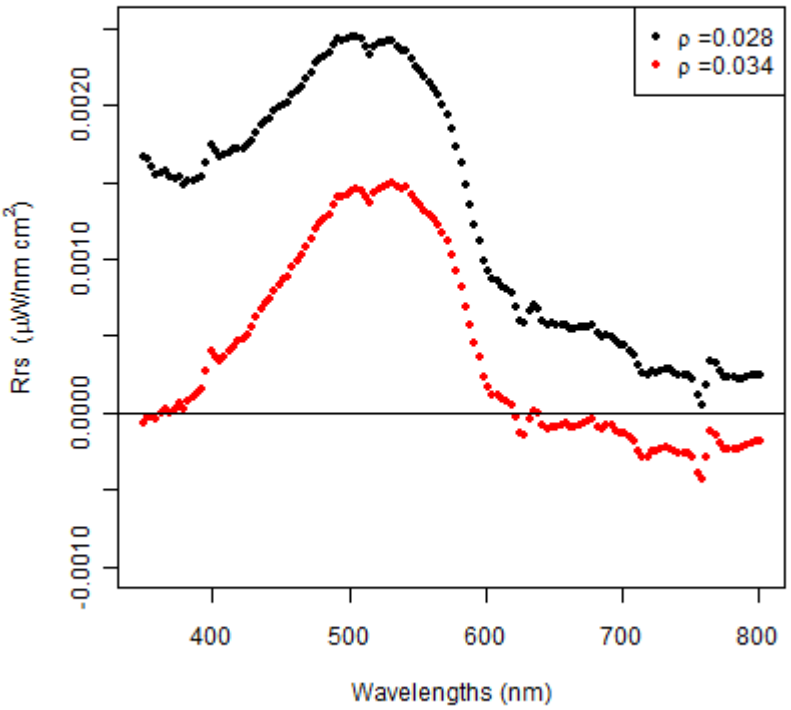

Figure 5.3. Estimated Rrs using different values for ρ. The optimum ρ was estimated minimizing the cost function and assuming the remote sensing reflectance being null in the NIR.

Finally, once the appropriate ρ is defined, the remote sensing reflectance (*Rrs*) can be computed as follows (see Figure 5.2):

$$Rrs = (Lt - \rho Li_{\lambda}) / Ed_{\lambda}$$

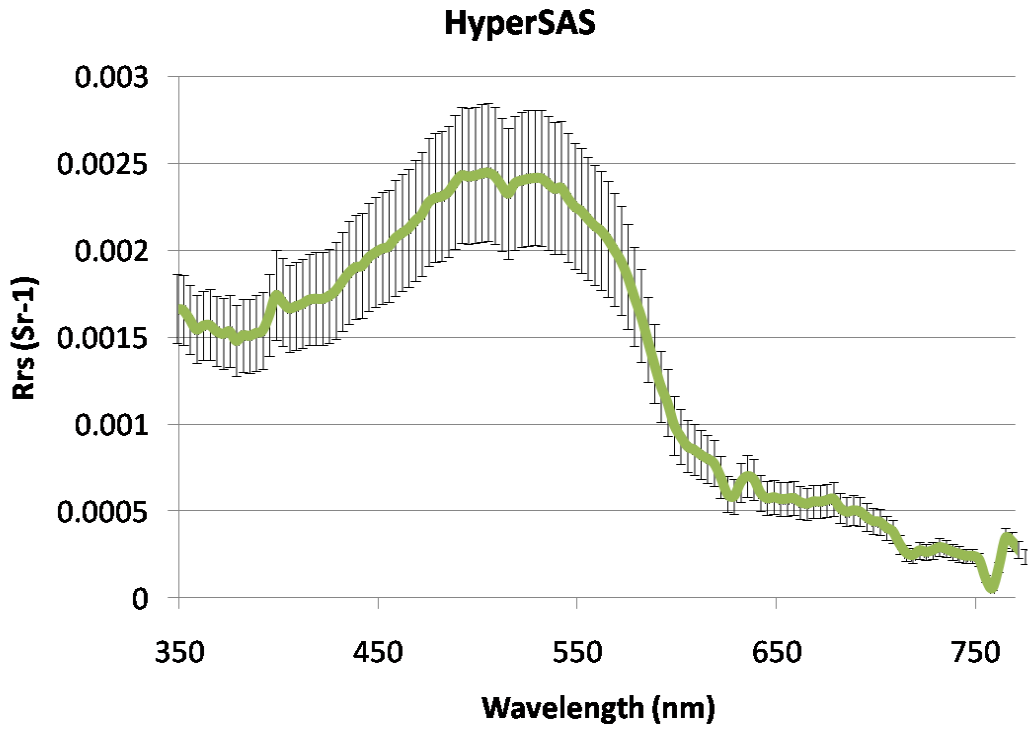

Figure 5.4 HyperSAS data collected on 20 July 2011 in the Gulf of Maine under clear sky conditions were processed using the method described above. The calculated Rrs is shown here with the standard errors (which reflect the temporal variance of the radiometer measurements). The green Rrs spectrum shows strong absorbption in the blue, suggestive of CDOM rich water .

5.3.2 HTSRB

With the HTSRB, *Lu* (60 cm below the sea surface) and *Ed* data are recorded over a defined time-series, and these data are used to finally calculate *Rrs*. An example of a *Lu* and *Ed* from a deployment with the HTSRB is shown in Figure 5.5. Here, median and standard deviation for *Lu* and *Ed* are shown for a 10 minute-long time series in the Gulf of Maine.

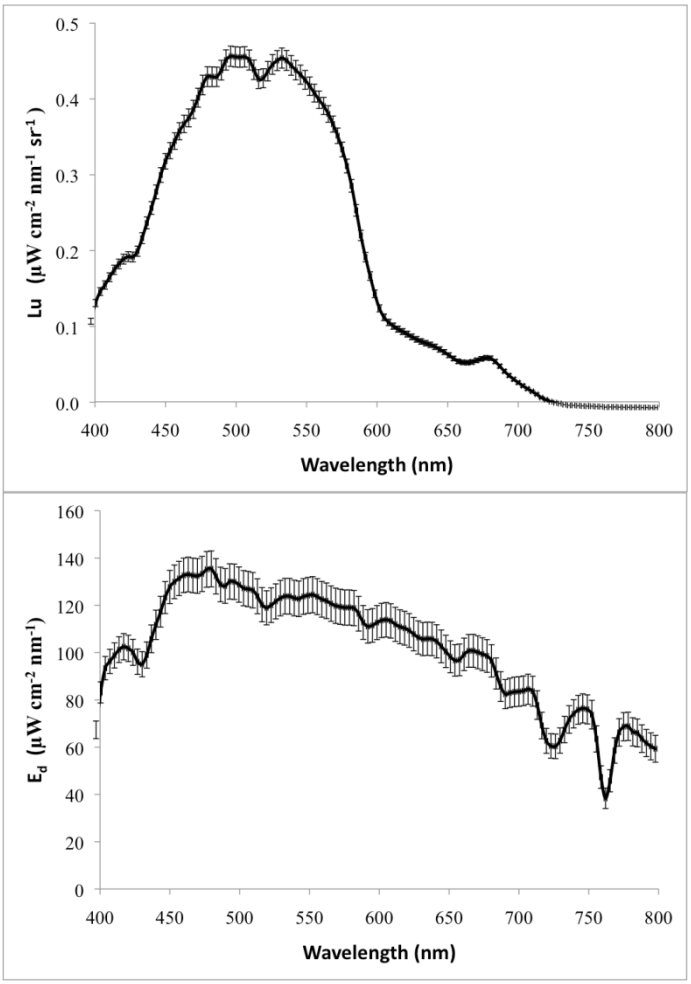

Fig. 5.5. Example of Lu and Ed (at 60cm depth) and related uncertainties (collected on 07/20/2011, coastal waters of Maine)

Since *Lu* is measured at 60 cm below the sea surface, it is necessary to calculate *Lu* just below the surface (*Lu(*0-)) before estimating water leaving radiance and therefore remote sensing reflectance. *Lu(*0-) can be obtained by the equation:

$$Lu(\lambda, 0\text{-}) = Lu(\lambda, z)\, e^{(-KLu*z)}$$

where z is equivalent to 60 cm, and K_{Lu} is the diffuse attenuation coefficient (refer to Section 5.2 for *K* calculation methods).

The radiance just above the surface, water leaving radiance, (*Lw*, in µW $cm^{-2}nm^{-1}$ sr^{-1}) is calculated from *Lu(*0-) by

$$Lw(\lambda)=t* Lu(0\text{-}, \lambda)/(n^2)$$

where n is water refractive index (for seawater, n~1.34) and t is the radiance transmittance of the surface (t~0.98) (Chang et al., 2003). Comparisons between *Lu*(0-) and *Lw* can be seen in Figure 5.5. The plot is in agreement with what is expected, notably that *Lu* decreases with depth. Based on the equation above, we also expect a large decrease in *Lu* when the light goes through the water surface from the water to air. This is also shown in Figure 5.6.

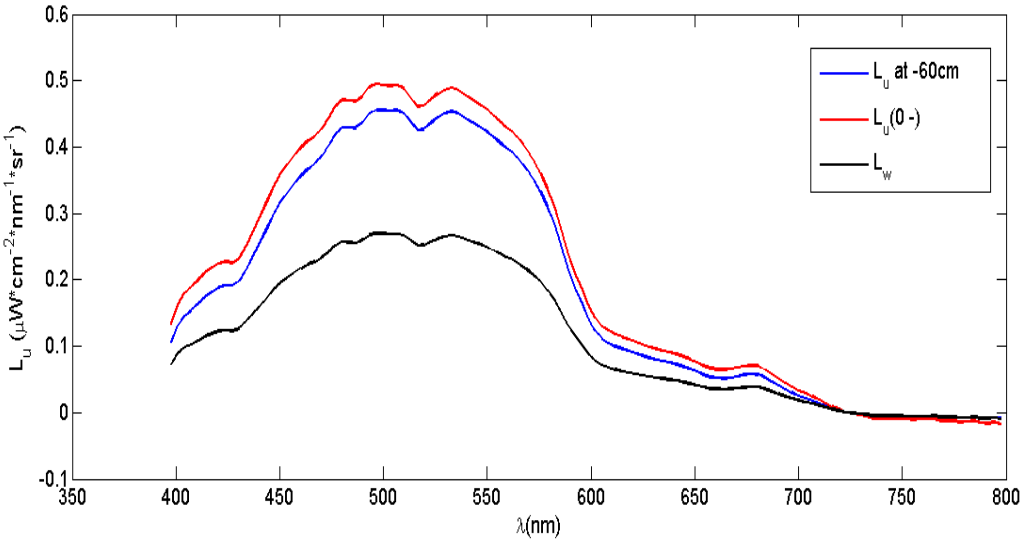

Figure 5.6 Comparison of Lu at a depth of 60 cm, right below the sea surface (Lu(0-)) and right above the sea surface (Lw).

Remote sensing reflectance (*Rrs*) for all wavelengths can then be calculated from *Lw* and *Ed*:

$$Rrs\ (\lambda) = Lw(\lambda)/Ed\ (\lambda)$$

It is important to note, however, that HTSRB measures *Ed* and *Lu* at slightly different wavelengths (~1 nm), so it is necessary to interpolate the data to allow appropriate matching in the *Lw*/*Ed* ratio.

Uncertainties to *Rrs* values can be obtained by propagating the errors associated with *Lu* at 60 cm depth and *Ed*, since those are the fundamental quantities used to derive *Rrs*. Uncertainties in *Rrs* per wavelength can thus be described by the equation:

$$Rrs(\lambda) * \sqrt{(SdLu(\lambda)/Lu(\lambda))^2 + (SdEd(\lambda)/Ed(\lambda))^2}$$

where *SdLu* is the temporal standard deviation of the *Lu* signal time series (measured at 60 cm depth), *Lu* is the median of *Lu* time series, *SdEd* is the temporal standard deviation of *Ed* time series, and *Ed* is the median of Ed time series.

Note that uncertainties associated with the extrapolation of subsurface *Lu* values upward to just under the surface (*Lu(*0-)) are not included here. The extrapolation of *Lu(*0-) requires an esimate of the diffuse attenuation coefficient, *KLu*, and so uncertainties in the *Lu(*0-) estimate (and conequently *Rrs* estimate) will also reflect uncertainties in the K values. Depending on the method used to calculate *KLu* (See Section 5.2 for more information), different methods can be used to determine the error associated with each calculation. If using methods K1 and K2, the error in *KLu* is related to the standard deviation in measured *Lu* values. If using methods K3 and K4, the error in *KLu* is the error in calculated slope values. In addition, the transformation between *Lu(*0-) and *Lw* was assumed not to carry any errors with the conversion factors. Statistical simulations could be used to understand the effect of slight changes in index of refraction and transmittance factors in estimating *Lw*, but that was considered out of the scope of this report. *Rrs* measurements and related uncertainties after correction with the diffuse attenuation coefficient (right above the surface) are plotted in Figure 5.7.

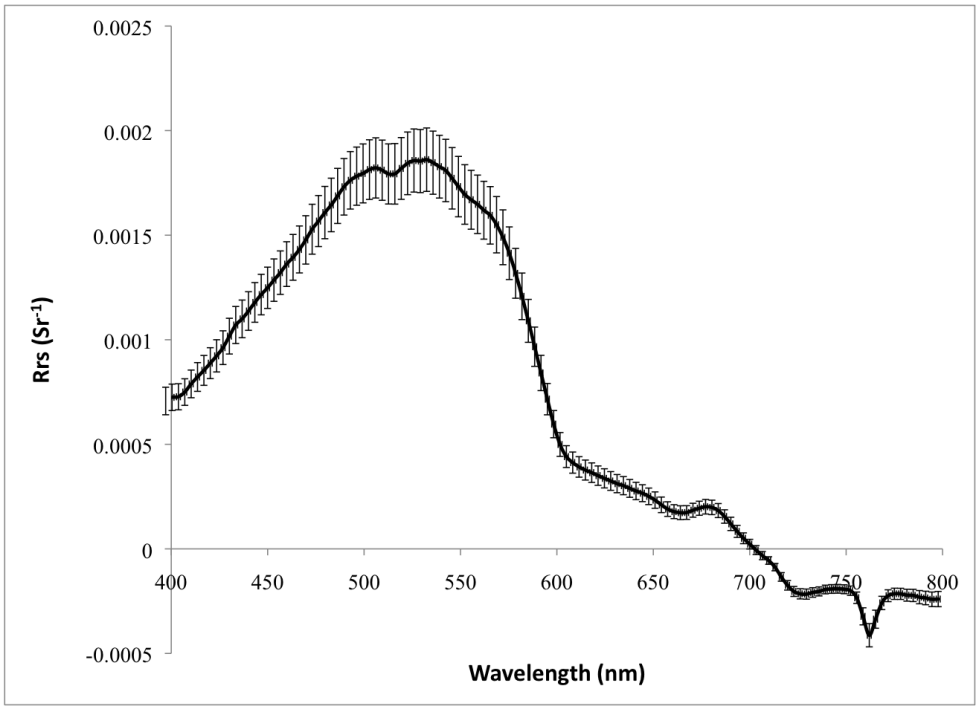

Figure 5.7 Rrs calculated above the surface and uncertainties (Final correction, after extrapolating Lu from 60 cm to Lu just below the sea surface, and then converting to Lw).

Uncertainties in the *Rrs* spectrum shown in the figure above could possibly be attributed to the sensor internal calibrations, variations in the tilt of the sensors, ship shadow and changes in the light field due to cloud cover, even though the latter two were not observed during the deployment in the field. The *Rrs* spectrum is typical of coastal waters rich in CDOM with high absorption in the blue as compared to the green part of the spectrum. There is also an evident fluorescence peak at around 680 nm. *Rrs* cannot be negative, but beyond 700 nm the *Rrs* spectrum shows negative values in the NIR. This could be due to the fact that the NIR signal is low due to water absorption, which causes an increase in the sensitivity of these wavelengths to error in the measurement. This issue also arises when sensors need recalibration, so perhaps this HTSRB is due for a factory calibration.

5.3.3 HyperPro

5.3.3.1 Buoy Mode

When using data collected from the HyperPro, take the median value for *Lu*, *Eu*, and *Ed* (from the HyperSAS as a reference sensor) and subtract their corresponding median dark values. In addition, the wavelength bands are slightly different for each sensor. Before further calculations, interpolate your data so the wavelength bands match. In order to extrapolate *Lu* measurements made below the surface ($Lu(z, \theta, \phi, \lambda)$) to *Lu* just below the surface ($Lu(0-, \theta, \phi, \lambda)$ use the equation:

$$Lu(0-, \theta, \phi, \lambda) = Lu(z, \theta, \phi, \lambda)e^{KLu\, dz}$$

where *KLu* (m^{-1}) is the diffuse attenuation coefficient for *Lu* and *dz* is the difference in depth between the surface and the *Lu* sensor location (refer to section 5.2 for calculating *K* values).

To calculate *Rrs*, one must convert $Lu(0, \lambda)$ to water leaving radiance ($Lw(0+, \lambda)$), which is the surface reflected radiance (in air) subtracted from the total upwelling radiance (in air). Since *Lw* cannot be calculated directly, it is estimated by extrapolation using the equation:

$$Lw(\theta, \phi, \lambda) = Lu(0-, \theta, \phi, \lambda)\,(1 - \rho)/n_w^2$$

where ρ is the Fresnel reflectance of the air-sea interface and n_w is the refractive index of seawater. Finally, *Rrs* is calculated with the equation:

$$Rrs\,(\lambda) = Lw(\lambda)/Ed(\lambda)$$

Figure 5.8. compares *Rrs* spectra that were calculated from varying *Lw* values. *Lw* was calculated by estimating the transmission of three different subsurface *Lu* values through the sea surface. Two *Rrs* spectra used *Lu* values extrapolated to the surface with two different *K* estimation methods (K2 and K4, Section 5.2). The third *Rrs* spectrum was computed from an *Lu* value left uncorrected by a *K* value.

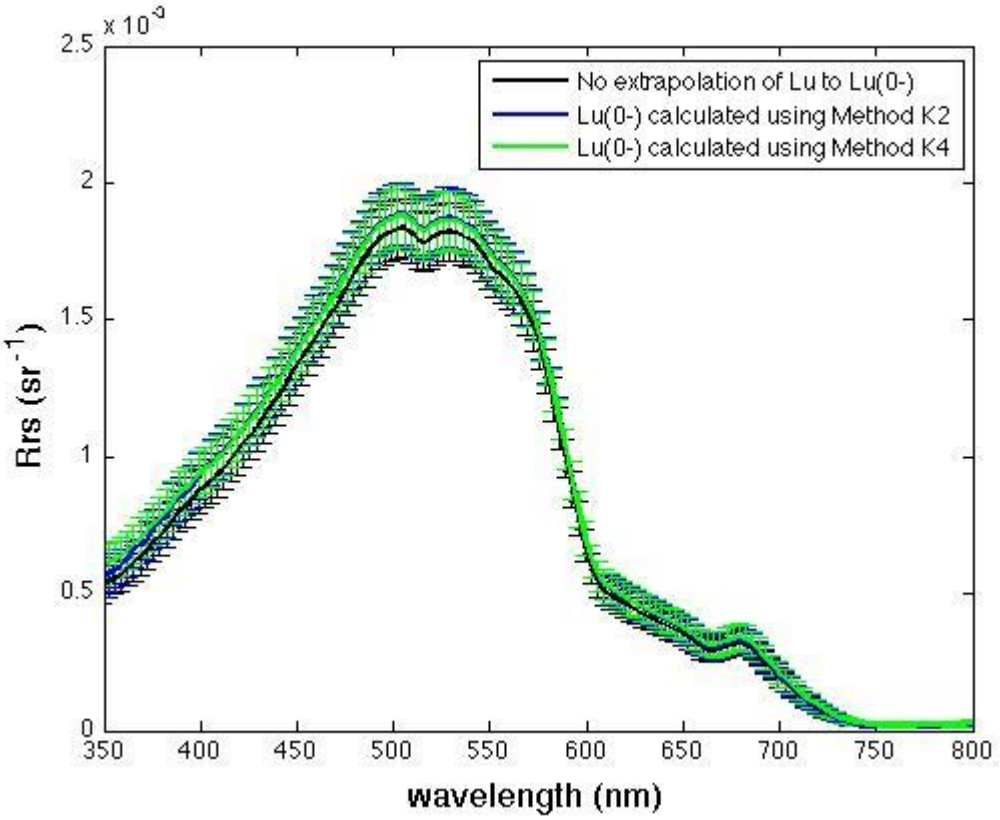

Figure 5.8. Three estimates of Rrs (sr^{-1}), calculated as Lw/Ed, were made using data collected in the Gulf of Maine in July 2011. All three estimates use the same Ed, which was measured using a reference HyperSAS irradiance sensor mounted above water on the ship. In contrast, Lw was calculated by estimating the transmission of 3 different subsurface Lu values through the sea surface: 1) Lw was calculated from the Lu measured at depth, without extrapolating a value for just below the surface (black line); 2) Lw was calculated with an Lu(0-) value calculated using a K value determined by method K2 (blue line); and 3) same as 2, but using a K value determined by method K4 (green line). See section 5.2 for details on methods for determining K. Note that the blue and green do not differ much and that the error bars for the three different Rrs spectra overlap.

5.4 Irradiance reflectance (R) and Upwelling radiance distribution (Q)

Two additional apparent optical properties calculated from HyperPro floating casts are reflectance (*R*) and the upwelling radiance distribution (*Q*). *R* is the ratio of *Eu* to *Ed* and *Q* is the ratio of *Eu* to *Lu*. Figure 5.9. shows that the *R* spectrum has the same shape as the *Rrs* spectrum (Figure 5.8.) calculated for the same location. Since both *R* and *Rrs* have the same *Ed*, the ratio of *Eu* to *Lu* should be a constant for *R* and *Rrs* to have the same spectral shape. In fact, for a Lambertian surface, where the apparent radiance is the same regardless of viewing angle, *Q* is equal to π. Figure 5.9, however, shows that *Q* is not a constant for every wavelength and that error increases in the red end of the spectrum. Q is important in relating IOPs and AOPs.

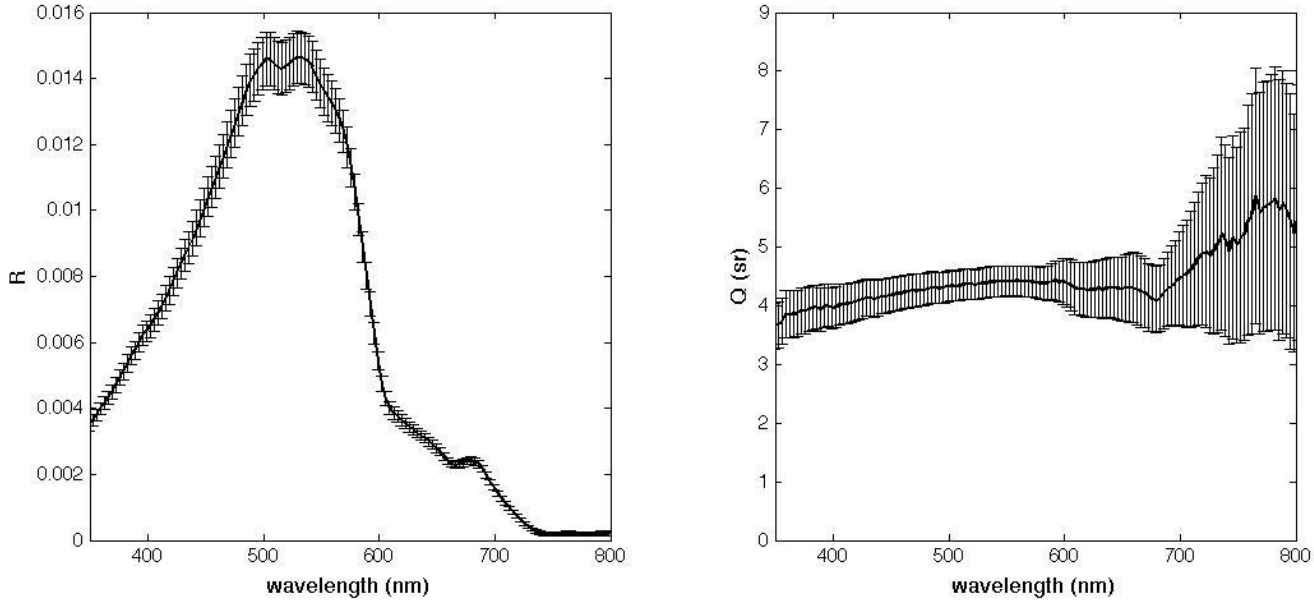

Figure 5.9. R (left) and Q (right) calculations from HyperPro in buoy mode. The shape of the R spectrum is very similar to that of the Rrs spectrum, suggesting that the ratio of Eu to Lu is a constant. The Q(λ) spectrum shows that Q is not constant over all wavelengths.

5.5. Radiometric closure

Field data obtained from the simultaneous deployment of three separate instrument systems in the Gulf of Maine in July 2011 provide an excellent opportunity to assess closure between disparate radiometric measurements. Figure 5.10 shows that estimates of *Rrs* (*Lw*/*Ed*) from the different instruments are in close agreement (<10% apart) over blue and green wavelength bands. In the red wavelength band, estimates of *Rrs* show significantly greater variation (up to 50%).

The differences between *Rrs* estimates reflect in part the techniques used to transform subsurface and above-water measurements into *Lw* and *Ed* values. In the case of subsurface measurements, this entailed extrapolation of *Ed*(z) and/or *Lu(*z) up to just below the sea surface and then estimation of their transmission through the surface. In the case of above-water measurements, this entailed the deconvolution of *Lt* into its *Lw* and sea-surface reflectance components, using assumptions about the reflectivity of the sea surface. Thus, in all cases, *Rrs* estimates were impacted by the state of the sea surface. In addition, because the different instruments may not a*Lw*ays be deployed simultaneously, temporal changes in the light field due to cloud effects or the diurnal cycle would also contribute to differences between *Rrs* estimates. The comparison presented here, however, probably represents an optimal case, since the data for these estimates were collected within 2 hours near noon on a day with a clear, blue sky and almost flat sea surface.

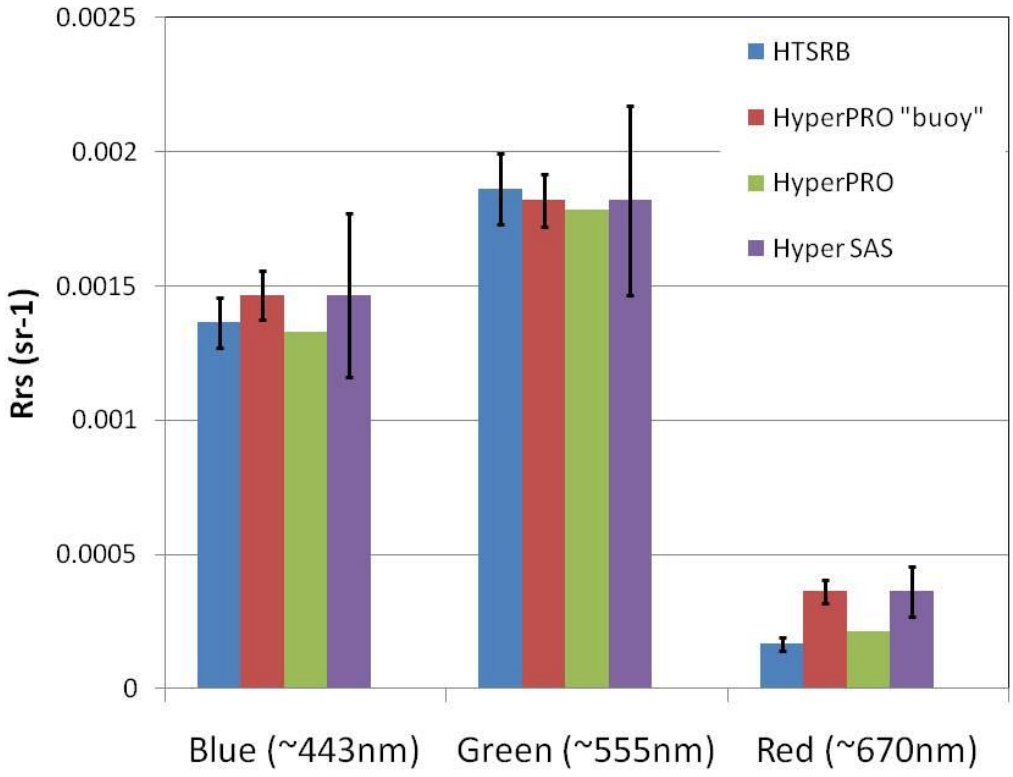

Figure 5.10. Comparison of Rrs estimates from four distinct radiometer systems deployed in the Gulf of Maine in July 2011. Error bars indicate standard deviation of each estimate, and are largely reflective of the temporal variance of the radiometers' signals.

6. Cautionary notes

The user should keep in mind that radiometer measurements will, by definition, be impacted by any features of the local light field, including those that arise 'artificially' due to the presence of the observing platform. Thus, care should be taken to design the platform and deploy instruments from it in a way that minimizes their optical footprint. For example, instruments should be deployed far enough away from a ship (or on its sunward side) so that the the ship's shadow does not interfere with the measurements. Figure 6.1 shows the effect of boat shadowing on *Rrs* estimated from HyperPro deployments in the Gulf of Maine in July 2011. In this case, *Rrs* was calculated using *Lu* from the profiler and *Ed* measurements from a deck-mounted reference radiometer. Therefore, when the profiler is shadowed by the boat, *Lu* values were attenuated but not *Ed*, thus producing a similar spectral shape but lower *Rrs*. The color of a ship's hull might also affect radiometer measurements. For example, a white coloured ship hull might reflect light back towards the water surface which could then be re-reflected or backscattered towards the HyperSAS assembly and result in an overestimation of the measured sea-water radiance (*Lt*).

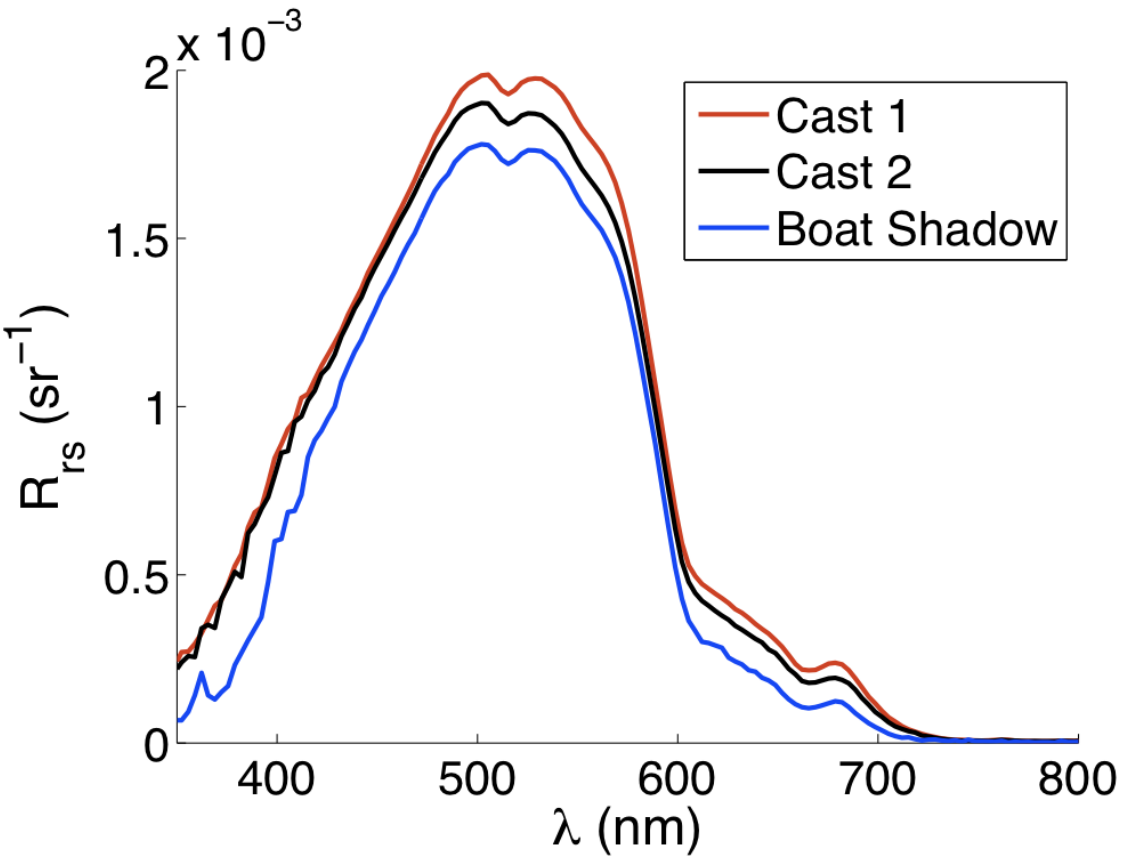

Figure 6.1 Hyperpro-derived remote sensing reflectance for three casts, one of which was conducted in the shadow of the boat. Rrs is calculated using Lu from the profiler and Ed measurements from a deck-mounted reference radiometer. The shape of the spectrum is similar but Rrs values are attenuated due to boat shadowing effects on Lu and not on Ed.

7. References

Chang G. C., Tommy D. Dickey, Curtis D. Mobley, Emmanuel Boss, and W. Scott Pegau, (2003). "Toward Closure of Upwelling Radiance in Coastal Waters," Appl. Opt. **42**, 1574-1582.

Mobley C. D., (1999). "Estimation of the Remote-Sensing Reflectance from Above-Surface Measurements," Appl. Opt. **38**, 7442-7455.

Mobley, C.D., Sundman, L.K., Davis, C.O., Bowles, J.H., Downes, T.V., Leathers, R.A., Montes, M.J., Bissett, W.P., Kohler, D.D.R., Reid, R.P., Louchard, E.M., Gleason, A., (2005). "Interpretation of hyperspectral remote-sensing imagery by spectrum matching and look-up tables," Appl. Opt. **44**(17), 3576-3592.

APPENDIX

The Satlantic OCR radiometers output dark-frame and light-frame data files that must be processed together to produce dark-corrected data. Specifically, a dark value is subtracted from each light reading. These 'dark readings' allow for a subsequent subtraction of the instrument's baseline reading in the absence of light. Because the dark and light data are not gathered simultaneously, the dark values must be interpolated in time to match up with the light values. After the interpolation (and removal of light data collected before the first dark measurement and after the last dark measurement), the data can be dark-corrected and made available for further processing. The following matlab script defines a function, 'readOCR_2.m', that performs the dark-correction.

The function requires two input arguments, the names of the dark-frame and light-frame data files.

FILE STARTS BELOW...

```
function [data,tt2,SN,INTtt2] = readOCR_2(fnamdark,fnamlight)

% ------------------------------------------------------------------------
% Read data into Matlab.  Data files are assumed to have already been
% converted to comma-delimited text and calibration and immersion
% coefficients applied in SatCon.  One header line is assumed (to ensure
% this, UNcheck "extra output header information" in SatCon parameters),
% and tt2 tags are assumed to have been processed and formatted (should be
% 2 last columns of .dat file).
%
```

```
% INPUTS:
% fnamdark  = string containing the path/filename of the dark-frame
%           data file for a single sensor
% fnamlight = string containing path/filename of the corresponding
%           light-frame data file
%
% OUTPUTS:
% data      = radiometric data with tt2-interpolated dark-frame
%           values subtracted
% tt2       = Matlab datenumber-formated tt2 vector (sensor-
%           specific)
% SN        = Sensor serial number
% INTtt2    = vector of measurement integration tt2s (seconds)
% ------------------------------------------------------------------------


% 1) READ IN THE DARK-FRAME DATA FILE ...
% fnamdark=HED;
fid = fopen(fnamdark);

% create a text string of conversion specifiers that textscan to use when
% it reads in the data file (user must inspect the data file to determine
% the type and total number of data fields, then adjust the following
% code accordingly):
formatpattern = [];
number_of_floating_point_columns = 146; % inspect data file to determine
number_of_string_columns= 2;            % inspect data file to determine
for ii = 1:number_of_floating_point_columns
          formatpattern = [formatpattern '%f'];
```

```
end

for ii = 1:number_of_string_columns
        formatpattern = [formatpattern '%s'];
end

% read in the file contents
A = textscan(fid,formatpattern,'headerlines',1,'delimiter',',');
fclose(fid);

% read numeric data (not all are output; see "rawheader" variables in
% OCRstuff.mat)

% if the file is empty, then set output as NaNs, otherwise write in the
% dark data and date/time info, then proceed to the light data file
if isempty(A{1})
        data=NaN;
        tt2=NaN;
        SN=NaN;
        INTtt2=NaN;
else

 % write the dark file numerical data to a 'darkdata' array
        for i = 1:number_of_string_columns
   darkdata(:,i) = A{1,i};
        end;

        % read date and time data (renamed as 'tt2') as formatted by SatCon
        for i = 1:number_of_floating_point_columns
```

```
tt2(:,i) = A{1,number_of_floating_point_columns+i};
        end;

        % Convert SatCon date/tt2 to Matlab datenumber format
        for i = 1:size(tt2,1)
        B = [sscanf(tt2{i,1},'%f-%f')' sscanf(tt2{i,2},'%f:%f:%f')'];
        C = datevec(datenum([B(1) 0 B(2)]));
        C(4:6) = [B(3) B(4) B(5)];
        darkdate(i,1) = datenum(C);
        end;

% clean up
        clear tt2 A B C;

        %repeat all of the above for light-frame datafile

        % fnamlight=HSE;
        fid = fopen(fnamlight);
        A = textscan(fid,formatpattern,'headerlines',1,'delimiter',',');
        fclose(fid);

        if isempty(A{1})==1
data=NaN;
tt2=NaN;
SN=NaN;
INTtt2=NaN;
        else

for i = 1:number_of_floating_point_columns;
```

```
  lightdata(:,i) = A{1,i};
end;

for i = 1:2;
  tt2(:,i) = A{1,number_of_floating_point_columns+i};
end;

for i = 1:size(tt2,1);
  B = [sscanf(tt2{i,1},'%f-%f')' sscanf(tt2{i,2},'%f:%f:%f')'];
  C = datevec(datenum([B(1) 0 B(2)]));
  C(4:6) = [B(3) B(4) B(5)];
  lightdate(i,1) = datenum(C);
end;

% clean up
clear tt2 A B C;

% Prior to interpolating dark-frame data to light-frame tt2scale,
% discard light frames collected before the first or after the last
% dark frame
first = darkdate(1,1);
last = darkdate(length(darkdate),1);
good = intersect(find(lightdate>first),find(lightdate<last));

% retrieve the data. user must specify the columns where the
% radiometer data are located:
start_col = 4; % first colunm of radiometric data
end_col = 140; % last column of radiometric data
lightdata = lightdata(:,start_col:end_col);
```

```
    darkdata = darkdata(:,start_col:end_col);

    % retrieve the serial number of the OCR sensor:
    SN = lightdata(1,1);

    % retrieve the vector of measurement integration tt2s (seconds)
    INTtt2 = lightdata(good,2);

    % loop through each of the data columns and interpolate dark-frame
    % data to light-frame tt2scale
    for i = 1:size(lightdata,2);
      darkfill(:,i) = ...
        interp1(darkdate,darkdata(:,i),lightdate(good),'linear');
    end;

    data = lightdata(good,:)-darkfill;
    tt2 = lightdate(good);

  end
end
```

Closure: Measurement-model and Measurement-measurement

Section Guide

1. Introduction

Closure is the process of obtaining the same value for a quantity (Rrs, chlorophyll concentration, particle backscatter, etc.) in (at least) two independent ways. For example, if Rrs calculated from two different radiometers agrees, given the uncertainties for each instrument, then you have closure between the two methods. Closure is an important process in data analysis because it convinces you that your measurements are sound. The two types of closure investigated in this report are measurement-model closure and measurement-measurement closure. The former refers to agreement between field measurements and the outputs of models that use field data, the latter to the agreement between the same measurement for two data sets, collected using either different instruments or different algorithms to derive the desired variable.

2. Measurement-Model Closure

2.1 Remote sensing reflectance (Rrs) measured and modeled

Hydrolight (Hydrolight - Ecolight 5 © 2008 by Curtis D. Mobley) is a radiative transfer model that can be used to model radiometric variables and apparent optical properties (AOPs), like remote-sensing reflectance (Rrs), for a given water type, sun angle, and atmospheric state. The user can supply inherent optical properties (IOPs) measured in the field, such as absorption (a), scattering (b), backscattering (b_b), attenuation (c) and chlorophyll concentration into the model which in turn computes the desired IOPs and/or AOPs (for technical documentation see Mobley and Sundman, 2008). In the present research,

measurement-model closure is achieved by investigating whether or not the Rrs spectra generated by Hydrolight with field-measured IOPs (absorption, backscatter, attenuation and chlorophyll concentration) agree with the Rrs spectra generated from field data.

Before imputing IOP data into Hydrolight, extreme care has to be taken to ensure proper data processing with all corrections for dark signals, blanks, and temperature/salinity differences (see ac-9/ac-s (pg 73) and BB9 (pg 91) chapters for details). Chlorophyll concentration as a function of depth (mg m^{-3}) is calculated using the *in-situ* fluorometer method described in the flurometers chapter (pg 3). In the present study the chlorophyll absorption specification model is selected based on Case I water. IOPs, a (m^{-1}) and c (m^{-1}) coefficients are measured using an ac-s (described in the ac-9/ac-s chapter, pg 73), while b_b coefficients (m^{-1}) are measured using a BB9 (described in the BB9 chapter, pg 91). Additionally, the model utilizes a Pope and Fry pure water model, considers inelastic scattering effects and an infintely deep water column and estimates a_{CDOM} (m^{-1}) with a filtered ac-s cast. The wind speed is 3 kt and the sky is as 100% clear. In order to compute the sun position and intensity, the specific location while taking the insitu IOP measurements and date and time are also supplied to the model. Finally, the Rrs output from Hydrolight is compared to the Rrs measured using the HyperSAS, the HyperPRO (in buoy mode) and the HTSRB instruments (how Rrs are estimated from these instruments is detailed in radiometers chapter, pg 116). Figure 1 shows the measurement-measurement closure and model-measurment closure for a single cast. The Rrs values measured with the three different instruments all agree within the error limits. Furthermore, the Rrs spectrum generated from Hyrdolight (red line) agrees with the field measurements of Rrs and both HTSRB and Hydrolight Rrs spectra show the characteristic chlorophyll peak around 670 nm. Note that for this specific cast, the Rrs spectrum for the HTSRB appears to drop below zero at about 700 nm. Negative values for Rrs are irrealistic. In the present research this negative offset most likely results from an old calibration file when processing the data. A good way to compare the offset between radiometers is to point them at the same surface and look at the difference between measurements (for both radiance and irradiance sensors).

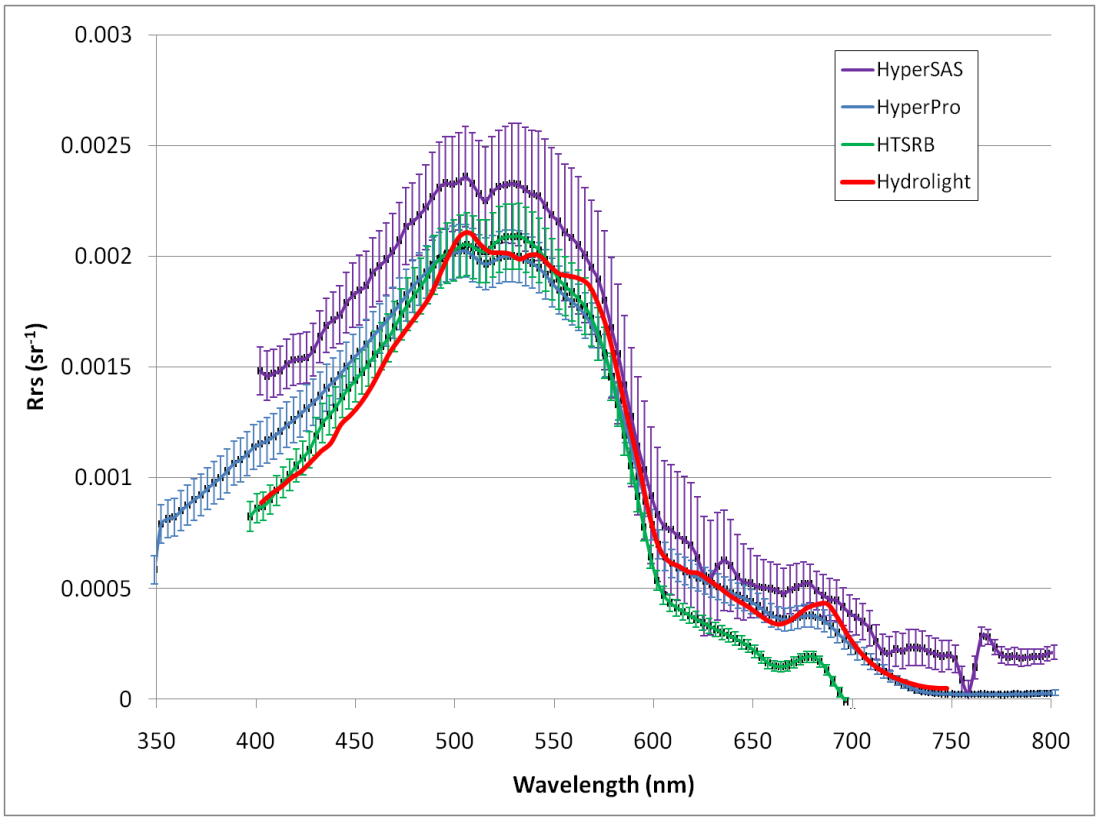

Figure 1. Measurement-model and measurement-measurement closure for Rrs (sr^{-1}) spectra measured in the Gulf of Maine (43 44.9 N 69 29.9 W) on July 20, 2011. Rrs from field measurements using the HyperSAS (purple line), HyperPRO (buoy mode) (blue line) and the HTSRB (green line).

3. Measurement-measurement closure

3.1 Agreement between chlorophyll concentrations and fluorescence with depth

Using ac-s measured a_p (as described in the ac-9/ac-s chapter, a_p is determined by substracting a_{cdom} from a_{total}) and chlorophyll concentration ([chl]) from discrete water samples at three depths (5, 10, and 15 m; [chl] measured with a spectrophotometer as described in the spectrophotometer chapter, pg 35), the specific absorption of chlorophyll (a*(676 nm)) for each depth is. The specific absorption of chlorophyll is defined as follow: a*(676 nm) = a□(676 nm)/chl. To find a□(676 nm), a baseline is fitted between 650nm and 715nm on the a_p spectrum. Using the slope of this baseline, at 676 nm is calculated between the a_p peak at 676 nm and the baseline is calculated. Considering that $a_p = a_{nap} + a$□□and with assumptions about the shape of the a_{nap} curve, the lineheight can be defined as the contribution of a□ to a_p at 676 nm. The average a*(676 nm) value (here egual to 0.015 m^2/mg) over the 3 different depths and the measured a□□(676 nm) at each depth (1-meter binned increments) is then used to estimate a value of chlorophyll concentration at each depth. As shown in figure 2 the calculated profile of chlorophyll concentration has good agreement with the calibrated fluorescence data in shape, and fairly good agreement in magnitude.

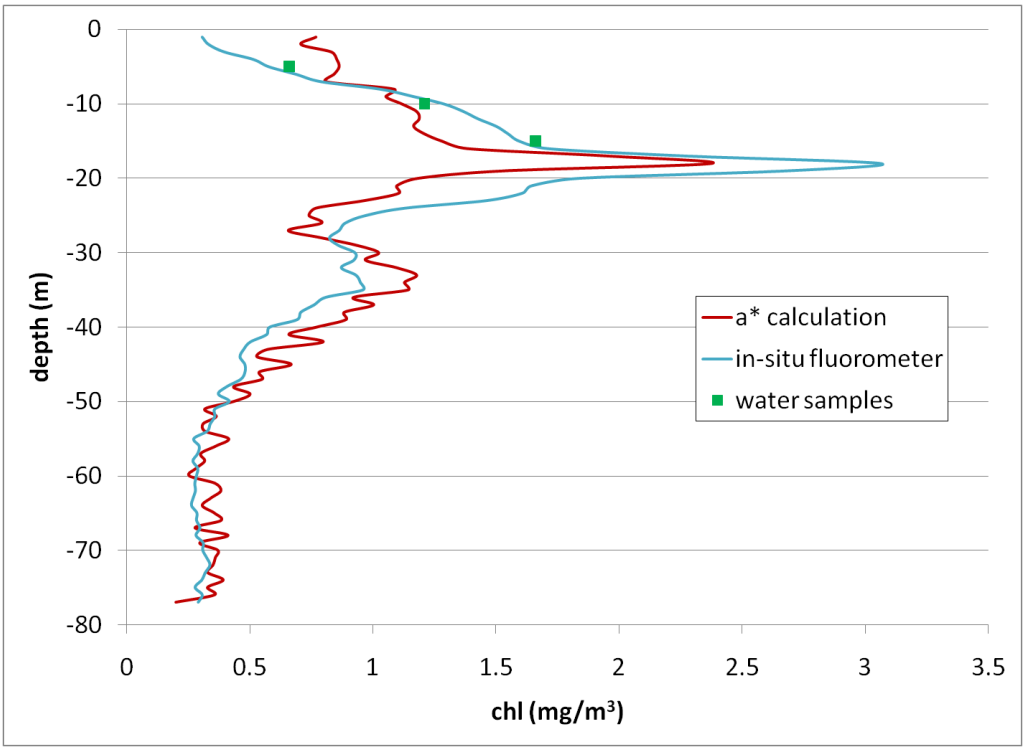

Figure 2. Profile of chlorophyll concentration created using two methods; the blue line is calibrated Wetlabs ECO-FL voltage, and the red line is created using discrete Niskin bottle samples at 5, 10 and 15 m. The green points are the locations of the three water samples. Note the effect of quenching near the surface, which is seen in the in-situ fluorometer profile but not in the specific absorption profile. Further analysis is required to examine different methods of a*(676 nm) calculation.

3.2. Diffuse attenuation Kd estimated from IOP versus Kd estimated from AOP

The diffuse attenuation coefficient (K_d) is an apparent optical property related to the decrease in downwelling irradiance (E_d) with depth (see radiometers chapter, pg 116). However, the attenuation of light with depth also results from the inherent optical properties. Subsequently, K_d can be derived from the measured IOPs (here referred as K_dIOP). Indeed, and as described by Gordon (1989), K_d is proportional to the total absorption (a_t) and the total backscattering (bb_t):

$$K_dIOP= 1.0395*(a_t+bb_t)/\mu_d$$

$$\mu_d= \cos\theta =E_d/E0_d$$

with E_d being the plane downwelling radiance and E_{od} the scalar downwelling radiance (the ratio of the 2 variables gives you information about the directional pattern of the radiance). The total absorption a_t and backscattering bb_t have both been computed previously with the ac-s and bb9 respectively (see portfolio about BB9 and AC-S), however μ_d remains unknown. Note that a_t and bb_t also include the absorption and backscattering and absorption of sea-water.

Section 4.4.2 of the portfolio 'Hyperspectral radiometers', outlines the several methods of computing Kd from the AOP's (here referred as K_dAOP) derived from the radiances measured with the HyperPro. In the present research, the K_d is computed as follow (referred as 'method 1' in the portfolio 'Hyperspectral radiometers'):

$$K_d AOP = dE_d/dz$$

K_dAOP and K_dIOP should be equal to each other. Equalizing both variables will enable us to estimate the remaining unknown μ_d. A way to find μ_d over a range of different possible values is to minimize the following cost function:

$$\chi^2 = \sum_{z=1}^{n} \left[(1.0395 * (a_t + bb_t)/\mu_d) - K_d^{AOP} \right]^2$$

Figures 3. to 5. show K_d computed from both AOP and IOP for 3 different wavelengths. Table 1. gives an overview of the different values of μ_d, estimated with the cost function, for each wavelength and at each depth. Overall the μ_d values varies between 1 and 0.2 which is in agreement with the definition of μ_d, notably that a cosinus varies between 0 and 1. As observed with other instruments (e.g. see figure 2 for the same cast), the peak in chlorophyll is distinctive by an significant peak in attenuation around 20 m depth.

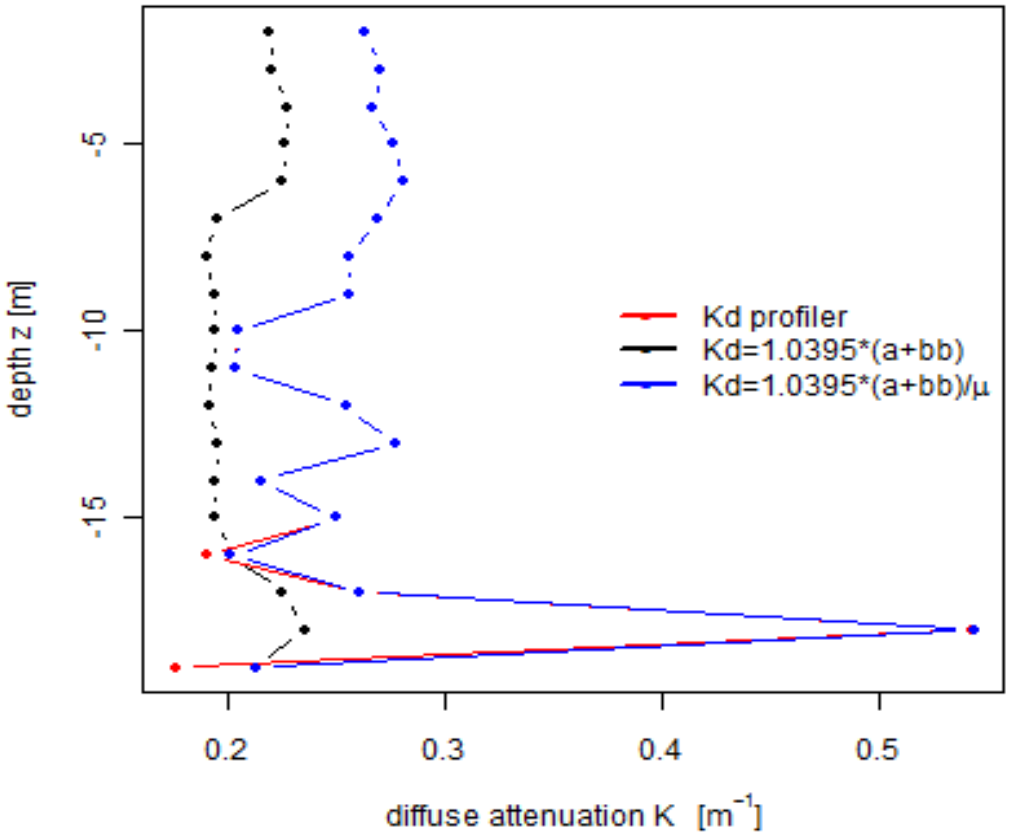

Figure 3. Diffuse attenuation Kd with depth estimated from the IOP's and AOP's for the wavelength at 440 nm.

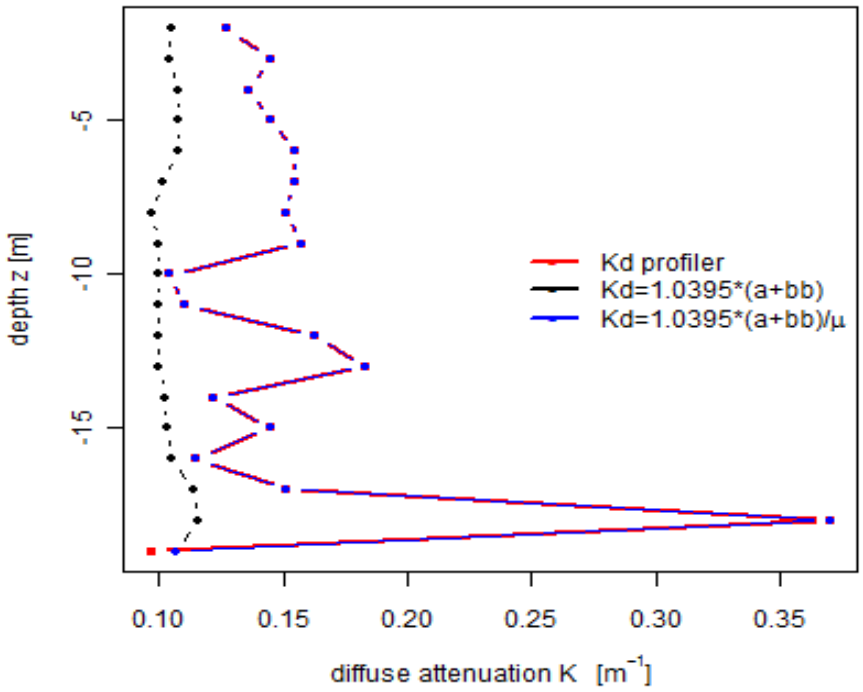

Figure 4. Diffuse attenuation Kd with depth estimated from the IOP and AOP for the wavelength at 555 nm.

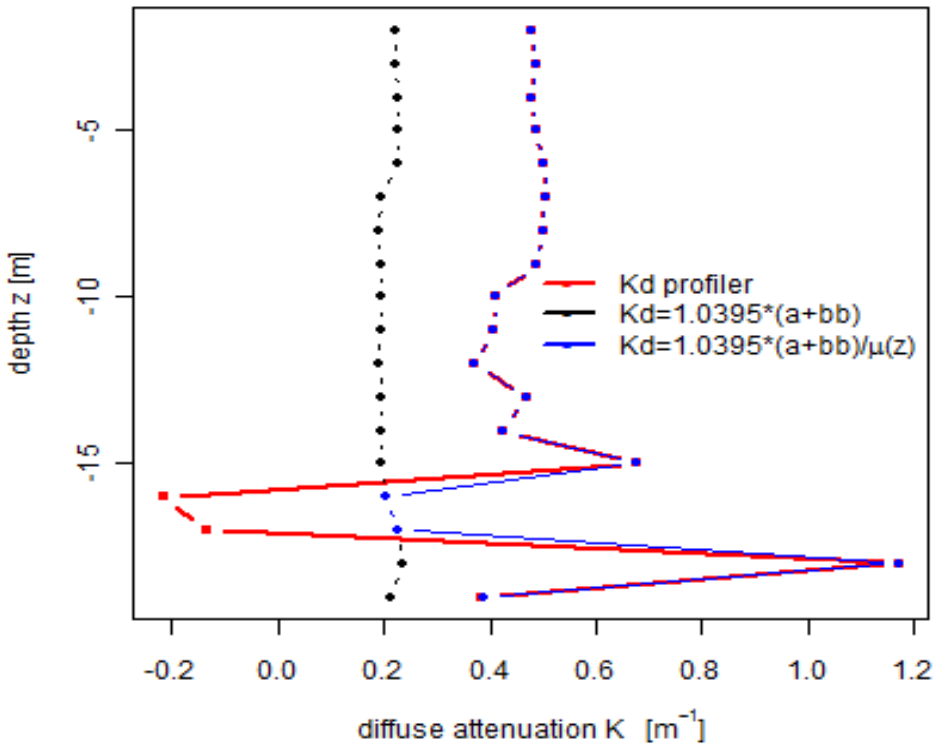

Figure 5. Diffuse attenuation Kd with depth estimated from the IOP's and AOP's for the wavelength at 668 nm.

Depth	mu(442)	mu(555)	mu(668)
1	-	-	-
2	0.84	0.82	0.46
3	0.81	0.72	0.45
4	0.85	0.79	0.48
5	0.82	0.74	0.47
6	0.8	0.7	0.45
7	0.73	0.66	0.39
8	0.74	0.65	0.38
9	0.76	0.63	0.4
10	0.95	0.96	0.47
11	0.95	0.9	0.47
12	0.75	0.61	0.52
13	0.71	0.55	0.42
14	0.9	0.84	0.46
15	0.78	0.71	0.29
16	1	0.91	1
17	0.86	0.75	1
18	0.43	0.31	0.2
19	1	1	0.55

Table 1. μ_d values for the different wavelengths and for each depth.

4. References

Gordon, H. R., 1989. Can the Labert-Beer law be applied to the diffuse attenuation coefficient of ocean water. Limnology and Oceanography, 34 (8), 1389-1409

Mobley, C.D. and L.K. Sundman, 2008. HydroLight 5 - EcoLight 5 Technical Documentation (2008), Sequoia Scientific, Inc. *Available online:* http://misclab.umeoce.maine.edu/boss/classes/RT_Weizmann/HE5TechDoc.pdf